**DISSERTATION**

# ION AND SUBSTRATE EFFECTS ON THIN FILM DEPOSITION AND SUBSTRATE-RADICAL INTERACTIONS IN RF PLASMAS

Submitted by

Carmen I. Butoi

Department of Chemistry

In partial fulfillment of the requirements

for the degree of Doctor of Philosophy

Colorado State University

Fort Collins, Colorado

Fall 2000

Bell & Howell Information and Learning Company
300 North Zeeb Road
P.O. Box 1346
Ann Arbor, MI 48106-1346

COLORADO STATE UNIVERSITY

October 10, 2000

WE HEREBY RECOMMEND THAT THE DISSERTATION PREPARED UNDER OUR SUPERVISION BY CARMEN I. BUTOI ENTITLED **ION AND SUBSTRATE EFFECTS ON THIN FILM DEPOSITION AND SUBSTRATE-RADICAL INTERACTIONS IN RF PLASMAS** BE ACCEPTED AS FULFILLING IN PART THE REQUIREMENTS FOR THE DEGREE OF DOCTOR OF PHILOSOPHY.

Committee on Graduate Work

Advisor

Department Head

## ABSTRACT OF DISSERTATION

## ION AND SUBSTRATE EFFECTS ON THIN FILM DEPOSITION AND SUBSTRATE-RADICAL INTERACTIONS IN RF PLASMAS

Fluorocarbon plasmas (FCP's) have applications such as generation of interlevel dielectric films and etching in the microelectronics industry, as well as production of biocompatible materials. Ammonia glow discharges are equally useful with applications in nitride passivation for integrated circuit manufacture along with polymer surface modification. This work aims to elucidate the underlying chemical mechanisms that control substrate modification in the two plasma systems. The research performed to achieve this goal combines substrate modification and plasma molecular beam studies.

The structure and composition of fluorocarbon materials deposited in pulsed and continuous wave (CW) hexafluoropropylene oxide (HFPO) plasmas were investigated. Results indicate a substantial dependence on substrate position relative to the rf coil. When the substrate was placed 8 cm downstream from the rf coil (25 W CW), highly amorphous, cross-linked films were obtained. In contrast, materials deposited further downstream at 28 cm contained less cross-linked moieties and a higher degree of order.

Difluorocarbene radicals are believed to play a key role in FCP substrate

modification. The surface scatter coefficients, $S$, of $CF_2$ radicals were determined during plasma processing of substrates using the imaging of radicals interacting with surfaces (IRIS) technique. The plasma molecular beam sources were 100% $C_2F_6$, 50/50 $C_2F_6/H_2$, and 100% HFPO. CW and pulsed glow discharges were investigated. Rf power and substrate material effects on difluorocarbene reactivity were studied along with ion bombardment effects. The radical-surface interaction data were correlated with data from surface characterization of plasma processed substrates. The key finding is that the surface reactivity of $CF_2$ radicals is a good indicator of the overall plasma process: etching or deposition.

The interactions of $NH_2$ radicals with different substrate materials during $NH_3$ plasma processing were also investigated using the IRIS technique. For most conditions, $S > 1$, indicating that $NH_2$ generation occurs at the plasma-substrate interface. To obtain information on energy transfer between plasma species and the substrate surface during processing, the translational temperature, $\Theta_{Tsc}$, of scattered $NH_2$ molecules was determined under different experimental conditions. The correlation of $NH_2$ scatter coefficients and translational temperature results permitted the identification of the processes most likely involved in $NH_2$ radical surface generation.

Carmen I. Butoi
Department of Chemistry
Colorado State University
Fort Collins, Colorado 80523-1872
Fall 2000

## TABLE OF CONTENTS

# CHAPTER 1

## PLASMA FUNDAMENTALS AND OVERVIEW

This dissertation chapter provides an introduction to plasma science. Plasma types and modes of generating a glow discharge are briefly discussed. The fundamentals of gas-phase and plasma-surface interactions are also covered. In addition, this chapter contains an overview of the research presented in Chapters 2-6.

## 1.1. INTRODUCTION

Plasma enhanced surface modification has found uses in a wide range of industries.[1] Glow discharges can be used to deposit novel materials,[2,3] and also to selectively etch $SiO_2$/Si systems in the microelectronics industry.[4] In addition, plasma enhanced chemical vapor deposition techniques (PECVD) show great promise in generating biocompatible and robust materials for biotechnology industry applications.[5,6] A large body of work concerning plasmas does exist. However, most of the studies published to date are empirical in nature. While such research provides insight into the versatility of plasma processing, it does little to promote a solid understanding of plasma surface modification mechanisms. Hence, more in-depth fundamental investigations of glow discharges than what has been performed are needed to understand and control plasma induced surface modification processes.

## 1.2. PLASMA FUNDAMENTALS

A plasma is a quasi-neutral gas composed of ions, electrons, radicals, metastables, and parent gas species.[1] Based on the temperature of species in the plasma, three main classifications exist: (a) plasmas in complete thermodynamic equilibrium, where the temperatures of all species are equal; (b) plasmas in local thermodynamic equilibrium, where thermodynamic equilibrium is achieved in small plasma volumes; and (c) non-local thermodynamic equilibrium plasmas, where the temperature of electrons is always larger than the other species in the glow discharge. The last type of plasma is also known as a cold plasma, and is very useful because of its capability to induce chemical reactions at

relatively low gas temperatures (<1000 K).[1]

Cold plasmas are generated and sustained electrically by applying direct current, radio frequency, or microwave power across the parent gas. All the studies presented in this thesis are based on the use of inductively coupled rf plasmas. Hence, details for these glow discharges are discussed further in the following section.

## 1.3. RF PLASMAS

When an alternating electric (AC) field is applied across a gas, the anode and cathode switch polarity at a frequency, ω, equal to that of the AC current. If ω surpasses the critical ion frequency, defined in equation 1.1, the amount of time taken by ions to move between the two electrodes is larger than half the period of the electric field,

$$f_{ci} = \frac{\langle v \rangle_{di}}{2L} \qquad (1.1),$$

where $f_{ci}$ is the ion critical frequency, $\langle v \rangle_{di}$ is the average drift velocity of the ion, and $L$ is the distance between the electrodes. The $f_{ci}$ value ranges from 500 kHz to several MHz based on ion properties (i.e. mass, charge).[1]

In contrast to ions, electrons have a much larger mobility due to their smaller mass.[7] Hence, they respond to the AC field when the ions have stopped doing so. An rf plasma is operated at 13.56 MHz, a frequency larger than the $f_{ci}$ but smaller than the electron critical drift velocity, $f_{ce}$, equation 1.2,

$$f_{ce} = \frac{\langle v \rangle_{de}}{2L} \qquad (1.2)$$

where $\langle v \rangle_{de}$ is the electron average drift velocity. Consequently, in rf glow discharges electrons collect most of the energy from the external electric field, and thus have temperatures in the 10-20 eV range, much larger than those of ion or neutral species which are typically < 5 eV.[7] The rf discharge is sustained through the elastic and inelastic collisions of the plasma energetic electrons with neutral or ionic species.

### 1.3.1. GAS-PHASE INTERACTIONS

Plasma gas-phase chemical reactions occur as a result of inelastic collisions between (A) electrons and heavy species (radicals and ions), or between (B) heavy species.

(A) Collisions between electrons and heavy species can result in atomic electronic excitation or molecular rotational, vibrational, or electronic excitation. As short-lived electronically excited species return to the ground state, electromagnetic radiation occurs in the UV or visible region of the spectrum. However, metastable species are also formed through electron-impact excitation. Since metastables are long lived, they can participate in other chemical processes before returning to their ground state.

Another process which can occur as a result of A-type collisions is dissociation of the heavy species. This type of process accounts for bond breaking and formation of radicals in the glow discharge. Molecular dissociation occurs through vibrational or

electronic excitations. In addition, electron-neutral collisions can also result in ionization of the neutral species, depending on ionization energy values. Positive atomic or molecular ions are usually generated through this type of process.

(B) Collisions between heavy species can be divided into radical-molecule, and ion-X interactions, where X comprises ions and neutral molecules. A significant B-type process is radical recombination. Radicals produced in the plasma through the interactions discussed previously can recombine through disproportionation or combination processes. New chemical species are thus formed in the plasma; these molecules can then be involved in other chemical processes within the glow discharge.

Another possible outcome of radical-molecule collisions is the ionization of one of the colliding species. This type of process is known as Penning ionization, and mainly occurs when an energetic metastable species is involved in the collision.[1,7] Of course, for the Penning process to take place, the energy of the metastable must be larger than the ionization energy of the collision partner.

Interactions between ions and other plasma species are also an integral part of bulk plasma chemistry. If negative ions are present, they can collide with positive ions, lose charge and radiatively recombine to form a new product as shown in equation 1.3.

$$X^- + Y^- \rightarrow XY + h\nu \qquad (1.3)$$

Another reaction involving ions which can occur in type B collisions is charge transfer, as shown in equation 1.4.

$$X^+ + Y \rightarrow X + Y^+ \qquad (1.4)$$

It is worth noting that in a cold plasma, the degree of ionization ranges from $10^{-7}$

to $10^{-5}$, resulting in ion densities much lower than those of neutral species (radicals and molecules). It is thus expected radical-molecule interactions predominate over those of ion-X type in the gas phase.[1] However, despite their relatively low densities in the plasma bulk, ions play crucial roles in substrate-plasma reactions as will be discussed in section 1.3.2.

### 1.3.2. GAS-SURFACE INTERACTIONS

All the species created in the plasma can interact with substrates at the plasma-surface interface. There are numerous ways through which these interactions can occur. Parent gas molecules and radicals can adsorb at the surface and stick, possibly resulting in film formation. Interactions between adsorbed and incident radicals can initiate polymerization reactions. In addition, the adsorbed neutral species can further diffuse and react at the substrate surface, or they can desorb.

One of the most significant types of plasma-surface interactions is the collision between ions and the substrate. Ions are thought to have a profound impact on the type of surface modification accomplished during the plasma processing of substrates.[8] Ion bombardment can result in the sputter of fragments from the underlying substrate or the film formed during the plasma process. It can also create reactive radical sites during film deposition.[11] The density of such sites controls the composition of the material generated via PECVD. Other interactions which affect the plasma process are the collisions between metastables and the substrate surface. These are believed to have similar effects to those of ion bombardment.[7]

All the processes discussed in this section contribute to modifying the substrate through etching, functional group implantation, or film deposition at the substrate surface. Because most of the species created in the gas phase directly interact with the substrate surface, it is difficult to determine the individual contributions to the overall plasma process mechanism. The present work aims to investigate the role of two important types of plasma species, radicals and ions, during substrate exposure to two industrially relevant glow discharges: fluorocarbon and ammonia plasmas. An overview of the studies conducted is presented in section 1.4.

## 1.4. OVERVIEW OF RESEARCH

As illustrated in the preceding sections, plasmas are non-equilibrium, complex systems. The systematic study of individual plasma species and their reactions is needed to elucidate process mechanisms but is very difficult to achieve. Some researchers have attempted to explore radical-surface interactions by using molecular beams which comprise the radical of interest only.[9,10] Such studies are useful in understanding radical behavior but fail to provide insight into plasma processing where many species concomitantly interact with each other and with a substrate. One technique which allows the investigation of plasma radicals as they react with substrates is the imaging of radicals interacting with surfaces (IRIS) technique.

The work presented here focuses on the study of two plasma systems: fluorocarbon and ammonia glow discharges. Both are used extensively to modify materials for specific applications. To elucidate substrate modification mechanisms, a

two-faceted approach was used. One facet examines substrate modifications as a function of plasma parameters. The other facet consists of studying the types of interactions of specific plasma radicals with different substrate materials. By correlating these two facets, a deeper understanding of the overall plasma process was gained.

The experimental set-up used to perform substrate modification investigations is described in detail in Chapter 2. A typical glass reactor, rf inductive coil, and rf matching network are used to generate plasmas. Plasma parameters which include precursor gas, gas pressure, gas flow rate and rf power can be varied. The substrates thus processed are analyzed using a comprehensive suite of techniques such as FTIR, X-ray photoelectron spectroscopy (XPS), near-edge X-ray absorption fine structure (NEXAFS), secondary ion mass spectrometry (SIMS), and scanning electron microscopy (SEM).

In Chapter 3 a systematic study of materials deposited in hexafluoropropylene oxide (HFPO) plasmas is presented. Experimental parameters such as rf power, HFPO pressure, pulsed plasma duty cycle, and substrate distance from the rf coil are investigated. Fluorocarbon films deposited under different experimental conditions are analyzed using a battery of surface compositional and structural analysis techniques. The effects of ions on material composition are also directly investigated.

To explore the role of specific radicals participating in substrate modification during plasma processing, the IRIS method was used. The IRIS apparatus is described in detail in Chapter 4. This technique generates spatially resolved images of plasma radicals as they interact with substrates by combining a gated and intensified charge coupled device (CCD) camera, laser induced fluorescence (LIF), and molecular beam techniques. Radical

scatter coefficients can be determined from comparing densities of radicals incident to the substrate surface to the densities of radicals which emanate from the substrate surface. In addition, the IRIS technique can be used to obtain kinetic energy information by monitoring the movement of radicals as a function of gate delay.

In fluorocarbon plasma polymerization, $CF_2$ radicals are often cited as critical deposition precursors and are believed to play a crucial role in fluorocarbon plasma polymeric film formation.[8,11,12] Chapter 5 explores this hypothesis by using the IRIS method to investigate $CF_2$-substrate interactions in a variety of fluorocarbon plasmas. The surface scatter behavior of $CF_2$ radicals is investigated as a function of applied rf power, pulsed plasma duty cycle, and substrate material. Also discussed are difluorocarbene interactions when ions are removed from the plasma molecular beam. The results obtained are compared to data from other fluorocarbon plasma systems. $CF_2$ radical behavior is correlated to the overall plasma process, etching or depositing.

$NH_2$ radical behavior at the ammonia plasma-substrate interface is investigated in Chapter 6. $NH_3$ plasmas are widely used for polymer surface modification as they are known to implant groups which render substrate surfaces hydrophilic.[17,18] While substrate modification in ammonia plasmas has been extensively explored, little is understood about the modification mechanism. The scatter coefficients of $NH_2$ radicals produced in ammonia plasmas during processing of metallic, semiconductor and polymer substrates have been measured with IRIS. In addition, radical-substrate translational energy transfer is probed through comparison of incident and scattered radical translational temperatures. Ion bombardment is shown to greatly affect both $NH_2$ radical reactivity and scattered $NH_2$

translational temperature.

## 1.5. REFERENCES


1. A. Grill, *Cold Plasma in Materials Fabrication*, IEEE Press, New York, (1994).

2. H. Yasuda, *Plasma Polymerization*, Academic Press, New York, 1985.

3. F. Yamagishi, D. D. Granger, A. E. Schmitz, and L. J. Miller, *Thin Solid Films* **84**, 427 (1981).

4. K. Endo, *Mat. Res. Soc. Bull.* **22,** 55 (1997), and references therein.

5. Bohnert, J. L.; Fowler, B. C.; Horbett, T. A.; Hoffman, A. S. *J. Biomat. Sci:Poly. Ed.* **1990**, *1*, 279.

6. Kiaei, D.; Hoffman, A. S.; Horbett, T. A. *J. Biomat. Sci.: Poly. Ed.* **1992**, *4*, 35.

7. M. A. Lieberman, and A. J. Lichtenberg, *Principles of Plasma Discharges and Materials Processing*, John Wiley&Sons, New York, (1994).

8. R. d'Agostino, F. Cramarossa, F. Fracassi, and F. Illuzi, *Plasma Deposition, Treatment, and Etching of Polymers*, R. d'Agostino ed., Academic Press, San Diego, p. 99 (1990).

9. D. C. Gray, H. H. Sawin, and J. W. Butterbaugh, *J. Vac. Sci. Technol. A* **9**, 779 (1991).

10. J. W. Butterbaugh, D. C. Gray, and H. H. Sawin, *J. Vac. Sci. Technol. B* **9**, 1461 (1991).

11. N. E. Capps, N. M. Mackie, and E. R. Fisher, *J. Appl. Phys.* **84**, 4736 (1998).

12. J. P. Booth, G. Hancock, N. D. Perry, D. C. W. Blaikley, J. A. Cairns, and R. Smailes, *Mat. Res. Soc. Symp Proc.* **98**, 135 (1987).

# CHAPTER 2

## EXPERIMENTAL METHODS FOR THIN FILM DEPOSITION AND ANALYSIS

This chapter contains a description of the plasma reactor used to process materials in rf glow discharges. Experimental conditions for fluorocarbon and ammonia plasma material processing are also discussed. In addition, a detailed list and description of film analysis methods is presented.

## 2.1 INTRODUCTION

All of the plasma generated materials studied in this work are produced in a home-built tubular glass inductively coupled rf plasma reactor. This chapter describes the components of this PECVD apparatus along with the analytical techniques used to analyze the substrate processed. In a typical deposition experiment, the system is evacuated to base pressure (<5 mtorr), followed by introduction of the precursor gas into the plasma reactor through a mass flow controller. Flow rate is measured in standard cubic centimeters per minute (sccm). The pressure is monitored by a MKS capacitance manometer, which is not sensitive to the type of gas flowing through the system. After the plasma is ignited, the reflected power, which is the rf power lost to the system, is minimized. Processing times vary with the plasma conditions and the precursors used. At the end of the plasma processing, the reactor and gas lines are again evacuated to base pressure. After bringing the system to atmospheric pressure, the processed sample is removed and analyzed.

## 2.2 PLASMA REACTOR

The plasma reactor consists of two cylindrical Pyrex tubes held together by a 50 mm o-ring and a Thomas pinch clamp. Glass sleeves are employed to reduce the amount of deposits on the reactor walls. For fluorocarbon film depositions, the reactor was modified relative to what was used previously[1] by extending one glass tube section to allow for far downstream depositions, Fig. 2.1. Gas products are removed from the system through a liquid $N_2$ trap by an Alcatel 2012A mechanical pump at a speed of

4.2 $Ls^{-1}$.

An RFPP power supply is used to apply 13.56 MHz of power through a matching network to the system. An eight-turn, 10 gauge nickel coated copper wire is used as the rf coil. The RFPP has both CW and pulsed power capabilities. For CW plasmas, the rf power is programmed from the power supply, whereas for pulsed plasmas, the rf power, duty cycle, and cycle on-time, $t_{on}$, can be adjusted. Along with equivalent power these parameters are used to classify pulsed plasmas. Duty cycle is defined in equation 2.1,

$$Duty\ cycle = \left(\frac{t_{on}}{t_{on} + t_{off}}\right) x100 \qquad (2.1),$$

where $t_{off}$ is the cycle off-time during which no rf power is applied to the system; and equivalent power is defined in equation 2.2,

$$Equivalent\ power = \left(\frac{t_{on}}{t_{on} + t_{off}}\right) \cdot P \qquad (2.2),$$

where $P$ is the peak applied rf power, which is transferred to the gas during the on-time only. On-times can be varied from 2 to 98 ms using the internal pulse generator of the power supply, and duty cycles can be varied from 1 to 99%.

## 2.3 CONDITIONS FOR PLASMA PROCESSING OF SUBSTRATES

To generate the fluorocarbon materials discussed in Chapter 3, input power for CW depositions was varied from 5-120 W, and the applied peak power was kept constant

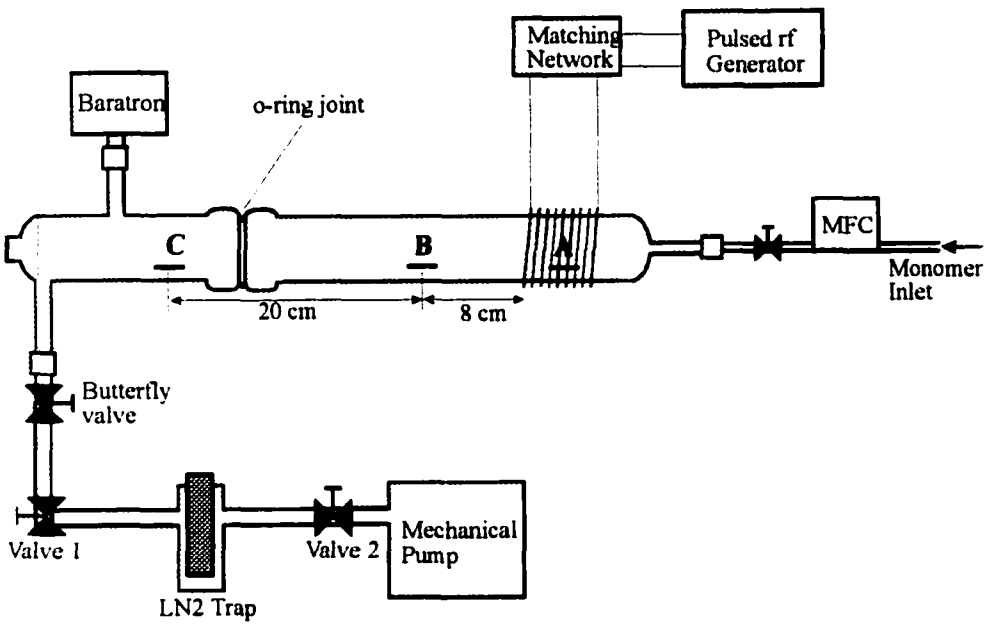


**Figure 2.1.** Schematic diagram of the inductively coupled rf plasma reactor used for all depositions. The HFPO flow is controlled by a mass-flow controller (MFC). Substrates placed at position A are within the visible glow. Positions B and C correspond to substrate positions of 8 cm and 28 cm downstream from the rf coil, respectively.

at 300 W for pulsed experiments. In the latter case, the equivalent CW power can be determined by calculating the time averaged power applied over the entire pulse cycle. A 10/190 ms pulse sequence, where the plasma is on for 10 ms and off for 190 ms, corresponds to an equivalent CW power of 15 W, and a duty cycle of 5%. For all pulsed plasma experiments, the on-time was 10 ms.

FTIR grade KBr (Aldrich) pellet and a silicon wafer (p-type, 110) with 40 - 60 Å of native oxide were used as substrates. These were placed on glass microscope slides oriented parallel to the gas flow within the coil region (position A, Fig. 2.1) as well as at 8 and 28 cm downstream (positions B and C, respectively in Fig. 2.1). CW and pulsed deposition times ranged from 30 min to 2 h. For pulsed experiments, deposition time was defined by the total time the sample was exposed to both pulse on and off cycles.

For $NH_3$ plasma treatments Si, Cu, PTFE and polyimide substrates were processed at two rf powers: 50 W and 100 W. Samples were placed in the plasma glow and also 12 cm from the rf coil. All treatment times were 5 minutes. Multiple samples of each substrate were treated.

## 2.4 FILM ANALYSIS

The fluorocarbon materials generated in our inductively coupled plasma reactor were analyzed using a suite of analytical tools. To determine film composition, transmission FTIR and X-ray photoelectron spectroscopy were used. For structural information, secondary ion mass spectrometry (SIMS) and near-edge X-ray absorption fine structure (NEXAFS) analyses were performed. Finally, scanning electron microscopy

(SEM) and atomic force microscopy (AFM) were used to investigate the morphology of fluorocarbon materials deposited on copper wires and silicon wafers. Deposition rates were determined from film thickness values obtained from AFM and profilometry measurements. The instrumental parameters utilized are described in detail in the following sections.

### 2.4.1 FTIR SPECTROSCOPY

Transmission FTIR spectral analysis on films deposited on KBr pellets and Si wafers was performed *ex situ* using a Nicolet Magna 760 FTIR spectrometer (resolution of 8 $cm^{-1}$ and averaging 128 scans). Spectra shown are corrected for residual carbon dioxide not purged from the FTIR spectrometer (absorbances at ~2340 and 2360 $cm^{-1}$). For materials deposited on KBr pellets, an air background spectrum was subtracted from the sample spectrum. When fluorocarbon films were deposited on Si wafers, a blank Si wafer was used for background subtraction.

### 2.4.2 X-RAY PHOTOELECTRON SPECTROSCOPY

X-ray photoelectron spectroscopy (XPS) is an analytical tool used extensively in the determination of solid material elemental composition along with chemical environment.[2] X-ray light with sufficient energy to eject elemental core electrons illuminates the solid's surface. By comparing the energy of the incoming X-ray photon to the energy of the electron ejected from the sample, valuable information about the element which donated the electron along with its bonding environment can be determined.

XPS analyses were performed on a Surface Science Instruments S-probe spectrometer located at the University of Washington NESAC-BIO center. This system has a monochromatic Al Kα X-ray source (hν = 1486.6 eV), hemispherical analyzer, and resistive strip multichannel detector. A low energy (~5 eV) electron gun was used for charge neutralization on the nonconducting samples. The binding energy (BE) scales for the samples were referenced by setting the $CF_2$ peak maxima in the $C_{1s}$ spectra to 292.0 eV. High resolution $C_{1s}$ spectra were acquired at an analyzer pass energy of 50 eV and a X-ray spot size of 1000 μm and were fit using Gaussian functions with FWHM of 1.3-1.5 eV. XPS elemental compositions were obtained using a pass energy of 150 eV. To obtain information about the composition of the fluorocarbon film at different depths, Photoelectron take-off angles of 0, 55 and 80° were used; where the take-off angle is defined as the angle between the axis of the analyzer lens and the surface normal.

### 2.4.3 NEAR-EDGE X-RAY ABSORPTION FINE STRUCTURE

The NEXAFS technique uses polarized X-ray light to excite sample core electrons into antibonding orbitals. Based on dipole moment selection rules, X-ray absorption is most intense when the antibonding orbital is parallel to the electric field of the polarized X-ray beam. If the bond being probed exhibits a particular orientation, X-ray absorption varies in intensity as the X-ray-substrate angle changes. Hence, NEXAFS is a useful technique for obtaining structural information of materials.

NEXAFS analysis was performed at the National Synchrotron Light Source at Brookhaven National Laboratory on beamline U7A. The 600 lines/mm grating

monochromator was calibrated using the graphite $C_{1s} \rightarrow \pi^*$ transition (285.35 eV) and had an energy resolution of ~0.15 eV (FWHM) at the carbon K edge. Photoelectrons and Auger electrons were collected with a negatively biased channeltron to obtain partial electron yield (PEY) spectra. These spectra were normalized by using the PEY from a 90 % transmission grid which was gold coated *in situ*, and positioned in the incoming X-ray beam. The incidence angle is defined as the angle between the incident X-ray beam and the sample surface. Data were obtained at different incidence angles by rotating the sample with respect to the X-ray beam.

### 2.4.4 SECONDARY ION MASS SPECTROMETRY

All time-of-flight SIMS (ToF-SIMS) spectra were acquired on a Physical Electronics PHI 7200 ToF-SIMS spectrometer. The instrument is equipped with a $Cs^+$ ion source operated at 8 keV, a reflectron mass analyzer, and chevron-type multichannel plate detectors. For acquisition of spectra, a bunched primary $Cs^+$ beam (50 μm diameter, approximately 1 ns pulse width) is used, and the bin width of the time-to-digital converter (TDC) is set at 1.25 ns, resulting in mass resolutions ($m/\Delta m$) of >8000 at m/z = 27 for electrically conducting samples. The beam is rastered over a square area that is 100 μm on a side. Data acquisition times were adjusted to ensure that the spectra were taken in static mode, i.e. the total ion dose was less than $2 \times 10^{12}$ ions/cm$^2$ during the acquisition.

### 2.4.5 FILM SURFACE ANALYSIS

The hydrophobicity of the fluorocarbon materials deposited in CW and pulsed HFPO plasmas was measured using a Ramé Hart Model 100 contact angle goniometer. Static contact angles for water were measured using the sessile drop method. Measurements were taken on both sides of water drops at ambient temperature, 30-40 s after 1 μL drops were applied to the surface and the needle tip was removed from each drop. For each sample, four drops were placed at different locations on the surface of the film. Each reported contact angle is an average of these measurements for three samples.

To assess surface modification during $NH_3$ plasma processing, static contact angles were measured using a Krüss DSA10 drop shape analysis system with a G1041 video measuring system and a volume control apparatus. For each sample, 2-3 measurements were made using 0.5 μL drops. In addition, aging studies on all treated samples were performed by determining static contact angles over a period of 6 weeks following $NH_3$ plasma treatment.

To investigate the topology of the fluorocarbon materials deposited in HFPO plasmas (Chapter 3), scanning electron microscope (SEM) images were obtained using a Philips 505 apparatus. The accelerating voltage was 26.0 KV and the spot size was 20 nm. For more detailed morphological information, an atomic force microscope (AFM) was utilized in tapping mode. The Digital Instruments Nanoscope III apparatus was used to measure root mean square (rms) surface roughness values on 5 x 5 μm sample areas.

### 2.4.6 FILM DEPOSITION RATE

Deposition rates of fluoropolymers in HFPO plasmas were calculated using AFM and profilometry analysis. For films with thickness >500 Å, deposition rates were calculated based on step height measurements with a Tencor Alpha Step 100 profilometer. To form a step during the deposition process, half of the processed silicon substrate was masked with cellophane tape. After depositing for a known period of time, the tape was removed. AFM analysis of materials deposited on silicon wafers was used to determine deposition rates for films thinner than 500 Å.

## 2.5 PLASMA GAS PHASE DIAGNOSTICS

To understand plasma processing it is necessary to monitor species produced in the plasma along with analyzing substrate modifications. Since for most plasma species a fraction of the population is generated in the excited state, optical analysis techniques are valuable in evaluating the plasma content. Optical emission spectroscopy is such a technique that is widely used in plasma research.[3]

### 2.5.1 OPTICAL EMISSION SPECTROSCOPY

Optical emission spectroscopy (OES) is used to monitor plasma content by detecting the electromagnetic radiation emitted by gas phase excited state species as they lose energy. Most excited state radicals are produced through electron impact dissociation of precursor species.[4] It is important to note that most plasma species exist in the ground state. Hence, monitoring excited state neutrals does not provide information

on the behavior and absolute densities of plasma radicals.[5] However, OES remains a very useful tool in identifying species generated in the glow discharge.

To obtain OES data on our inductively coupled plasmas, an Ocean Optics S2000 triple spectrometer is employed. The downstream end of the plasma reactor was fitted with a fused silica optical window for coaxial detection of emitting species. OES from 240 - 700 nm were obtained for the fluorocarbon plasmas investigated in Chapter 5. Emitted light was collected through a quartz window situated ~15 cm downstream of the coil region, resulting in coaxial sampling of the plasma emission. Emission was imaged onto a 10 $\mu$m entrance slit of an Ocean Optics S2000 spectrograph using an optical fiber. The spectrograph was equipped with three 1800 grooves/mm holographic gratings and three 2048-element linear CCD-array detectors.

## 2.6. REFERENCES


1. K. H. A. Bogart, N. F. Dalleska, G. Bogart, E. R. Fisher. *J. Vac. Sci. Technol. A* **13**, 476 (1995).

2. E. A. Leone, and A. J. Signorelli, *Materials Characterization and Chemical Analysis*, 2nd ed., VCH, New York (1996).

3. R. W. Dreyfus, J. M. Jasinski, R. E. Walkup, aand G. S. Selwyn, *Pure and Appl. Chem.* **57**, 1265 (1985).

4. W. L. Lite, *Chemical Reactions in Electrical Discharges*, American Chemical Society, Washington D. C. (1969).

5. G. Hancock, L. Lanyi, J. P. Sucksmith, and B. K. Woodcock, *Pure and Appl. Chem.* **66**, 1207 (1994).

# CHAPTER 3

## DEPOSITION OF HIGHLY ORDERED $CF_2$-RICH FILMS USING CW AND PULSED HEXAFLUOROPROPYLENE OXIDE PLASMAS



This dissertation chapter contains the manuscript of a full paper that has been published in *Chemistry of Materials*. It describes novel materials produced in hexafluoropropylene oxide (HFPO) plasmas. In addition, this chapter discusses the effects of changing plasma parameters on the properties of materials generated in HFPO glow discharges. The structure and composition of fluorocarbon materials deposited in pulsed and continuous wave (CW) hexafluoropropylene oxide (HFPO) plasmas are investigated.

## 3.1. INTRODUCTION AND BACKGROUND

Over the past 20 years, pulsed rf plasmas have been successfully employed in plasma polymerization of a variety of monomers.[1,2,3] With pulsed plasma polymerization, high retention of the monomer functional group in the resulting polymeric film can be achieved.[4] In addition, pulsed plasmas provide access to lower continuous wave (CW) equivalent powers because the rf power is on for only a portion of the cycle time. Use of pulsed sources reduces trapped radicals in the film, lowers deposition surface temperatures, decreases high energy ion bombardment and UV flux to the surface, and provides greater control over the resulting film chemistry.[5] In contrast, films deposited from CW plasmas are often amorphous polymeric materials with little resemblance to the original monomer.[6,7] This is partially because CW plasmas can significantly fragment and scramble monomer functional groups through complex recombination and addition reactions.[8] We have previously reported the use of pulsed rf plasmas to produce a variety of hydrogenated and fluorinated organic films with a high degree of controllability over film composition.[4]

Alternatives to pulsed plasma film deposition are provided by plasma-enhanced chemical vapor deposition (PECVD) using downstream and remote CW plasmas, which also decrease energetic species bombardment of the deposited material. Again, this eliminates undesired effects usually associated with the use of CW plasmas and can produce films with unique properties.[9,10,11] Such materials have been shown to possess low dielectric constants[12] and increased biocompatibility.[13,14] O'Kane and Rice reported pronounced composition differences between films generated at different distances from the rf glow of a tetrafluoroethylene (TFE) plasma.[10] Fluoropolymers deposited at the

longest distances contained the highest percentage of $CF_2$ and less than 5% $CF_3$. Castner and coworkers found that depositions performed downstream from the discharge glow in a TFE plasma produced highly ordered materials with high $CF_2$ content.[15]

Along with TFE plasmas, other fluorocarbon systems have been utilized for the deposition of polymeric films with low dielectric constants as well as for producing biocompatible materials.[16,17,18] One monomer that has been used extensively in pulsed plasma polymerization work is hexafluoropropylene oxide (HFPO). Timmons and coworkers deposited films in HFPO plasmas under pulsed conditions but observed no film formation at 300 W under CW conditions.[19] Gleason and coworkers also found that the use of pulsed HFPO plasmas (0.5% duty cycle, 280 W) results in high $CF_2$ content fluoropolymers. In contrast to Timmons' results, Gleason's group did observe film formation under CW conditions, but these films were highly cross-linked unlike those obtained in the pulsed plasma system.[20] Neither Timmons' nor Gleason's studies probed film orientation with respect to the substrate surface.

An early communication from our laboratory presented limited results for films deposited in CW HFPO plasmas.[21] The present work aims to provide a more comprehensive perspective into the nature of films deposited in HFPO plasmas under CW as well as pulsed conditions. To identify the best conditions for the deposition of highly ordered, $CF_2$ rich materials, plasma parameters were varied along with distance from the discharge visible glow for both CW and pulsed systems. Film composition was investigated with Fourier transform infrared (FTIR) spectroscopy, angle-resolved x-ray photoelectron spectroscopy (XPS), and static secondary ion mass spectrometry (SIMS), while near-edge x-ray absorption fine structure (NEXAFS) analysis was used to determine

structural attributes. We have also determined film deposition rates under different plasma conditions and tested the mechanical stress properties of fluoropolymers deposited on Cu wires.

## 3.2. RESULTS

### 3.2.1. FTIR SPECTROSCOPY

Figure 3.1 shows FTIR spectra of films deposited at 8 cm (position B) downstream from the rf coil, using rf powers of 15, 30 and 60 W in a CW HFPO plasma. For materials deposited at position B at low rf powers (15 and 30 W), the spectra contain absorbance bands associated with amorphous plasma polymerized fluorocarbon materials, Fig. 3.1a. The most prominent feature in both spectra is the absorbance band at 1100-1400 $cm^{-1}$, attributable to all $CF_x$ (x=1-3) stretching modes.[22] The weaker absorbance band at 1700-1850 $cm^{-1}$ corresponds to either $C=CF_2$ or $CF=CF_2$ moieties in the film.[23] In contrast, the film obtained from a 60 W CW plasma shows a feature corresponding to SiO stretching at ~1100 $cm^{-1}$, but very little $CF_2$ signal. The SiO band results from etching of the glass reactor walls followed by redeposition of the etched material on the KBr substrate.[7] This constitutes strong evidence that etching is the predominant plasma process at high rf powers.

Figure 3.2 shows FTIR spectra of films deposited at position C with applied rf powers of 15, 30, and 60 W. The spectra of materials obtained in 15 and 30 W CW plasmas are different from those shown in Fig. 3.1. Two distinct absorption bands at 1217 and 1165 $cm^{-1}$, corresponding to the $CF_2$ asymmetric and symmetric modes, respectively, are observed.[23]

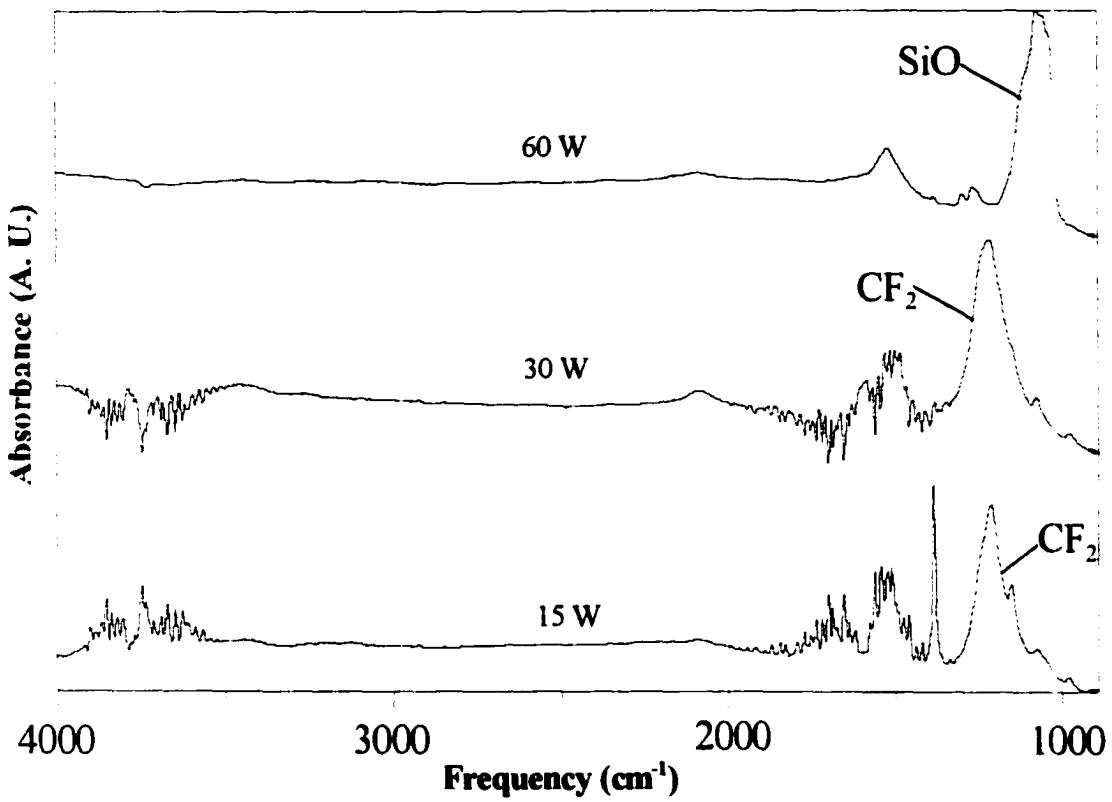


**Figure 3.1.** FTIR spectra of films deposited at position B in a CW HFPO plasma at three different rf powers 15, 30 and 60 W. The monomer gas pressure was 233 mtorr.

In addition, the intensity of the $CF_x$=$CF_2$ (x=0,1) stretch at ~1700-1800 $cm^{-1}$ is considerably lower in these films compared to what was observed in the films deposited at position B, Fig. 3.1. Along with the separation of $CF_2$ asymmetric and symmetric stretch bands, this indicates a lower degree of cross-linking than that of the fluorocarbon materials deposited at position B. In contrast, the FTIR spectrum of the 60 W film contains a broad absorption band at ~1200 $cm^{-1}$, consistent with a relatively amorphous fluorocarbon film.

The monomer pressure also affects the composition of materials deposited in our CW plasmas, Fig. 3.3. Figure 3.3 displays the IR spectra for materials obtained at position B for a 30W CW plasma and different HFPO pressures: 233 mtorr, 490 mtorr, and 900 mtorr. The presence of a broad band at ~1200 $cm^{-1}$ indicates that the fluorocarbon film deposited at 233 mtorr is highly amorphous. For films generated at higher pressures, the symmetric and asymmetric $CF_2$ vibrational bands separate, consistent with less amorphous materials. FTIR spectra of films deposited at position C, however, contain clearly separated $CF_2$ symmetric and asymmetric stretching bands at all monomer pressures, Fig. 3.4. Figure 3.5, 3.6, and 3.7 show FTIR spectra of films deposited at positions A, B, and C, respectively, using pulsed HFPO plasmas with different duty cycles. The spectrum of a film obtained at position A, at the highest duty cycle, 33% (10/23 ms), shows no absorbance band corresponding to the $CF_x$ stretching modes, but does contain an SiO absorbance band, Fig. 3.5. This indicates that although a fluorocarbon film is not generated, material etched from the reactor walls is deposited on the substrate. The film produced at a lower duty cycle of 16% (10/52 ms) the parent gas along with SiO moieties etched off the glass walls.

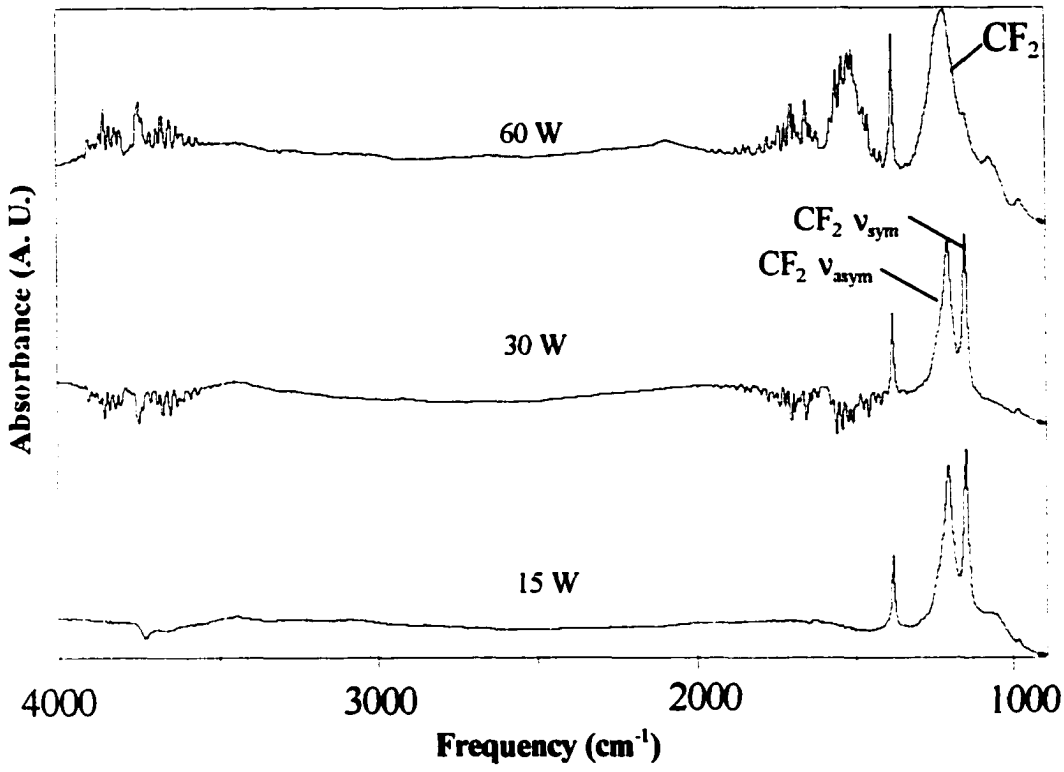


**Figure 3.2.** FTIR spectra of films deposited at position C in a CW HFPO plasma at three different rf powers 15, 30 and 60 W. The monomer gas pressure was 233 mtorr.

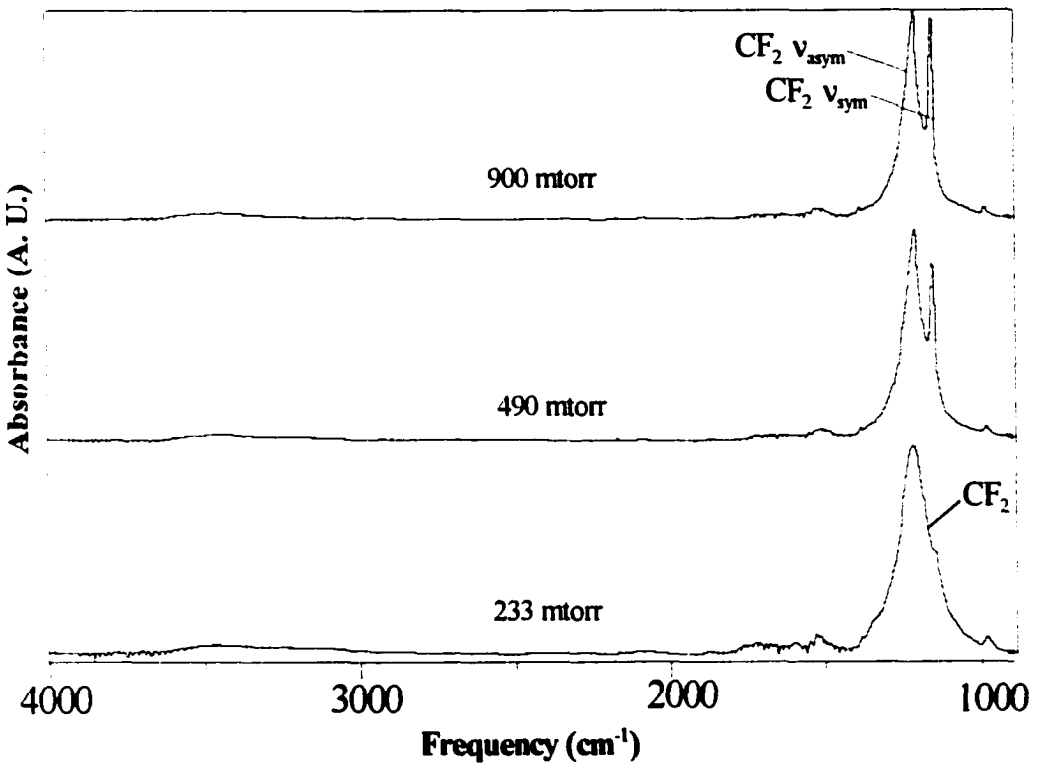


**Figure 3.3.** FTIR spectra for films deposited in a 30 W CW plasma at Position B using three different monomer pressures, 233, 490, and 900 mtorr.

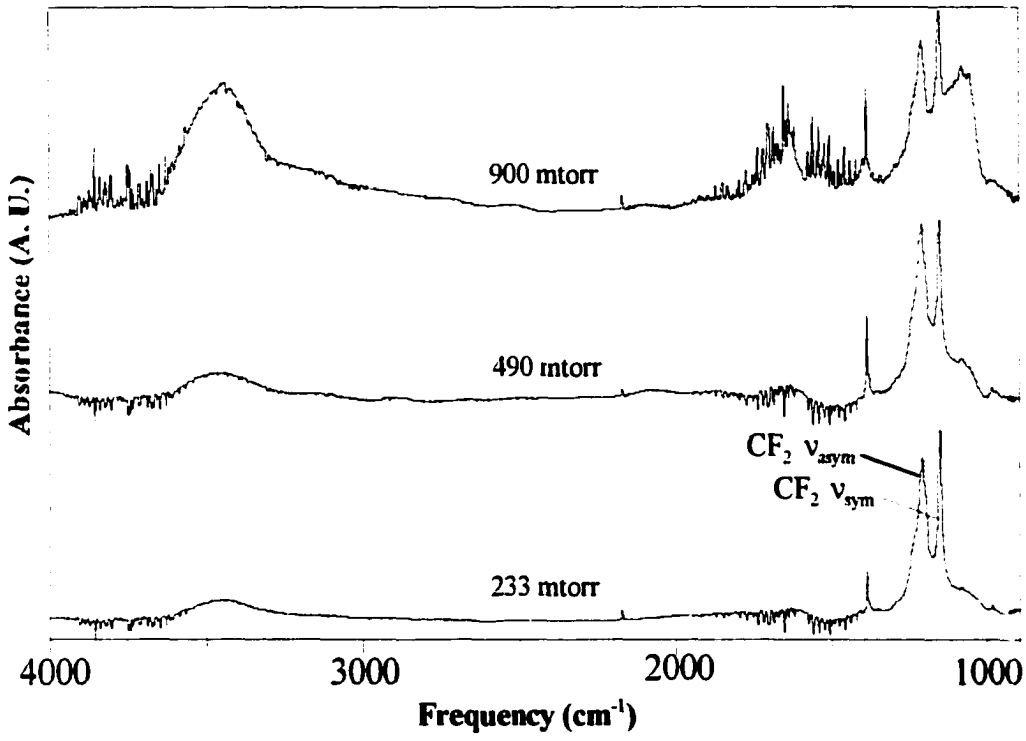


**Figure 3.4.** FTIR spectra for films deposited in a 30 W CW plasma at Position C using three different monomer pressures, 233, 490, and 900 mtorr.

The IR spectrum of the film deposited using a 5% duty cycle (10/190 ms) pulsed HFPO plasma, however, displays two distinct absorption peaks at 1217 and 1165 $cm^{-1}$ corresponding to $CF_2$ stretching modes. No other features are observed in the spectrum. Figure 3.6 indicates that further downstream at position B, both the 5% and 16% duty cycle plasmas deposit fluorocarbon materials for which the $CF_2$ symmetric and asymmetric stretching bands are clearly separated. The IR spectrum of the film generated at the 33% duty cycle (10/23 ms) still exhibits the SiO peak caused by reactor wall etching along with a new broad shoulder in the 1200-1300 $cm^{-1}$ region. This corresponds to the $CF_2$ vibrational signal and indicates that an amorphous material is obtained under these conditions. In contrast, at position C, Fig. 3.7, all three pulse sequences give rise to films whose IR spectra contain distinct $CF_2$ stretching bands and small degrees of unsaturation. Note that the IR spectra shown in Fig. 3.7 are nearly identical to those of films deposited at position C in 15 and 30 W CW plasmas, Fig. 3.2.

### 3.2.2. XPS ANALYSIS

Figure 3.8 shows the XPS spectra obtained at a 55° photoelectron take-off angle for fluorocarbon films deposited at positions B and C in a 25 W CW plasma. Peaks corresponding to C-$CF_x$ (287 eV), CF (290 eV), $CF_2$ (292 eV) and $CF_3$ (294 eV) moieties are present in the spectrum of the film generated at position B, with a content distribution of 39% (C-$CF_x$ + CF), 36% ($CF_2$), and 25% ($CF_3$). In contrast, the sample deposited under the same plasma conditions but further downstream, at position C, contains significantly more $CF_2$ (80%) and less $CF_3$ (12%).

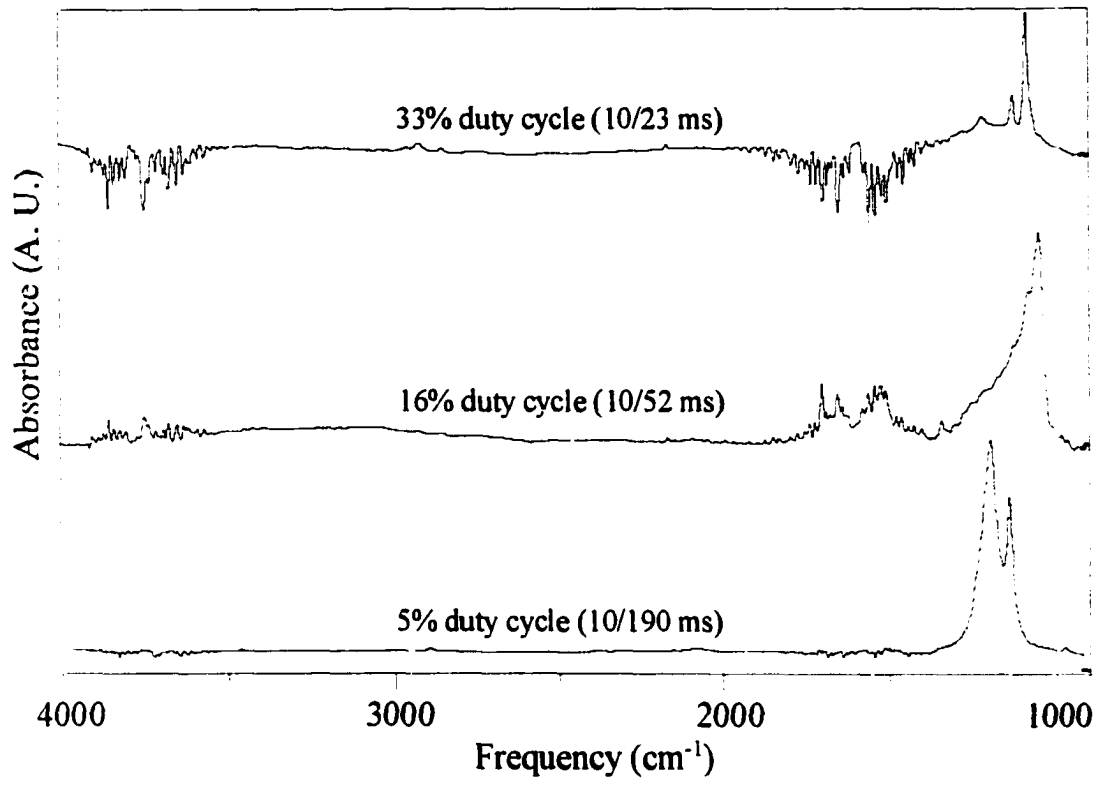


**Figure 3.5.** FTIR spectra of materials deposited at Position A in pulsed plasmas with pulse sequences of 10/190 msec (5% duty cycle), 10/52 msec (16% duty cycle), and 10/23 msec (33% duty cycle). The monomer gas pressure was 233 mtorr.

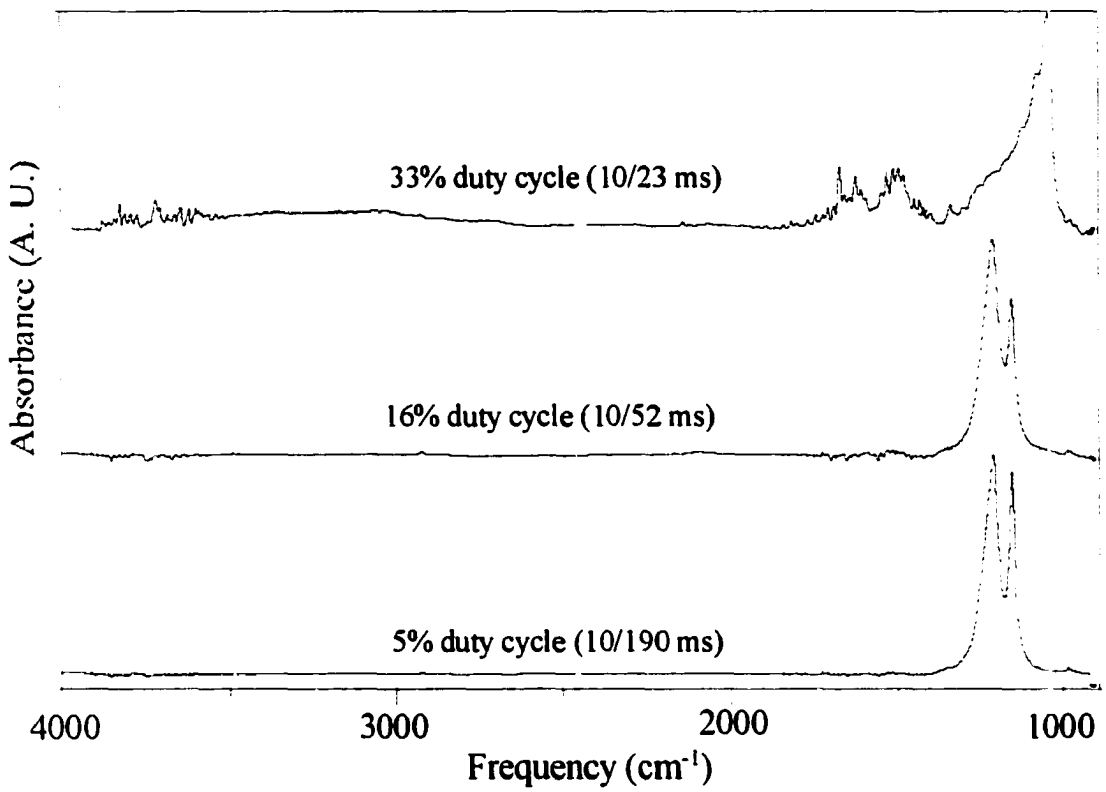


**Figure 3.6.** FTIR spectra of materials deposited at Position B in pulsed plasmas with pulse sequences of 10/190 msec (5% duty cycle), 10/52 msec (16% duty cycle), and 10/23 msec (33% duty cycle). The monomer gas pressure was 233 mtorr.

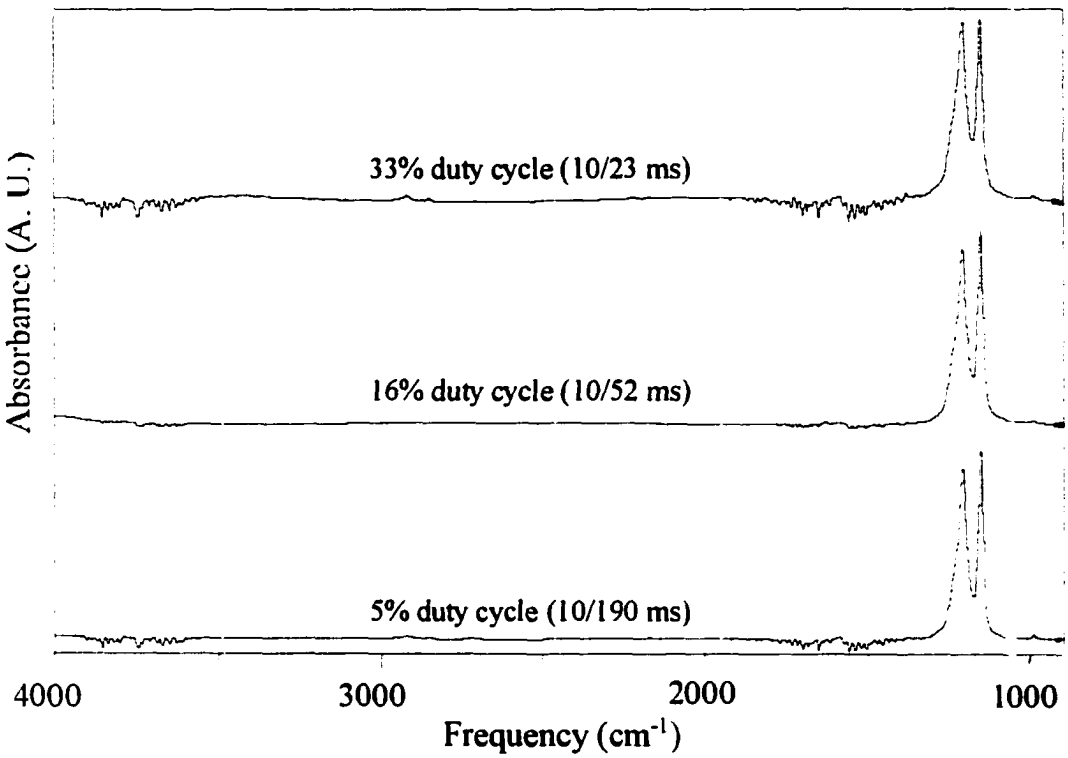


**Figure 3.7.** FTIR spectra of materials deposited at Position C in pulsed plasmas with pulse sequences of 10/190 msec (5% duty cycle), 10/52 msec (16% duty cycle), and 10/23 msec (33% duty cycle). The monomer gas pressure was 233 mtorr.

To investigate film composition as a function of sampling depth, materials generated at position C, in both a 25 W CW and a 16% duty cycle (10/52 ms) pulsed plasma were studied using two photoelectron take-off angles, 0° and 80°, Table 3.1. The use of a 0° photoelectron take-off angle provides information about the material composition ~90 Å deep, whereas at an 80° angle, only the outermost surface layers of the film are probed. The $C_{1s}$ analysis from these measurements is listed in Table 3.1. For the CW film, the 0° XPS data showed the approximate percentage of each species detected in the spectrum is 76 ± 0.5% $CF_2$ and 12 ± 0.7% $CF_3$. As the photoelectron takeoff angle is increased to 80°, these percentages change significantly. The uppermost surface layers contained 69 ± 1% $CF_2$ and 20 ± 0.9% $CF_3$. Similar behavior was also observed for the materials obtained using a 16% duty cycle pulsed plasma, Table 3.1. Here, the XPS data obtained at 0° indicate that the film contains 77 ± 0.4% $CF_2$ and 11 ± 0.5% $CF_3$. At 80°, XPS analysis revealed slightly lower $CF_2$ (72 ± 0.9%), but higher $CF_3$ content (14 ± 0.7%) for the outer most layers of the film.

We also investigated the composition of our films formed in the pulsed systems as a function of duty cycle and distance from rf coil, Table 3.2. Two significant trends are apparent from the XPS analysis of these materials. First, for each reactor position, A, B, or C, the use of higher duty cycle (shorter plasma off time) results in fluorocarbon materials with higher C-$CF_x$ content, but lower $CF_2$ content. The amount of $CF_3$ present in the films also increases with increasing duty cycle (decreasing off times). Second, the closer the substrate is placed to the rf glow, typically the higher the degree of unsaturation and $CF_3$ content in the film, and the lower the $CF_2$ content. The 50% duty cycle sample at position A does not follow some of these trends due to the presence of higher levels of

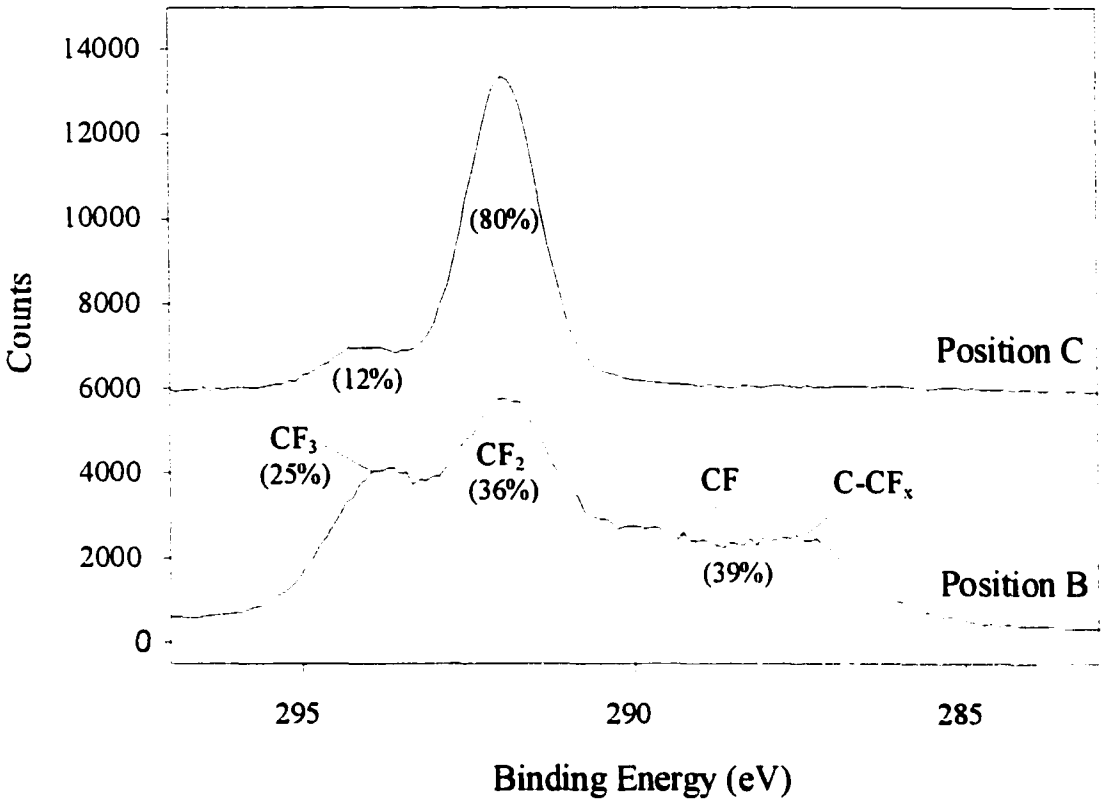


**Figure 3.8.** XPS $C_{1s}$ spectra for films deposited at positions B and C in a 25W CW plasma using a photoelectron take-off angle of 55°. Percent content for $CF_2$, $CF_3$ and C-$CF_x$ groups is shown.

glass and hydrocarbon contamination detected on this sample.

Table 3.3 shows the elemental composition for films generated in CW and pulsed HFPO plasmas as a function of distance from the rf coil. For materials obtained at position A in CW and high duty cycle pulsed systems, the highest amounts of Si and O are detected, indicating redeposition of $SiO_2$ etched from the walls of the glass reactor. This is consistent with what we observe in the FTIR spectra of these films. The Si and O content decreases with decreasing duty cycle. The most dramatic change in the F/C ratio with position occurs in the CW films. As the distance from the rf glow increases, the F/C ratio increases by a factor of 2. For the highest duty cycle (50%), a similar increase in F/C ratio is observed, Table 3.3. Although the same trend is observed in the 16% duty cycle data, the difference is much less pronounced. Interestingly, in the lowest duty cycle (5%) data, F/C=2.0 at all substrate positions.

### 3.2.3. SIMS AND NEXAFS ANALYSIS

SIMS and NEXAFS analyses were employed to further characterize the composition and structure of materials generated in CW and pulsed HFPO plasmas. Figure 3.9 shows the SIMS spectrum for a film deposited at position C in a 25 W CW plasma. The presence of $OC_nF_{2n+1}$ molecular ions is consistent with some oxygen incorporation in the films deposited at position C. This agrees well with the XPS data given in Table 3.3. Oxygen incorporation was not observed for downstream depositions when a nonoxygenated fluorocarbon monomer (i.e. TFE) was employed.[15] In the 1000 - 1800 amu region, the series of peaks separated by 50 amu correspond to $C_nF_{2n+1}$ molecular ions. The persistence of these mass peaks out to very high masses indicate the presence of

**Table 3.1.** Composition of fluorocarbon films deposited CW and pulsed HFPO plasmas.

| 25 W CW | $CF_2$ (%) | $CF_3$ (%) | Other (%) |
|---|---|---|---|
| 0 deg | 76 ± 0.5 | 12 ± 0.7 | 12 ± 0.6 |
| 80 deg | 69 ± 1 | 20 ± 0.9 | 11 ± 0.4 |
| **16 % duty cycle** | | | |
| 0 deg | 77 ± 0.4 | 11 ± 0.5 | 12 ± 0.5 |
| 80 deg | 72 ± 0.9 | 14 ± 0.7 | 16 ± 0.5 |

[a] All films were deposited at position C. Composition was determined by angle resolved XPS $C_{1s}$ analysis.

**Table 3.2.** Composition of fluorocarbon materials deposited in pulsed HFPO plasmas as a function of distance from rf coil[a]

| Duty cycle (%) | Position | $CF_3$ (%) | $CF_2$ (%) | CF (%) | CC (%) |
|---|---|---|---|---|---|
| 5 | A | 13.0 ± 0.8 | 76.6 ± 1.1 | 6.8 ± 0.4 | 3.6 ± 0.6 |
| | B | 14.8 ± 0.5 | 73.6 ± 0.6 | 6.1 ± 1.1 | 5.4 ± 1.0 |
| | C | 13.8 ± 1.2 | 86.2 ± 1.2 | 0.0 | 0.0 |
| 16 | A | 18.9 ± 1.4 | 35.8 ± 2.8 | 19.7 ± 0.5 | 25.7 ± 2.9 |
| | B | 18.4 ± 0.4 | 56.6 ± 0.5 | 13.4 ± 1.3 | 11.6 ± 1.1 |
| | C | 11.5 ± 0.3 | 75.8 ± 0.4 | 5.2 ± 1.0 | 7.5 ± 1.3 |
| 50 | A | 9.1 ± 0.4 | 13.6 ± 1.0 | 12.5 ± 2.4 | 64.8 ± 3.7 |
| | B | 21.4 ± 1.4 | 31.7 ± 1.6 | 19.4 ± 0.5 | 27.4 ± 0.6 |
| | C | 15.2 ± 1.0 | 51.3 ± 0.7 | 13.9 ± 0.3 | 19.5 ± 1.2 |

[a]Determined from $C_{1s}$ XPS analysis performed at a 55° take-off angle.

**Table 3.3.** Elemental composition for films deposited in CW and pulsed HFPO plasmas at positions A, B and C as determined by XPS analysis.[a]

| | C(1s) | F(1s) | O(1s) | Si(2s) | F/C |
|---|---|---|---|---|---|
| **25 W CW** | | | | | |
| Position A | 28.6 ± 0.7 | 29.3 ± 0.4 | 15.2 ± 0.2 | 26.9 ± 0.7 | 1.0 |
| Position B | 36.5 ± 0.1 | 62.3 ± 0.2 | 1.2 ± 0.2 | 0.0 | 1.7 |
| Position C | 32.3 ± 0.9 | 63.4 ± 0.6 | 1.9 ± 0.4 | 2.3 ± 0.2 | 2.0 |
| **5 % duty cycle** | | | | | |
| Position A | 33.3 ± 0.2 | 66.7 ± 0.2 | 0.0 | 0.0 | 2.0 |
| Position B | 33.6 ± 0.5 | 66.4 ± 0.0 | 0.0 | 0.0 | 2.0 |
| Position C | 33.0 ± 0.6 | 66.7 ± 1.1 | 0.3 ± 0.5 | 0.0 | 2.0 |
| **16 % duty cycle** | | | | | |
| Position A | 39.8 ± 0.7 | 58.0 ± 1.3 | 1.8 ± 0.7 | 0.3 ± 0.5 | 1.5 |
| Position B | 34.9 ± 0.5 | 64.8 ± 0.1 | 0.3 ± 0.4 | 0.0 | 1.9 |
| Position C | 33.3 ± 0.2 | 66.4 ± 0.7 | 0.3 ± 0.5 | 0.0 | 2.0 |
| **50 % duty cycle** | | | | | |
| Position A | 40.1 ± 1.8 | 35.8 ± 1.5 | 9.1 ± 0.7 | 9.1 ± 0.1 | 0.9 |
| Position B | 36.0 ± 0.5 | 62.6 ± 0.6 | 1.4 ± 0.2 | 0.0 | 1.7 |
| Position C | 35.9 ± 0.3 | 62.3 ± 0.3 | 1.8 ± 0.0 | 0.0 | 1.7 |

[a]Determined from XPS analysis performed at a 55° take-off angle.

long $CF_2$ chains in our films. For comparison, the films produced by Castner and coworkers showed a similar trend, with molecular ions corresponding to additions of $CF_2$ units up to at least 250 amu.[15] One important note is that since the secondary ion yield for $OC_nF_{2n+1}$ can be significantly different than that for $C_nF_{2n+1}$, the relative intensities of the fragment signals are not indicative of the relative concentrations of the two species.

To determine the orientation of these chains with respect to the substrate surface, NEXAFS analysis was employed. Figure 3.10a shows the NEXAFS spectra of a film deposited in a 25 W CW plasma at position B. Data obtained at 20° (grazing) and 90° (normal) incidence angles is presented. Absorption features assigned to transitions of C-F (292 eV and 298 eV) and C-C (295 eV) core electrons to $\sigma^*$ orbitals are observed. There is no difference in the intensity of these features between the 20° and 90° spectra, indicating no particular orientation of the C-F and C-C bonds. Similar behavior is observed for films deposited at position A. In contrast, for films deposited at position C, Fig. 3.10b, the intensity of the C-F absorption bands decreases as the angle between the substrate and X-ray beam changes from 90° to 20°. This type of decrease is consistent with C-F bonds oriented parallel to the substrate surface. In contrast, the C-C peak intensity is lowest when the X-ray is perpendicular to the film surface, showing that the helical axis of the C-C backbone is perpendicular to the C-F bonds in the film. These NEXAFS results, along with the SIMS data indicate that the fluoropolymers deposited at position C comprise long $CF_2$ chains which are oriented normal to the substrate surface. Clearly, long $CF_2$ chains are also deposited at the other positions, but the perpendicular orientation of the chains is observed only in the films deposited at position C.

Similar $CF_2$ chain orientation dependence on distance from rf glow occurs with

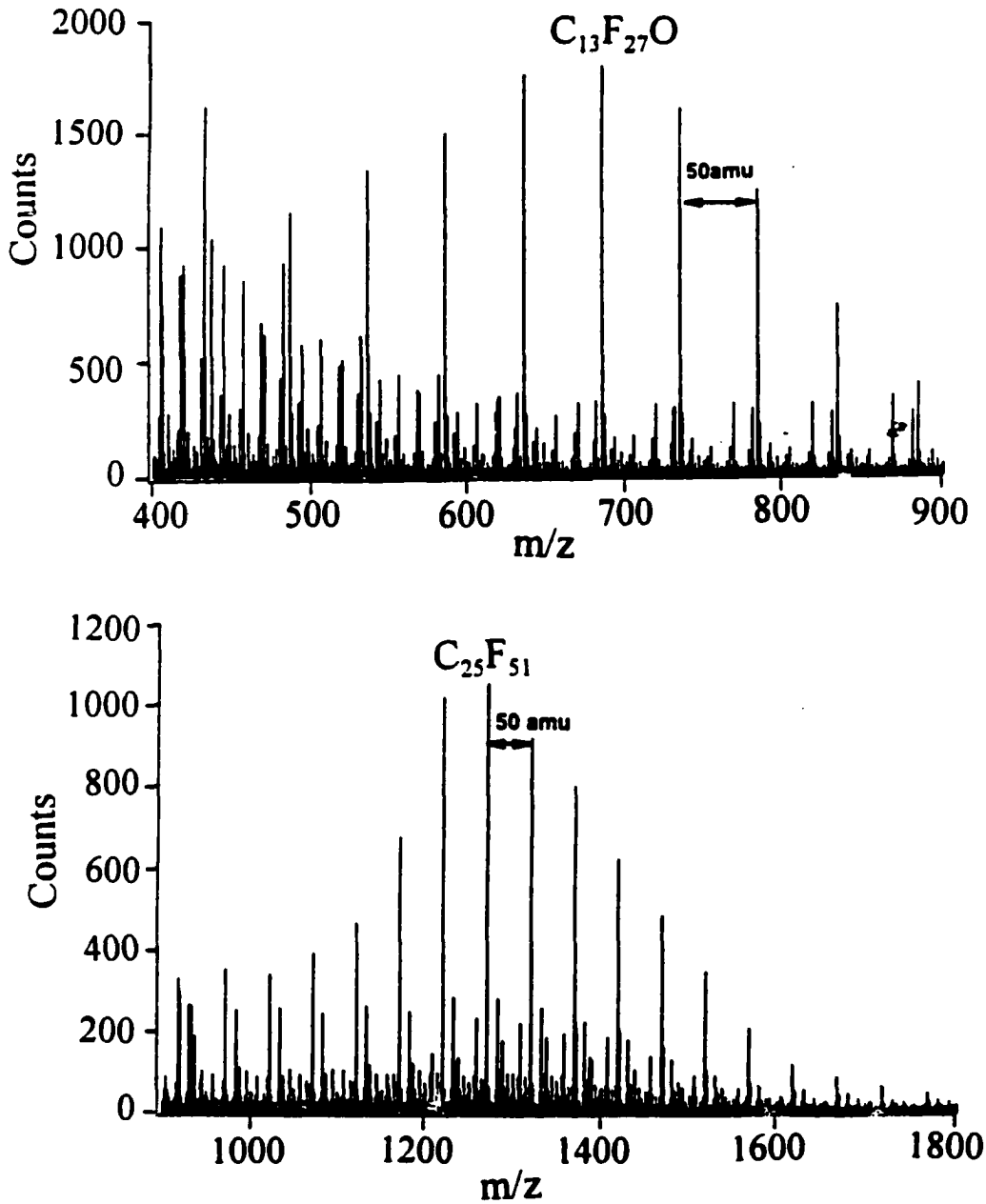


**Figure 3.9.** SIMS spectrum for the fluoropolymer deposited at position C in a 25W CW system.

films deposited in pulsed HFPO plasmas. Films obtained at position C contain chains which are perpendicular to the substrate surface while those generated at positions A and B show very little or no particular orientation. The effect of duty cycle on film structure was also studied. The difference in 20° and 90° NEXAFS peak intensity is largest in Fig. 3.11 which corresponds to a film produced in a 5% duty cycle plasma system. No particular orientation of the 50% duty cycle film was observed at position B, but a small degree of orientation was detected for the 16% and 5% duty cycle films at position B. These data demonstrate that materials deposited at position C have the highest degree of order for the lowest duty cycle, 5% (10/190 ms). As the duty cycle increases to 16% (10/52 ms) and 50% (10/23 ms), Figs. 3.12 and 3.13, respectively, this difference decreases. Thus, a lower degree of $CF_2$ chain ordering is observed as the plasma off time decreases (duty cycle increases).

### 3.2.4. CONTACT ANGLE MEASUREMENTS

To determine the wettability of film surfaces, static contact angles were measured for materials deposited at positions B and C in CW plasmas with different applied rf powers, Fig. 3.12. At applied powers ≥60 W, the contact angles of films generated at position C are nearly identical to those deposited at position B. All films deposited at rf powers <60 W are hydrophobic (contact angles of 105-117°), but those deposited far downstream, at position C, have higher contact angles than the films deposited at position B. These data support the XPS analysis findings, because the higher hydrophobicity of films generated at position C is likely caused by increased $CF_3$ incorporation at the film surface. Indeed, $CF_3$ moieties have been shown to contribute to the hydrophobicity of

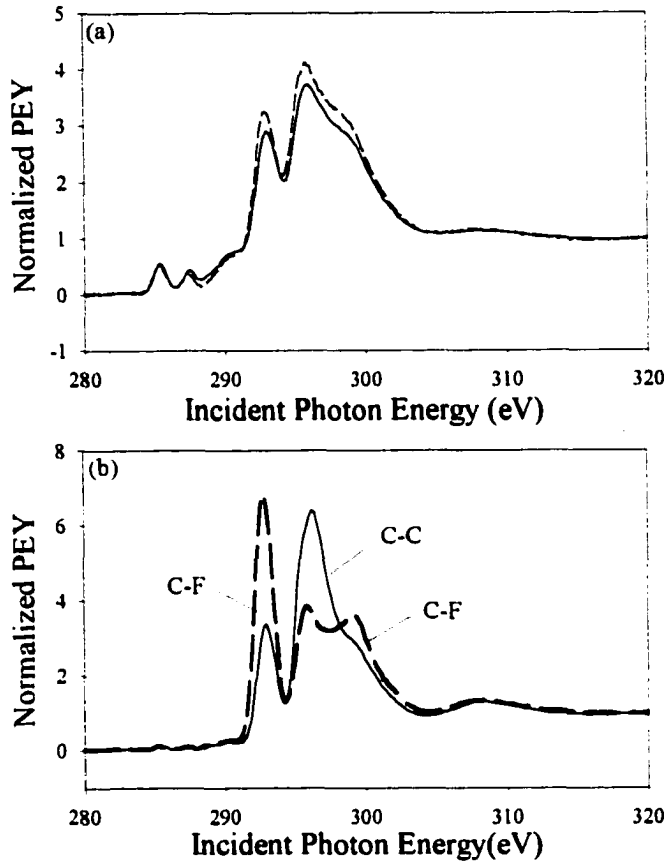


**Figure 3.10.** NEXAFS spectra for films deposited at (a) Position B and (b) Position C in a 25 W CW plasma. Results for two X-ray angles of incidence are shown: 20° (solid line) and 90° (dashed line)

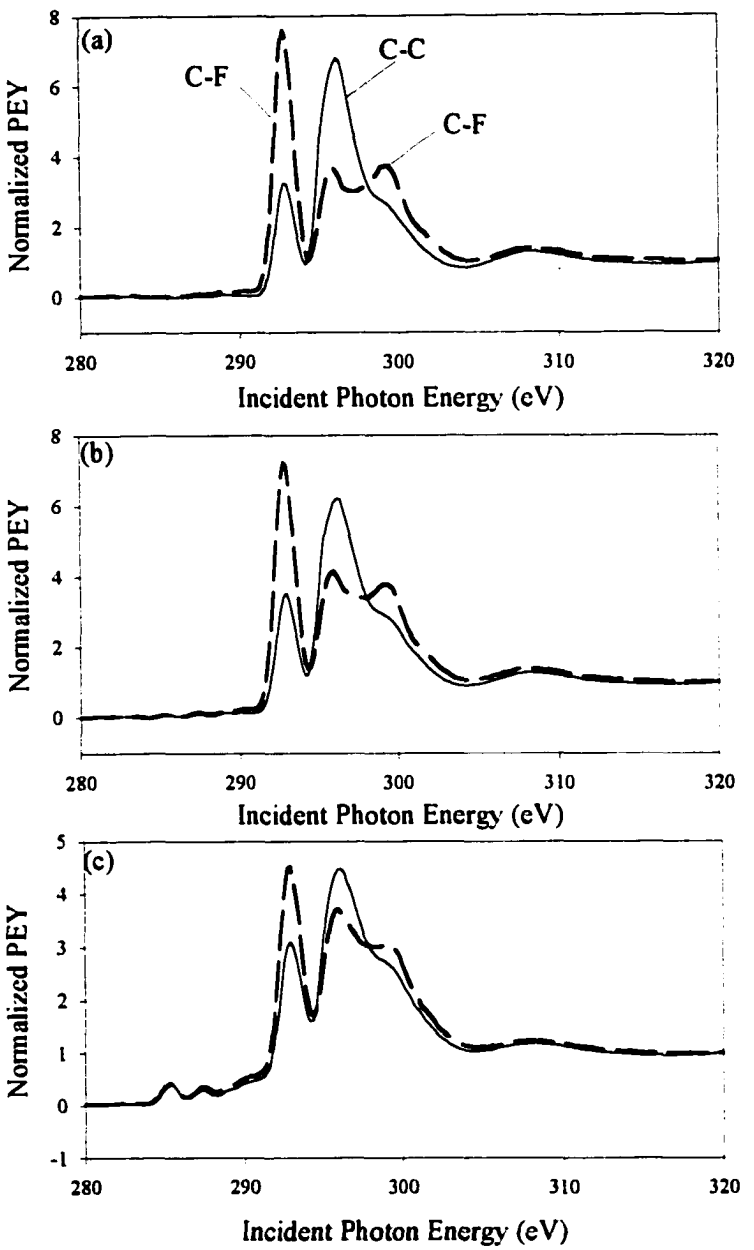


**Figure 3.11.** NEXAFS spectra for films deposited at Position C in pulsed plasmas with duty cycles of (a) 5%; (b) 16%; and (c) 50%. The angles of incidence were 20° (solid line) and 90° (dotted line).

fluorinated films.[23]

Contact angles were also measured for fluorocarbon materials deposited in pulsed plasmas at duty cycles ranging from 2% to 50%, Fig. 3.13. At low duty cycles, when the plasma is off for long times, no difference in contact angle is observed for films generated at positions B and C. However, position C films are more hydrophobic than position B materials when duty cycles >5% are employed. As with the CW films, this is likely due to more surface $CF_3$ incorporation in films deposited at position C relative to position B.

### 3.2.5. DEPOSITION RATES

Table 3.4 lists the deposition rates measured for materials generated in a 25 W CW plasma at positions B and C. A relatively high deposition rate of 30 Å/min is observed at position B compared to the 1.6 Å/min observed at position C. For comparison we also measured deposition rates in pulsed plasma systems. As shown in Table 3.4, these deposition rates are higher for materials generated at both positions B and C, relative to what was observed for CW systems. Indeed, at position C, there is an order of magnitude increase in the deposition rate for the 16% duty cycle pulsed system compared to the 25 W CW system. Also important to note, deposition rates are higher closer to the glow under all plasma conditions (CW and pulsed).

### 3.2.6. SEM AND AFM IMAGING.

We have investigated the mechanical flexibility of the fluorocarbon films deposited in HFPO plasmas by coating a 200 $\mu$m copper wire placed at position C under both CW and pulsed conditions. In Fig. 3.14a the SEM image of a wire coated in a 5% duty cycle

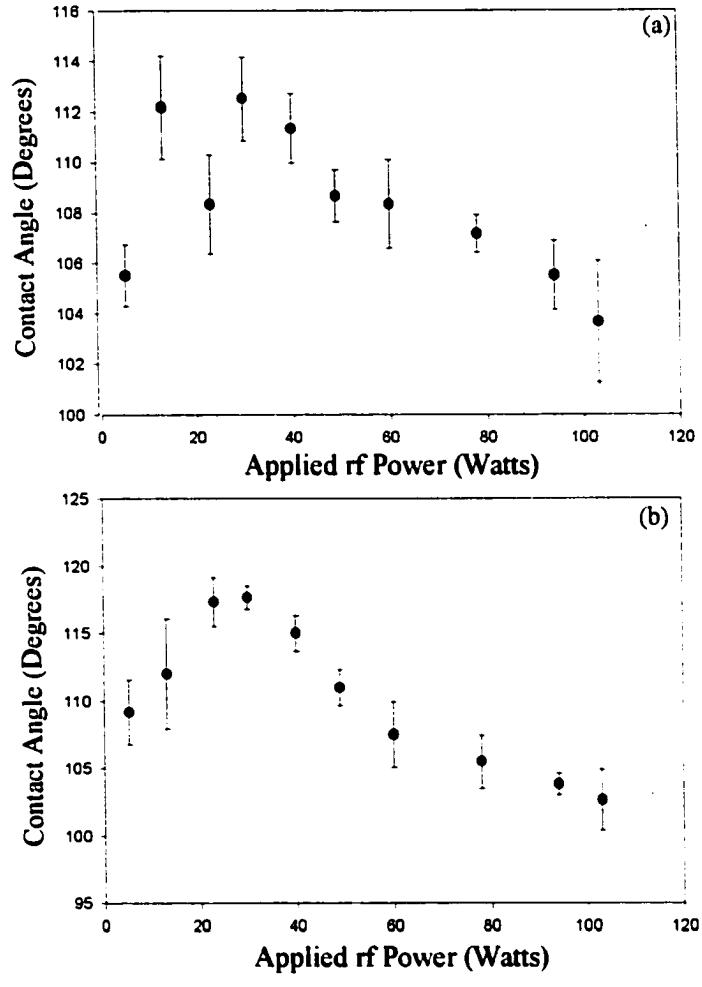


**Figure 3.12.** Dependence of the static contact angle on applied rf power for films deposited in CW plasmas at (a) Position B and (b) Position C. The monomer gas pressure was 233 mtorr.

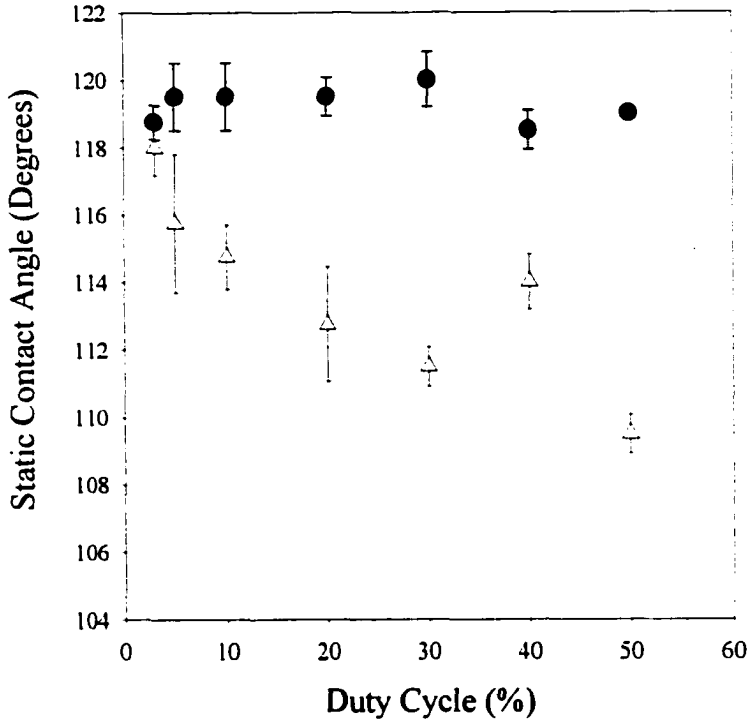


**Figure 3.13.** Dependence of the static contact angle on duty cycle for films deposited in pulsed plasmas at Position B (open triangles) and Position C (closed circles). The monomer gas pressure was 233 mtorr.

pulsed plasma shows a very smooth film. Figure 3.14b displays the same wire after it has been bent in a loop ~0.5 cm in diameter. No significant cracking of the fluorocarbon coat is observed, suggesting that the material has a high degree of flexibility. Figure 3.14c shows a similar wire that was coated in a 25 W CW plasma and bent into a loop. Just as for the film produced under pulsed conditions, bending does not result in any noticeable film deterioration.

AFM imaging was used to determine the surface rms roughness for materials deposited in CW and pulsed HFPO plasmas at positions A, B, and C. Values ranged from 2 nm to 20 nm, comparable to the 0.88-31.7 nm range reported by Gleason and coworkers.[24] For Gleason's materials, the lowest rms roughness of 0.88 nm was measured for materials deposited at the highest duty cycle of 33%, while a 31.7 nm value was reported for films generated at the lowest duty cycle, 4.8%. We did not observe trends similar to these, likely due to the differences in design between the two experimental apparatus.

## 3.3. DISCUSSION

The goal of the present work was to identify the optimal conditions for obtaining highly ordered films with high $CF_2$ content as well as to compare the structure and composition of films obtained under CW and pulsed HFPO plasma conditions. Despite the extensive study of pulsed HFPO plasmas, the CW regime has not been fully investigated. Our results show that under the appropriate experimental conditions, fluorocarbon materials generated in CW systems display attributes virtually identical to those of films produced in pulsed plasmas. In this work, we show that films deposited far

**Table 3.4.** Film deposition rates (Å/min) in CW and pulsed HFPO plasmas.

| | **Position B** | **Position C** |
|---|---|---|
| 25 W CW | 7 ± 1 | 1.6 ± 0.3 |
| 16 % duty cycle | 50 ± 5 | 17 ± 3 |
| 50 % duty cycle | 183 ± 8 | 52 ± 3 |

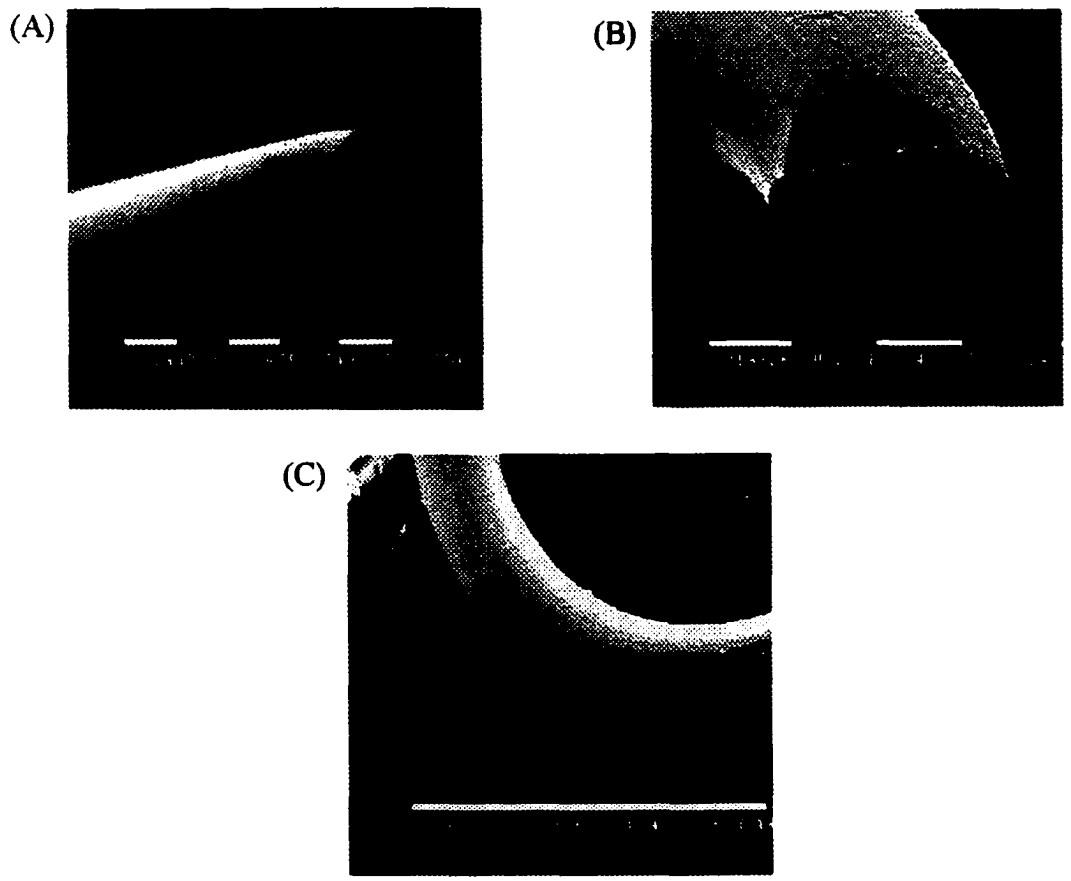


**Figure 3.14.** (a) Scanning electron micrograph of film deposited on 200 $\mu$m diameter Cu wire placed at position C in a 5% duty cycle pulsed plasma (magnification x143). (b) Scanning electron micrograph of the same wire after being tied in a loop (magnification x231). (c) Scanning electron micrograph of film deposited on 200 $\mu$m diameter Cu wire placed at position C in a 25 W CW plasma (magnification x89).

downstream from the rf glow (Position C), under both CW and pulsed conditions, have the lowest degree of cross-linking and are the least amorphous. This is demonstrated convincingly by the FTIR spectra, Figs. 3.1-3.7, which contain clearly separated asymmetric and symmetric stretching bands and no other features. Moreover, these compositional attributes correlate well with XPS data which show that materials generated at position C also have the highest $CF_2$ content and F/C ratios, Tables 3.1-3.3. Position C films also contain long $CF_2$ chains, as demonstrated by the SIMS data of Fig. 3.9, which display a pronounced orientation, as determined via NEXAFS experiments. The following discussion highlights and interprets the major trends observed from our extensive parameter study and analysis.

The two experimental parameters that primarily control the type of material obtained in CW HFPO rf glows are distance from the rf coil and applied rf power. Gleason and coworkers did explore CW power dependence in a parallel plate system but generated only amorphous films.[20] Materials generated in the glow of our CW HFPO plasmas are similar to those reported by Gleason. Unlike previous researchers, however, we have also explored the dependence of film composition as a function of distance from the HFPO plasma rf glow. While we were the first to perform distance dependence studies for materials generated in HFPO plasmas, other researchers have investigated distance effects on the composition of films generated in TFE plasma systems. Castner and coworkers found that materials deposited 10-30 cm downstream with CW rf powers $< 10$ W contained a high $CF_2$ content (~90 %), and a high degree of orientation.[9] Conversely, films generated in the rf glow comprised significantly more $CF_3$ as well as CF

groups.

Similar to Castner's results with TFE, we also discovered that the position of the substrate relative to the visible glow plays a very significant role in the type of material obtained in HFPO plasma systems. For depositions performed at position B and rf powers > 50 W, etching of the glass reactor walls occurs as indicated by the intense SiO peak (~1100 $cm^{-1}$) present in the FTIR spectrum shown in Fig. 3.1. In contrast, materials generated at position C have IR spectra in which the dominant feature is the 1200 $cm^{-1}$ band corresponding to $CF_x$ stretches, Fig. 3.2. At lower rf powers (15 W, 30 W), however, no sign of reactor etching is observed for position B films, while position C materials have a low degree of cross-linking and high $CF_2$ content, Figs. 3.1 and 3.2, respectively. The composition dependence on distance from the rf glow is not surprising when one considers that many of the energetic species in the plasma, which are primarily responsible for etching and cross-linking, decay before reaching a substrate placed far downstream.[9]

The pressure dependence of the films obtained at an applied rf power of 30 W CW is also very interesting, Fig. 3.3. At low pressures, the fluorocarbon films generated at position B are highly amorphous as indicated by the broad IR absorbance band at 1200 $cm^{-1}$. At higher HFPO pressures, however, the separation between the $CF_2$ symmetric and asymmetric IR bands is consistent with a less amorphous fluoropolymer, similar to that deposited at position C. Increasing the pressure has a dual effect on the rf glow: both electron energy and particle mean free path decrease.[8] Both of these effects serve to decrease the amount of UV radiation reaching the deposited fluoropolymer

because most excited state neutral species, which fluoresce in the UV, are created through collisions with electrons. As the electron energy decreases, the number of excited state neutrals formed decreases. Likewise, as the mean free path decreases, energy transfer occurs preferentially through molecule-molecule collisions, rather than through radiative decay (emission). In addition, as the electron energy decreases, fewer ions are formed. Those ions that are created through electron impact will have less energy than the ones formed at lower pressures (higher electron energies). Thus, at higher pressures, plasma polymerized fluorocarbon films generated at position B do not undergo as much bombardment from energetic particles as they do at lower pressures. This is also consistent with the lack of pressure dependence observed for the composition of films generated at position C, where most energetic species have already undergone recombination reactions.

Energetic charged species are directly shown to influence the degree of film amorphousness by the FTIR spectra displayed in Fig. 3.15. Films were generated 9.5 cm downstream from the rf coil in a 25 W CW plasma with a pair of Cu deflector plates located immediately upstream from the substrate.[25] Figure 3.15a shows the IR spectrum of a material deposited when the deflector plates were not charged. A broad absorption band corresponding to $CF_2$ vibrations is present at ~1200 $cm^{-1}$, suggesting the material is amorphous. Figure 3.15b shows the IR spectrum for a film generated when one deflector plate was biased at +200 VDC while the other was grounded. The electric field thus created prevents charged species from colliding with the substrate surface. A distinct separation between the symmetric and asymmetric $CF_2$ IR absorbance bands is observed

for materials deposited under biasing conditions, similar to what was observed for films deposited at reactor position C. The separation is not as dramatic, however, due to the presence of energetic neutral species and UV light, which are not deflected by the charged plates. The difference between the IR spectra displayed in Figs. 3.15a and 3.15b constitutes direct evidence that charged species bombardment is primarily responsible for the formation of highly amorphous and cross-linked materials at position B.

Similar to the CW system, there are two main experimental variables that affect film composition in pulsed HFPO plasmas: duty cycle and distance from glow. Fluorocarbon polymers deposited at position C in pulsed HFPO plasmas have higher $CF_2$ content and a higher degree of $CF_2$ chain orientation than materials generated at positions A and B, Table 3.2. Etching of the glass reactor walls occurs at duty cycles >5% at position A, Fig. 3.5 and Table 3.3. As the duty cycle increases, however, the $CF_2$ content decreases and the orientation of film chains becomes less distinct in materials deposited at position C, Table 3.2 and Fig. 3.11. Pulsed plasma dynamics studies show that during the on-time period radicals and charged species are created, followed by the rapid decay of short lived ionic fragments during the off-time of the pulse sequence.[26,27] The effect of energetic species on film composition and structure is significantly reduced at all reactor positions because the plasma is pulsed. With a constant on time, lower pulse duty cycles (longer off times) provide longer time for deposition to occur unhindered by charged

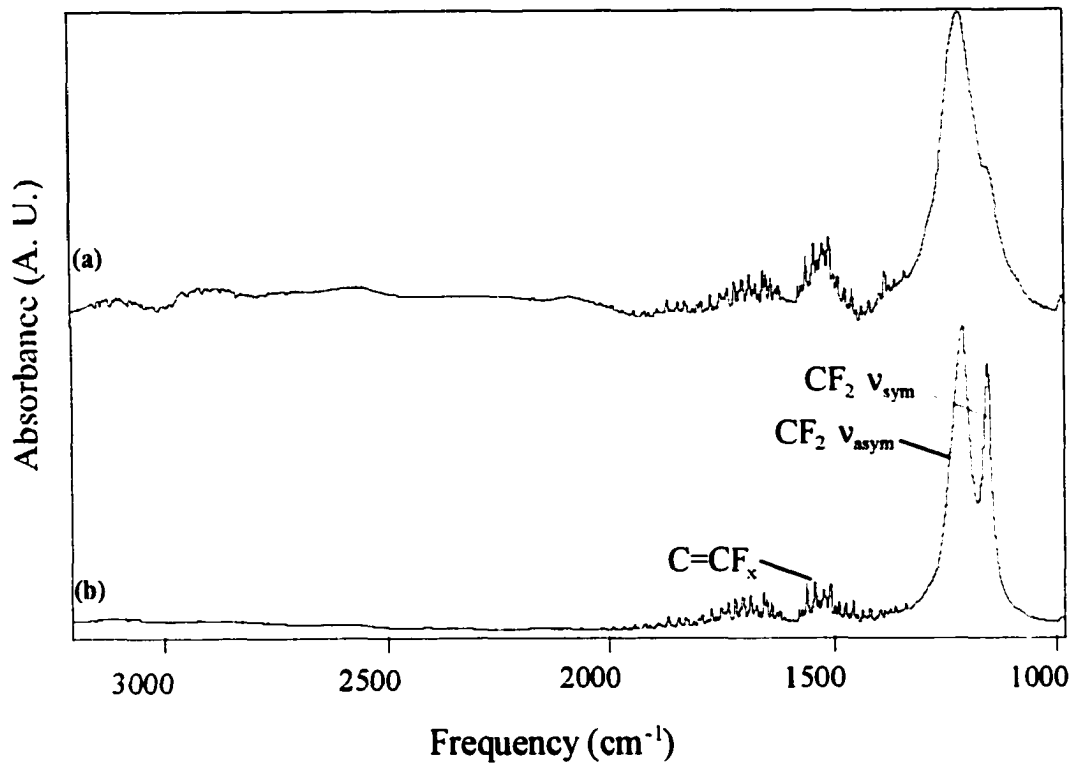


**Figure 3.15.** (a) FTIR spectrum for film deposited 9.5 cm downstream from the rf coil with deflector plates inserted in plasma chamber upstream from the substrate but not charged. This allows charged species to reach the substrate surface. (b) FTIR spectrum for film deposited at the same location with one of the deflector plates charged at +200 VDC and the other grounded. This prohibits charged species from colliding with the substrate surface.

species effects. In addition, lower duty cycles also mean lower equivalent power applied to the plasma. Indeed, as the duty cycle increases from 5% to 33%, the CW equivalent power rises from 15 W to 100 W. In a 100 W CW plasma, fluorocarbon film deposition occurs only at position C. In contrast, for the 33% duty cycle system (100 W equivalent CW power) fluorocarbon film deposition occurs at both position B and position C. One additional note is that at higher duty cycles, we observe a more marked dependence of film composition on reactor position, Tables 3.2 and 3.3.

Angle resolved XPS analysis results correlate well with the FTIR data and also provide additional information about composition differences between film surface and bulk. All the materials whose IR spectra did not contain features associated with cross-linked groups, had the highest $CF_2$ content and F/C ratios according to XPS data. XPS analysis also showed that for materials deposited at position C under CW conditions, the $CF_2/CF_3$ ratio changed from 3.5 to 6.3 when the sampling depth increased from ~20 Å to ~90 Å (photoelectron take-off angle changed from 80° to 0°). Likewise, the $CF_2/CF_3$ ratio for films generated at position C in a 16% duty cycle pulsed plasma changed from 5.2 for surface layers to 7.2 for film bulk at 0°. These changes suggest that the films deposited at position C in both systems have $CF_3$ enriched surfaces. This conclusion is further supported by static contact angle measurements which show that the surfaces of materials generated at position C are more hydrophobic than those at position B. The angle resolved XPS, and contact angle measurement information also agrees with the findings of static SIMS analysis. The former two show that position C films have $CF_3$ enriched surfaces, which indicates that the molecular ions of the form $C_nF_{2n+1}$ detected in

the SIMS spectrum are very likely to correspond to $(CF_2)_nCF_3$ moieties in the film. Similar conclusions were drawn by Castner and coworkers in regard to fluorocarbon materials obtained downstream from TFE plasmas. The same progression of molecular ions was observed and interpreted to indicate the presence of $(CF_2)_nCF_3$ chains.[15]

Another intriguing characteristic of the films deposited at position C is the high degree of orientation of the $CF_2$ chains observed for both CW and pulsed HFPO plasmas. Unlike PTFE, in which the $CF_2$ strands are parallel to the film surface,[15] fluorocarbon films deposited in our HFPO CW and pulsed systems at position C contain $CF_2$ chains perpendicular to the substrate surface. This is only the second plasma system for which this type of orientation is seen in the fluorocarbon materials generated.[15] One likely explanation for the perpendicular orientation of the $CF_2$ chains is the higher stability of the C-C (144 kcal/mol) bond relative to a C-Si (104 kcal/mol) bond.[28] This difference could lead to preferential C-C bond formation, once a carbon chain has been created on the underlying Si substrate. In contrast, the films deposited upstream do not have preferential orientation, most likely as a result of higher levels of ion and electron bombardment which lead to higher densities of chain nucleation sites.

Given the structural and compositional similarities between materials deposited in our CW and pulsed HFPO plasmas at position C, we also investigated how their flexibility compares under mechanical stress. SEM images indicate that our films are flexible enough not to crack under the stress of bending a coated wire into a loop of ~ 0.5 cm in diameter, Fig. 3.14. This is the first time a high degree of flexibility was observed for films obtained in HFPO plasmas under CW conditions. Gleason and coworkers generated flexible

materials in a 2.4% (10/400 ms) duty cycle pulsed HFPO plasmas, but their CW films were found to crack under bending stress.[29] The difference between our CW films generated at position C and the ones studied by Gleason is that the latter were deposited at high power densities in the rf glow of a parallel plate reactor. Gleason's previous research has shown that at high rf power, HFPO PECVD produces highly cross-linked materials which are less robust against mechanical stress than films with low degree of cross-linking.[20] Our films deposited at position C in a 25 W CW system contain virtually no cross-linked groups explaining their high degree of flexibility.

## 3.4. SUMMARY

PECVD using fluorocarbon systems is an extremely valuable technique in the quest for improved vapor deposited fluoropolymers. This study shows that HFPO plasmas can be employed to produce materials with high $CF_2$ content and low degrees of cross-linking. In addition, our results demonstrate that pulsing the HFPO plasma is not the only route to obtaining such films. CW downstream depositions produced similar high quality films. Note that the films generated in HFPO plasmas, similar to those seen in TFE systems, are not teflon-like in structure. PTFE contains $CF_2$ moieties linked parallel to substrate surfaces, whereas the materials we deposit comprise vertically oriented $CF_2$ chains which are terminated in $CF_3$ groups. However, only films obtained at the longest distance from the plasma glow display a high degree of orientation. As observed in other plasma systems, the energetic charged species produced in the rf plasma play a crucial role in the structure and composition of the materials generated. We conclude that with low rf

powers, far downstream depositions are virtually free of undesired energetic species bombardment effects simply because these species are lost through plasma recombination processes prior to reaching a substrate. A similar result is obtained for pulsing the HFPO plasmas despite the 300 W applied power because charged species rapidly decay during the time off period of the pulse sequence. Further investigations of gas-phase species in the HFPO system are presented in Chapter 5.

## 3.5. REFERENCES


1. H. Yasuda, T. Hsu, *J. Polym. Sci., Polym. Chem. Ed.* **1977**, *15*, 81-87.

2. C. L. Rinsch, X. Chen, V. Panchalingam, R. C. Eberhart, J. H. Wang, R. B. Timmons, *Langmuir* **12,** 2995 (1996).

3. C. R. Savage, R. B. Timmons, J. W. Lin, in Structure-Property Relations in Polymers; Advances in Chemistry Series 236, American Chemical Society: Washington D.C., 1993, p.745.

4. N. M. Mackie, D. G. Castner, E. R. Fisher, *Langmuir* **14,** 1227 (1998); N. M. Mackie, E. R. Fisher., *Polym. Prepr.* **38**, 1059 (1997); M. A. Leich, N. M. Mackie, K. L. Williams, E. R. Fisher, *Macromolecules* **31**, 7618 (1998); A. E. Lefohn, N. M. Mackie, E. R. Fisher, *Plasmas Polym.* **4**, 197 (1998).

5. V. Panchalingam, X. Chen, C. R. Savage, R. B. Timmons, R. C. Eberhart, *J. Appl. Polym. Sci., Polym. Symp.* **54**, 123 (1994).

6. H. Yasuda, *Plasma Polymerization*; Academic Press: Orlando, 1985.

7. N. M. Mackie, N. F. Dalleska, D. G. Castner, E. R. Fisher, *Chem. Mater.* **9**, 349 (1997).

8. *Plasma Deposition, Treatment and Etching of Polymers*; d'Agostino R., Ed.; Academic Press: Boston, 1990.

9. D. G. Castner, in *Plasma Processing of Polymers*, R. d'Agostino, P. Favia, F. Fracassi, Eds.; Kluwer Academic Publishers: Dordrecht, The Netherlands, 1997, pp. 221-230.

10. D. F. O'Kane, D. Rice, W. *J. Macromol. Sci. Chem. A* **10**, 567 (1976).

11. H. Yasuda, *J. Polym. Sci. Macromol. Rev.* **16**, 199 (1981).

12. P. Singer, *Semiconduct. Int.*, May, 88 (1996).

13. J. L. Bohnert, B. C. Fowler, T. A. Horbett, A. S. Hoffman, *J. Biomat. Sci:Poly. Ed.* **1**, 270 (1990).

14. Kiaei, D.; Hoffman, A. S.; Horbett, T. A. *J. Biomat. Sci.: Poly. Ed.* **1992**, *4*, 35.

15. D. G. Castner, K. B. Lewis, D. A. Fischer, B. D. Ratner, J. L. Gland, *Langmuir* **9**, 537 (1993).

16. K. Endo, T. Tatsumi, *Appl. Phys. Lett.* **68**, 2864 (1996).

17. W. W. Lee, P. S. Ho, *MRS Bull.* **22**, 19 (1997).

18. A. S. Hoffman, *J. Appl. Polym. Sci; Appl. Polym. Symp.* **42**, 251 (1988).

19. C. R. Savage, R. B. Timmons, *Chem. Mater.* **3**, 575 (1991).

20. S. J. Limb, D. J. Edell, E. F. Gleason, K. K. Gleason,. *J. Appl. Polym. Sci.* **67**, 1489 (1998).

21. C. I. Butoi, N. M. Mackie, J. E. Barnd, E. R. Fisher, L. J. Gamble, D. G. Castner, *Chem. Mater.* **11**, 862 (1999).

22. J. Seth, S. V. Babu, *Thin Solid Films* **230**, 90 (1993).

23. R. d'Agostino, F. Cramarossa, F. Fracassi, F. Illuzzi, *In Plasma Deposition, Treatment and Etching of Polymers*; Academic Press: San Diego, pp. 95-162 (1990).

24. C. B. Labelle, K. K. Gleason, *J. Appl. Polym. Sci.* **74**, 2439 (1999).

25. This location is essentially the same as position B used in other experiments.

26. S. Lin, C. Liao, R. Liang, *Polym. J.* **27**, 201 (1995).

27. J. P. Booth, G. Hancock, N. D. Perry, M. J. Toogood, *J. Appl. Phys.* **66**, 5251 (1989).

28. *CRC Handbook of Chemistry and Physics*, R. C. Weast, and S. M. Selby, Eds.; The Chemical Rubber Co., Cleveland, p. F-130 (1966).

29. S. J. Limb, K. K. Gleason, D. J. Edell, E. F. Gleason, *J. Vac. Sci. Technol. A* **15**, 1814 (1997).

# CHAPTER 4

## EXPERIMENTAL METHODS FOR THE IMAGING OF RADICALS INTERACTING WITH SURFACES

This dissertation chapter describes the methods used to obtain information on plasma radicals as they interact with substrate surfaces *during* plasma processing. The components of the imaging of radicals interacting with surfaces (IRIS) apparatus are described in the first part of the chapter. The second part describes data analysis methods for both radical reactivity and velocity profiling. In addition, IRIS experimental details are given for both $CF_2$ and $NH_2$ radicals. The interactions of these radicals with different substrate materials are discussed in depth in Chapters 5 and 6.

## 4.1. INTRODUCTION

The imaging of radicals interacting with surfaces (IRIS) technique used in our laboratories directly measures the steady-state surface reactivity of a gas-phase species during plasma processing of a substrate.[1] IRIS combines molecular beam and plasma technologies with laser induced fluorescence (LIF) to provide spatially-resolved 2D images of radical species. A schematic of the IRIS apparatus is shown in Figure 4.1. In a typical IRIS experiment, feed gases enter the glass reactor tube, rf power is applied and a plasma is produced as discussed in Chapter 2. Expansion of the plasma generates an effusive molecular beam consisting of virtually all species present in the plasma, including the species of interest.[2] A tunable laser beam intersects the molecular beam downstream from the plasma source and excites the species of choice. Spatially resolved LIF signals are collected by a gated, intensified charge coupled device (ICCD). The substrate of choice is rotated into the path of the molecular beam and LIF signals are again collected. Differences between spatial distributions with the surface in and out of the path of the molecular beam are used to measure the amount of scattering, or surface reactivity, for a particular radical.

## 4.2. VACUUM SYSTEM

The vacuum system contains three different pumping regions: (1) the glow discharge region; (2) the differentially pumped region; and (3) the chamber region. The existence of the middle, differentially pumped region is necessary to achieve the transition between the relatively high pressures required to sustain the plasma in region (1)

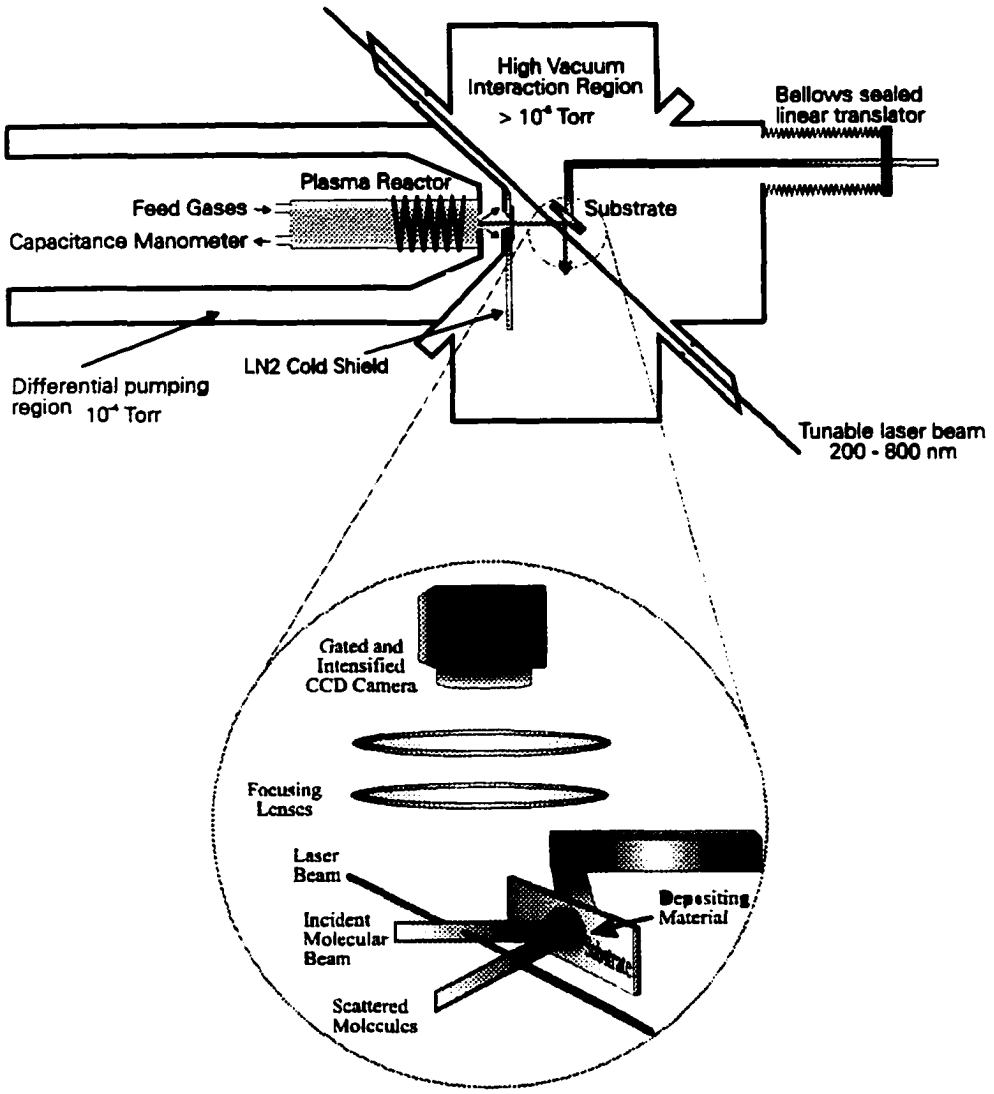


**Figure 4.1.** Schematic of the IRIS apparatus. In the upper part of the figure the schematic shows a transversal cross-section of the apparatus. In the lower part, an expanded view of the interaction region illustrates the relative locations of the substrate holder, the collimating and focusing lenses and the ICCD camera. Specular scattering of radicals is also illustrated.

and the low pressures needed in the interaction region to obtain spatial resolution.

The glow discharge region is pumped by a Varian HS-10 diffusion pump (4200 $Ls^{-1}$) which is backed by a Leybold D30A mechanical pump (12.6 $Ls^{-1}$). The pressure in the reactor is monitored with an MKS baratron connected to the rear of the reactor with an ultra-torr fitting. The differentially pumped region is evacuated with the same diffusion pump discussed above through a 10" opening provided by opening a manually operated gate valve. The volume of region (2) is equal to 19 L. The main chamber contains the interaction region where the substrate and a nearly effusive molecular beam intersect. The nearly effusive molecular beam is generated when the plasma created in region (1) passes through a pair of collimating slits, located immediately after the 1 cm diameter orifice which joins regions (1) and (2). Pumping is done with a Varian HS-10 diffusion pump through a 10" opening located between the pump and the main chamber.

## 4.3. LASER SYSTEM AND FLUORESCENCE DETECTION

To excite fluorescence for the radical of interest, an excimer (XeCl, 100 mJ/pulse, 100 Hz) pumped dye laser is used to provide monochromatic tunable light. The excimer laser is operated at 100 Hz and generates 100 mJ/pulse 308 nm light. The dye laser has frequency doubling capabilities when $\lambda < 308$ nm is necessary. Light with the desired wavelength is guided to the chamber by a series of silica prisms. The excitation laser beam enters the chamber through a quartz Brewster window, and intersects the nearly effusive plasma molecular beam at a 45° angle in the interaction region.

A gated Princeton Instruments intensified charge-coupled device (ICCD) camera

located directly above the interaction region is used to detect fluorescence and to obtain spatially resolved information. The camera is equipped with a microchannel plate image intensifier, and also with UV and IR enhancement coatings. During data collection the ICCD camera is cooled to -37°C and purged with 4.8 grade $N_2$ gas to avoid moisture accumulation. Radical fluorescence is collected by two 50 mm fused silica lenses. The camera optics demagnify the image making it possible for the 12.9 mm long array to view 55.0 mm along the laser-molecular beam interaction region. The total area imaged on the 586 x 384 pixel array with total area of 109 $mm^2$ is 1980 $mm^2$.

## 4.4. ADDITIONAL IRIS SYSTEM FEATURES

The IRIS apparatus also contains a rotatable substrate holder which can be placed in and out of the path of the molecular beam. This substrate can be positively or negatively biased to investigate the effects of ion bombardment on radical-substrate interactions. Another feature of the IRIS apparatus is that a grounded mesh can be placed in contact with the collimating slits, thus preventing plasma charged species from reaching the interaction region.

One difficulty that arises in the IRIS experiments for both fluorocarbon and ammonia glow discharges is that for $CF_2$ and $NH_2$ radicals which have low sticking coefficients can scatter from the collimating slits resulting in fluorescence signal along the laser axis throughout the LIF image. To minimize this problem, the slits are mounted on a liquid $N_2$ cold shield which results in freezing the molecules which collide with the slits. During the experiment, the slits are cooled to < 100 K, as monitored by a chromel/alumel

thermocouple attached to the shield.

## 4.5. $CF_2$ RADICAL STUDY EXPERIMENTAL DETAILS

The fluorocarbon plasma studies presented in Chapters 5 and 6 concern $CF_2$ radicals produced in molecular beams, the sources of which were plasmas generated with 100% $C_2F_6$ (Air Products 99.96%), a 50/50 mixture of $C_2F_6$ and $H_2$ (General Air 99.95%), or 100% HFPO (Aldrich, Lancaster Synthesis, 98%). Total pressure in the source was 25 mTorr for 100% $C_2F_6$ plasma, 30 mTorr for $C_2F_6/H_2$ plasmas, and 45 mTorr for the HFPO system, as measured by a capacitance manometer. The plasmas were produced by the inductive coupling of 13.56 MHz rf power ($P$ = 5-150 W) and were tuned by an rf matching network.

Ion effects were investigated using two methods. First, a grounded mesh was placed in the path of the plasma molecular beam. This removes the majority of the positively and negatively charged ions. No significant perturbations of the near-effusive molecular beam were believed to occur based on previous velocity studies of $NH_2$ radicals in $NH_3$ plasmas.[3] Second, the substrate was biased at +200 VDC. To further probe the mechanism of film deposition, the behavior of $CF_2$ radicals in pulsed HFPO plasmas was also investigated. Duty cycles of 5%, 10% and 33% were used while the peak rf power was kept constant at 300 W. Si, $SiO_2$, and PTFE substrates were used in the pulsed plasma experiments. In addition to these materials, copper was also investigated for CW HFPO plasma processing.

For the $C_2F_6$ and $C_2F_6/H_2$ plasma studies, the substrates processed were 25 x 40

mm Si (110), plasma or thermally deposited $SiO_2$ on Si wafers,[4] 0.5 $\mu$m System 8 photoresist (Shipley Corp.) spin coated on Si wafers, polyimide (Kapton E), platinum or copper foil (99.99% from Alfa Aesar) and PTFE. All substrates were placed 2-3.5 mm away from the laser.

The molecular beam was collimated by a combination of two slits. The slit width varied slightly between sets collected over a 13 month period. The first slit was 0.98-1.15 mm wide and was mounted on a liquid nitrogen cold shield cooled to -200°C. The second slit of 1.25-1.5 mm width was located 12 mm downstream from the first slit. Tunable laser light in the 229-240 nm range (~0.9 mJ/pulse) was produced by frequency doubling the output of the dye laser (Coumarin 47).

The laser was tuned to 234.323 nm, corresponding to the (0,11,0) - (0,0,0) vibronic band of the $CF_2$ $A_1B^1$ - $X_1A^1$ transition, unless otherwise noted. LIF from $CF_2$ radicals was directly imaged onto the ICCD using binned (4 x 4) pixels to increase signal to noise and reduce processing time. The ICCD camera had a 0.3 $\mu$s gate width and a 40-80 ns gate delay to maximize light collection for the $CF_2$ molecule, which has a 60 ns fluorescence lifetime.[5] LIF signals were collected for five accumulations of 1- 40 s exposure each. Multiple sets of data were taken for each experiment. To average these data, it was assumed that all measurements were made under steady-state conditions: the substrate processing time takes place on a much shorter time scale than the measurement. As described in Chapter 5, this assumption was explicitly tested by using previously processed Si substrates. Background images were taken with the laser tuned to a non-resonant frequency and were subtracted from the data image. A 1-D cross section of the

image was made by averaging 20 columns of pixels (7.74 mm) containing the LIF signal and plotting signal intensity as a function of distance along the laser beam path. Because we are operating in the power saturated regime of the laser, no corrections for laser power are made.[6]

## 4.6. $NH_2$ RADICAL STUDY EXPERIMENTAL DETAILS

For the $NH_2$ results presented in Chapter 6, the molecular beam source was a plasma produced with 100% $NH_3$ (Air Products 99.99%). The source total pressure was maintained in the 40-60 mtorr range as monitored by a capacitance manometer, and the flow rate was 20 sccm. Plasmas with $P$ = 50-175 W were produced by the inductive coupling of 13.56 MHz rf power and were tuned by an rf matching network.

The two collimating slits were 1.61-2.0 mm and 1.77-2.0 mm wide, respectively. The interactions between $NH_2$ radicals and Si (100), polyimide (Kapton E), polytetrafluoroethylene (PTFE), platinum, and copper foil (99.99% from Alfa Aesar) substrates were investigated. The polyimide, PTFE and Si substrates were cleaned by sonication in a 50:50 $H_2O$ (18MΩ)/ MeOH mixture for ~30 min prior to $NH_3$ plasma processing. The Pt and Cu substrates were cleaned by exposure to a 150 W Argon plasma for ~15 min prior to $NH_3$ plasma processing. All substrates were placed 2.0-3.5 mm away from the laser.

For reactivity experiments, the laser was tuned to 597.725 nm, corresponding to a collection of the $3_{03}$-$3_{13}$, $4_{04}$-$4_{14}$, $5_{05}$-$5_{15}$ rovibronic bands of the $NH_2$ $X_2B^1$ - $A_2A^1$ electronic transition. To obtain spatially resolved LIF images of $NH_2$ radicals the

molecular beam-substrate interaction region was directly imaged onto the ICCD using a binning of (4 x 4) pixels The ICCD camera had a 1.0 - 1.5 $\mu$s gate width and a gate delay of 2.0 - 2.5 $\mu$s. LIF signals were collected for multiple accumulations with exposure durations of 5 - 45 s. Multiple sets of data were taken for each experiment. Background images were taken with the laser tuned to the non-resonant wavelength of 581 nm and were subtracted from the data image.

To calculate the translational temperature of $NH_2$ radicals their spatially-resolved images were obtained at different camera delay times, ranging from 0.95 $\mu$s to 9.55 $\mu$s. The gate width was maintained at 1 $\mu$s. Most of the data sets were imaged using (2 x 2) pixel binning, and a few at (4 x 4) binning. The same transition used in the reactivity studies was also used here.

## 4.7. SIMULATIONS

### 4.7.1. RADICAL SCATTER

To obtain quantitative information on the density of radicals scattering from the substrate surface relative to incident molecular beam radical density, a simulation based on the geometry of the experiment is used. A Gaussian molecular beam 1-D profilsimulated based on the following experimentally measured parameters: slit widths, distance from the plasma orifice to the slits and laser, laser-surface distance, and size of the detector array. All these parameters are determined experimentally. A schematic of the orifice-slit-substrate region illustrating the geometrical arrangement of reactor orifice, slits and substrate is shown in Figure 4.2. In addition to the experimental parameters listed above,

Gaussian width and amplitude for the molecular beam are also input. Based on the input parameters which result in the best molecular beam fit, the simulation generates a scattered radical 1-D adsorption-desorption profile. This profile corresponds to all the incident radicals scattering from the substrate surface with a cosine function distribution around the surface normal. The only variable in the simulated scattered molecule profile is its amplitude which is adjusted such that it matches the experimental 1-D profile. The amplitude adjusting factor represents the radical scatter coefficient value, $S$. If $S < 1$, the radical of interest is consumed at the substrate surface, whereas if $S > 1$, radical surface generation is occurring.

### 4.7.2. MOLECULAR BEAM AND SCATTER VELOCITY

To obtain translational temperature information, the ICCD camera is gated at different delay times allowing the generation of "snap shots" of a radical's fluorescence in time relative to the excitation time. To simulate the velocity profiles of molecular beam radicals, our model assumes a Gaussian laser beam profile and calculates its time evolution using a Maxwell-Boltzmann distribution of speeds, described by equation (4.1),[7]

$$\frac{N_v}{N} = 4\pi\left(\frac{m}{2\pi k\Theta_{Tmb}}\right)^{3/2} v^2 e^{-mv^2/2k\Theta_{Tmb}} \qquad (4.1)$$

where $N_v/N$ is the fraction of molecules with velocity $v$, m is the mass of $NH_2$, $\Theta_{Tmb}$ is the translational temperature of radicals in the molecular beam, and $k$ is the Boltzmann constant.

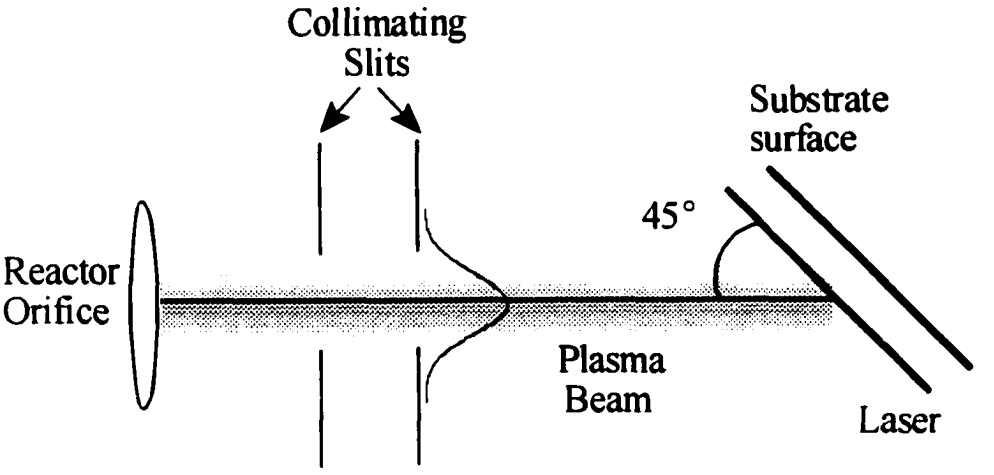


**Figure 4.2.** Schematic of the geometrical arrangement of the reactor, collimating slits, substrate, and laser. Also shown is a Gaussian distribution of densities for radicals emerging from the collimating slits. The laser intersects the plasma molecular beam at a 45° angle.

A crucial input parameter in the simulation process is the absolute length of time, $\tau$, traveled by a molecule before fluorescence is collected. To calculate $\tau$, the time necessary for the laser beam to reach the molecular beam, $\tau_0$, is experimentally determined and used to calculate $\tau$ as shown in equation (4.2).

$$\tau = \tau_1 - \tau_0 + \frac{1}{2}w \qquad (4.2),$$

where $\tau_1$ is the camera gate delay, and $w$ is the camera gate width.

A model similar to the one used to simulate the velocity profiles of molecular beam radicals is used to obtain information on the translational temperatures of scattered radicals, $\Theta_{Tsc}$. One additional factor needs to be considered in this case: the surface scatter distribution of radicals desorbing from the substrate surface is not Gaussian. As discussed in the section 4.7.1, plasma radicals scatter from substrate surfaces with a cosine function distribution around the surface normal. The velocity profile simulation takes this fact into account. Detailed descriptions of both models along with the program codes are given elsewhere.[8]

## 4.8. REFERENCES


1. P. R. McCurdy, K. H. A. Bogart, N. F. Dalleska, and E. R. Fisher, *Rev. Sci. Instrum.* **68**, 1684 (1997).

2. E. R. Fisher, P. Ho, W. G. Breiland, and R. J. Buss, *J. Chem. Phys.* **96**, 9855 (1992).

3. P. R. McCurdy, C. I. Butoi, K. L. Williams, and E. R Fisher, *J. Phys. Chem B.* **103**, 6919 (1999).

4. K. H. A. Bogart, N. F. Dalleska, G. R. Bogart, and E. R. Fisher, *J. Vac. Sci. Technol. A* **13**, 476 (1995).

5. D. S. King, P. K. Schenk, and J. C. Stephenson, *J. Molec. Spectrosc.* **78**, 1 (1979).

6. This has been discussed in detail previously for IRIS experiments. See reference 1.

7. P. R. McCurdy, V. A. Venturo, and E. R. Fisher, *Chem. Phys. Lett.* **274**, 120 (1997).

8. P. R. McCurdy, "Investigation of Surface Interactions and Deposition Mechanism in Plasma Enhanced Chemical Vapor Deposition of Silicon-Based Materials", Doctoral Dissertation, Colorado State University (1999).

# CHAPTER 5

## ION AND SUBSTRATE EFFECTS ON SURFACE REACTIONS OF $CF_2$ USING $C_2F_6$, $C_2F_6/H_2$ AND HEXAFLUOROPROPYLENE OXIDE PLASMAS

This dissertation chapter contains the manuscript of a full paper which will appear in the *Journal of Vacuum Science and Technology A*, Vol. 18, No. 6. The coauthors are N. M. Mackie, K. L. Williams, N. E. Capps, and E. R. Fisher. The work presented here encompasses a detailed comparison of $CF_2$ radical interactions in three different plasma systems: $C_2F_6$, $C_2F_6/H_2$, and hexafluoropropylene oxide (HFPO) glow discharges. The difluorocarbene scatter was measured for different substrate materials and plasma parameters. Both CW and pulsed glow discharges were investigated. The major finding of this work is that $CF_2$ radicals can be used to gauge the overall fluorocarbon plasma process: depositing or etching.

## 5.1. INTRODUCTION AND BACKGROUND

Plasma polymerization of fluorocarbons is a technique widely used to deposit films with many applications such as low k interlevel dielectric materials, moisture barriers and biocompatible thin films.[1,2,3,4,5,6,7,8] Fluorocarbon plasmas (FCPs) are also widely used in the semiconductor industry for selective etching of Si, $SiO_2$, and $Si_3N_4$.[9] In FCPs, substrate etching and film deposition are in direct competition and in many cases occur simultaneously. For some FCPs this competition can be driven towards deposition by using fluorocarbon feed gases with low F/C ratios or with the addition of a reductant such as $H_2$, Si, or hydrocarbon to the feed.[12] For other FCP systems, the transition from etching to deposition regimes occurs with decreasing applied rf power.[8]

It is the balance between etching and deposition that makes FCP chemistry both versatile and complex. This balance is largely controlled by $CF_x$ and fluorine atom concentrations in the gas phase. Using UV absorption spectroscopy, Booth and coworkers measured the absolute densities of $CF_2$ radicals in $CF_4$ and $C_2F_6$ capacitively coupled glow discharges to be $1.1 \times 10^{13}$ $cm^{-3}$ and $5.5 \times 10^{13}$ $cm^{-3}$, respectively.[10] Booth's group also compared $CF_4$ and $C_2F_6$ capacitively coupled discharges, and found the former to be F atom rich and the latter F atom poor.[11] They concluded that the fluorine atom concentration controls the amount of $CF_x$ groups in the gas phase. While some researchers believe $CF_2$ radicals to be direct film deposition precursors in FCP's,[12,13,14] Booth postulates that $C_xF_y$ oligomeric species formed in the gas phase from $CF_2$ units are also viable candidates as deposition precursors. Thus, further investigation of fluorocarbon plasma systems is required to fully elucidate and control deposition

mechanisms in these systems.

While there are some correlations between gas phase reactions and film deposition processes for $CF_4$ and $C_2F_6$ glow discharges, other systems have been studied little by comparison. Plasmas using hexafluoropropylene oxide (HFPO) as the monomer gas are one such example. HFPO plasmas have shown great promise for the generation of high $CF_2$ content materials.[7,8] Studies performed by the research groups of both Gleason and Timmons have generated useful but indirect correlations between plasma parameters and polymeric films produced utilizing HFPO plasma-enhanced chemical vapor deposition (PECVD).[15,16] While these investigations provide information on how HFPO pressure, flow rate, and plasma power affect the composition of the polymeric materials deposited, they generate little direct evidence on how plasma radicals and ions behave upon impact with a substrate surface. Our own work has demonstrated that under certain pulsed and CW experimental conditions, HFPO plasma systems deposit films comprising highly oriented $CF_2$ chains.[7,8] More importantly, we have shown that film composition can be tailored by controlling the amount of charged species reaching the substrate surface.[8] What has not been elucidated thus far is which radical species are involved in deposition processes in HFPO plasmas and how is their surface reactivity affected by experimental conditions.

A few studies are available on the gas-phase densities of $CF_x$ radicals in FCPs correlated with substrate materials. Hansen et al. measured spatially and temporally resolved $CF_2$ densities during $CF_4/O_2$ plasma processing of a wide variety of substrates, including Si, $SiO_2$, metals, and polymers.[17] They found that the density of $CF_2$ is strongly

dependent on substrate material, and in some cases was produced in large quantities with aluminum, $SiO_2$, and a photoresist polymer. Tserepi et al. further examined the interaction of fluorocarbon radicals with polymers and determined the surface loss coefficients for $CF_2$ radicals produced in $CF_4$ microwave discharges. For processing of hexatriacontane (HTC), $CF_2$ loss was dependent on the degree of fluorination of the HTC substrate.[18] In addition, surface generation of $CF_2$ occurred with fluorinated HTC sample. All of these studies, however, merely concentrated on the gas-phase densities and none directly measured the radical-surface interactions.

It is has been postulated that regardless of which regime an FCP belongs, depositing or etching, charged species play an important role.[19] However, few studies involving *in situ* investigations of this very important variable have been published. Tserepi and coworkers observed increased production of $CF_2$ in the presence of HTC at high rf powers, behavior which is consistent with ion assisted production of $CF_2$.[18] Li et al. measured ion density and flux in $C_2F_6$ and $CHF_3$ inductively coupled plasma systems.[20] For both FCPs, ion current densities were found to linearly increase with rf power between 600 and 1400 W CW. Previous work in our group has shown that ions contribute substantially to the surface production of $CF_2$ in $CHF_3$ plasmas,[6] and of $SiF_2$ in $SiF_4$ plasmas.[21] Clearly, elucidation of the exact nature of these effects necessitates further study.

The imaging of radicals interacting with surfaces (IRIS) technique used in our laboratories directly measures the steady-state surface reactivity of a gas-phase species during plasma processing of a substrate.[22] IRIS combines molecular beam and plasma

technologies with laser induced fluorescence (LIF) to provide spatially-resolved 2D images of radical species. Recently, many of our efforts have focused on the surface reactivity of $CF_x$ radicals in a variety of FCPs.[3,6,23,24] We have previously reported that the addition of $H_2$ to $C_2F_6$ plasmas can significantly alter the surface reactivity of $CF_2$ radicals.[3] In addition, we discovered that $CF_2$ scattering coefficients did not change appreciably when different substrate materials were processed in $CHF_3$ plasmas.[6] This was largely attributed to the amorphous fluorocarbon polymer layer deposited on all substrates.

The focus of the present IRIS experiments is to extend our reactivity measurements for $CF_2$ radicals to three very different FCPs: $C_2F_6$, $C_2F_6/H_2$, and HFPO plasmas. The overall goal is to develop a deeper understanding of how the molecular level chemistry is affecting the overall plasma process. Thus, we have measured $CF_2$ scattering coefficients on four industrially relevant substrate materials, Si, $SiO_2$, polyimide, and photoresist. In addition, IRIS measurements have been made for a totally fluorinated material, polytetrafluoroethylene (PTFE), and catalytic metals such as platinum. We also present relative gas-phase density measurements for ground state $CF_2$ radicals as a function of applied rf power. Additional information regarding gas-phase species in our plasmas comes from optical emission spectroscopy (OES) data. Correlations are made between these gas-phase measurements and X-ray photoelectron spectroscopy (XPS) and Fourier transform infrared (FTIR) analyses of substrates processed in the three plasma systems. Thus, this study provides in-depth information on $CF_2$ radical surface interactions in an FCP etching system ($C_2F_6$) along with two FCP deposition systems ($C_2F_6/H_2$ and HFPO).

## 5.2. RESULTS

The spectral selectivity of the LIF technique allows identification and independent study of one specific radical in a molecular beam populated with many different species. The $A^1B_1$ - $X^1A_1$ system of $CF_2$ has been thoroughly characterized by conventional flash-photolysis absorption[25] and LIF studies.[26,27] LIF excitation spectra for $CF_2$ recorded in our IRIS instrument from 100% $C_2F_6$ plasmas have been described previously and comparison to literature spectra verifies that the fluorescing species is indeed $CF_2$.[3] Spectra for 50/50 $C_2F_6/H_2$ and HFPO plasmas are similar to those produced from 100% $C_2F_6$ plasmas. In the following sections, fluorescence from the (0,11,0) $A^1B_1$ state of $CF_2$ ($\lambda$ = 234.323 nm) was used for all imaging experiments, unless otherwise noted.

### 5.2.1. PRODUCTION OF $CF_2$ IN $C_2F_6$, $C_2F_6/H_2$, AND HFPO PLASMAS

To understand the surface processes occurring during FCP processing, we must first determine the relative amounts of $CF_2$ radicals while varying processing parameters. $CF_2$ LIF intensities in a 100% $C_2F_6$ plasma molecular beam were measured as a function of applied rf power, Fig. 5.1a. Because we are operating in the power saturated regime of the laser, these intensities correspond to the relative $CF_2$ densities. LIF intensity for $CF_2$ in the 100% $C_2F_6$ plasma increases linearly above 20 W with increasing applied rf power. This increase in $CF_2$ LIF intensity closely matches the trends observed over a similar power range by Hargis and Kushner,[28] and by Kitamura et al.[29] Fig. 5.1b shows the relative $CF_2$ LIF intensities from 50/50 $C_2F_6/H_2$ plasmas. Here, $CF_2$ production increases rapidly to a maximum at 100 W and then decreases at higher applied rf powers. The

decrease in $CF_2$ production could be the result of increased fragmentation or the onset of $CF_2$ depletion reactions at higher powers.

We have also investigated the dependence of $CF_2$ density on HFPO plasma rf power with and without a grounded mesh in the path of the molecular beam.[24] With the grounded mesh, a lower $CF_2$ density is observed. In both systems, however, the relative density of the difluorocarbene radical follows the same linear trend observed in 100% $C_2F_6$ plasma systems: the higher the applied rf power, the higher the detected $CF_2$ relative density.

### 5.2.2. REACTIVITY OF $CF_2$ RADICALS USING $C_2F_6$ AND $C_2F_6/H_2$ PLASMAS

Fig. 5.2 shows a series of ICCD images of $CF_2$ LIF using a 100% $C_2F_6$ plasma molecular beam processing a $SiO_2$ substrate. LIF from $CF_2$ molecules in the molecular beam only is shown in Fig. 5.2a. Fig. 5.2b is the LIF signal acquired with the $SiO_2$ substrate rotated into the path of the molecular beam. Here, both the incident and scattered $CF_2$ molecules are being imaged. Fig. 5.2c is the difference between Fig. 5.2b and Fig. 5.2a, showing the $CF_2$ radicals scattered from the surface. It is clear from this figure that there is an appreciable amount of $CF_2$ emanating from the $SiO_2$ substrate. Fig. 5.3a shows the data of Figs. 5.2a and 5.2c converted to cross sections. The broad spatial distribution and the shift of the scattered signal peak maximum away from the molecular beam peak maximum indicate the $CF_2$ radicals scatter with a cosine angular distribution. Also shown in Fig. 5.3 are simulated curves (dashed lines) for the incident beam and for scattered molecules assuming an adsorption-desorption mechanism, with $S = 1.25 \pm 0.04$.

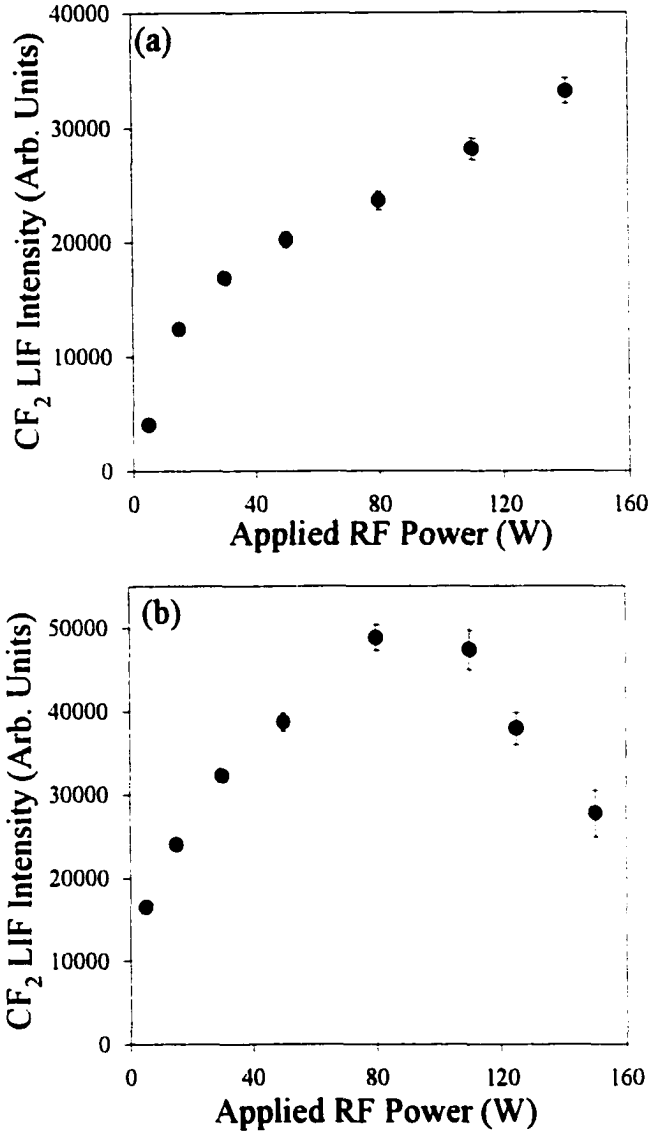


**Figure 5.1.** Relative LIF intensities of $CF_2$ radicals in (a) 100% $C_2F_6$ and (b) 50/50 $C_2F_6/H_2$ plasmas as a function of applied rf power. The LIF transition was the (0,11,0) vibronic band of the $A^1B_1$ - $X^1A_1$ system.

A scattering value greater than unity indicates that surface production of $CF_2$ (g) contributes to the observed scattering signal. Averaging all of our data sets for $SiO_2$ substrates yields a $CF_2$ scattering value of $S = 1.30 \pm 0.06$. Surface production of $CF_2$ has also been observed for $C_2F_6$ and for $CHF_3$ plasma processing of Si (100) and $SiO_2$.[3,6] For comparison, in 100% $SiF_4$ rf discharges, extremely high $S$ values of ~3 were determined for the isoelectronic difluorosilane radicals as they interacted with Si surfaces.[21] This is not surprising as the $SiF_4$ system is a completely etching plasma.

To determine the role of ions in the observed $CF_2$ scatter, a grounded mesh screen was placed in front of the first defining slit to remove charged species from the molecular beam. Figure 5.3b shows cross-sections for LIF of $CF_2$ in the incident molecular beam and scattered from a silicon substrate with the grounded mesh screen in the path of the molecular beam. The scattered $CF_2$ signal under these conditions is clearly less than that observed without the grounded mesh screen, Fig. 5.3a. Simulation of the data, also shown in Fig. 5.3b, yields a scatter value of $S = 1.07 \pm 0.06$, considerably lower than that observed without the mesh. To further explore the difluorocarbene surface generation phenomenon, IRIS measurements were performed using a variety of other substrate materials and the resulting data were modeled as above. $S$ values for $CF_2$ in these experiments are listed in Table 5.1.

Figure 5.4 shows a series of ICCD images of $CF_2$ using a 50/50 $C_2F_6/H_2$ plasma molecular beam processing a polyimide substrate. Figure 5.5 shows the cross sectional data for the IRIS images shown in Figs. 5.4a and 5.4c, along with the simulation curves. materials are listed in Table 5.1. The $S$ values obtained for Si, $SiO_2$ and polyimide are all

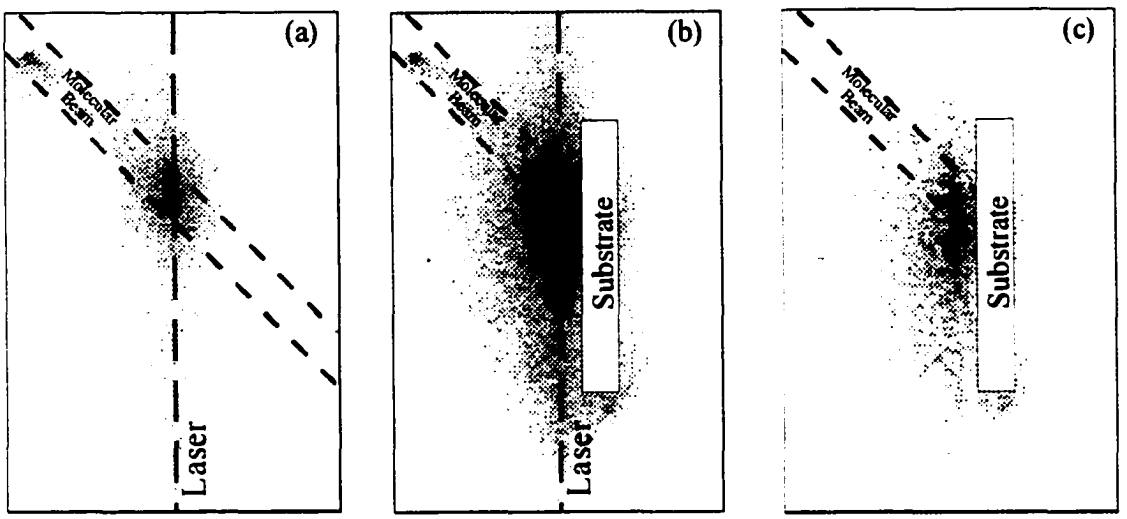


**Figure 5.2.** Spatially resolved two-dimensional ICCD images of the LIF signal for the $CF_2$ (0,11,0) state (a) in the 100% $C_2F_6$ molecular beam (no substrate) and (b) with a 300K $SiO_2$ substrate rotated into the path of the molecular beam at a laser surface distance of 2.0 mm. (c) Difference between the images shown in (a) and (b) displaying only $CF_2$ molecules scattering from the surface. LIF signals with the highest intensity appear as the darkest regions, dashed lines indicate the location of the molecular beam and the laser beam.

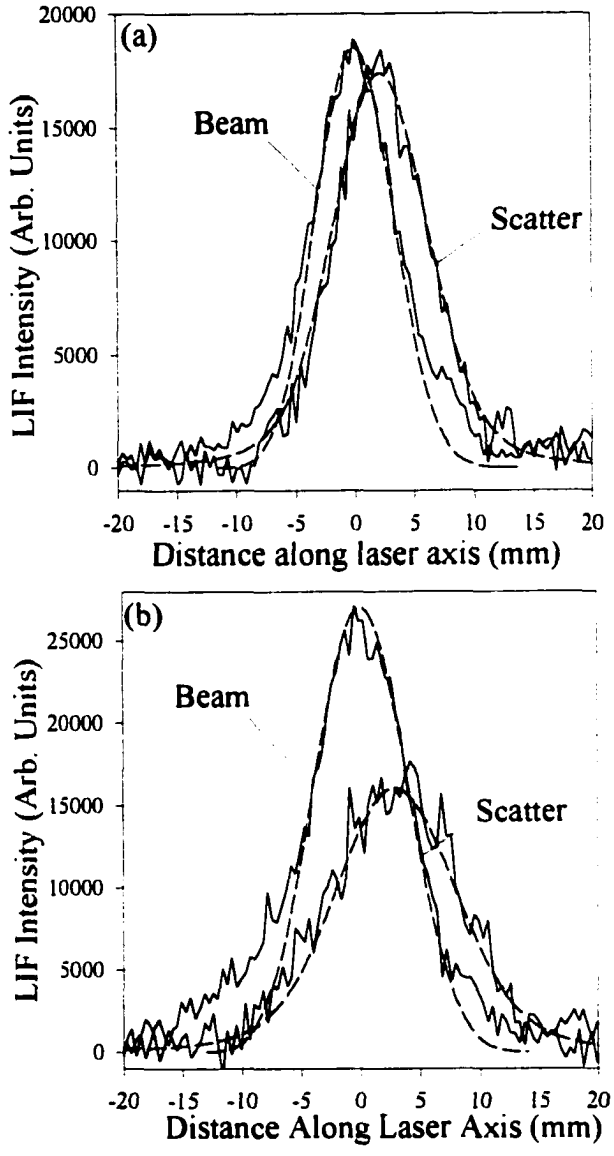


**Figure 5.3**. (a) Cross-sectional data for the LIF of $CF_2$ in the incident molecular beam and scattered from the $SiO_2$ substrate using a 100% $C_2F_6$ plasma molecular beam. The laser-surface distance is 2.0 mm. Dashed lines represent the simulated curves from the geometric model, assuming S = 1.25. (b) Cross-sectional data for the LIF of $CF_2$ in the incident molecular beam and scattered from a silicon surface using a 100% $C_2F_6$ molecular beam that has passed through a grounded mesh. The laser surface distance is 2.5 mm. Dashed lines represent the simulated curves from the geometric model assuming $S$ = 1.07. Results from these simulations as well as scattering data for $CF_2$ using other substrate <1

and are the same within the combined experimental error, while that for PTFE is > 1. Note, that the scattering values for Si, $SiO_2$ and polyimide are considerably lower than those obtained for the 100% $C_2F_6$ system.

### 5.2.3. REACTIVITY OF $CF_2$ RADICALS USING HFPO PLASMAS

Figure 5.6 depicts the experimental and calculated curves for $CF_2$ radicals interacting with a silicon substrate using a 135 W CW HFPO plasma as the molecular beam source. In Fig. 5.6a, the best fit to the scatter data was obtained with $S = 1.10 \pm 0.05$, suggesting that $CF_2$ radicals are neither lost nor produced at the surface. Shown in Fig. 5.6b are the experimental and simulated curves generated when the Si substrate was biased at +200 V under similar experimental conditions as Fig. 5.6a. The scatter coefficient decreases to ~0.8, corresponding to a surface reactivity of ~0.2.

To investigate the validity of the steady-state assumption for our IRIS measurements (see Chapter 4), we obtained $CF_2$ scatter coefficients for a Si substrate which was processed for 3 hours in an HFPO plasma prior to its use in IRIS experiments. $S$ values very close to the ones discovered for bare Si substrates were observed, Table 5.2. Thus, the steady state assumption appears to be valid. Table 5.2 also lists the scatter coefficient values obtained under CW conditions while varying several experimental parameters. Three different $CF_2$ vibronic transitions were probed, with no significant change in $S$ observed. In addition, the scatter coefficient of $CF_2$ displays no noticeable dependence on the type of substrate used. However, somewhat higher $CF_2$ scatter is observed for higher plasma rf powers. Table 5.2 also shows the difluorocarbene

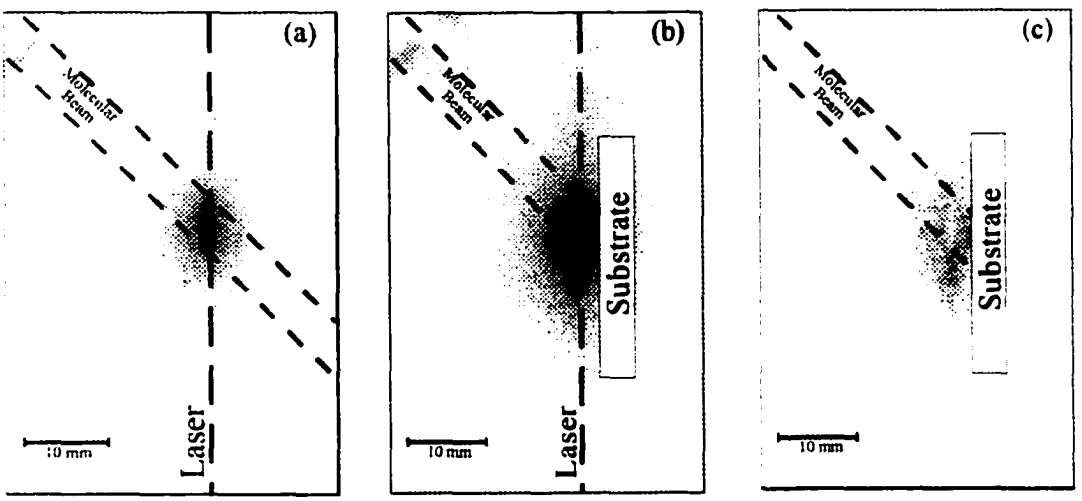


**Figure 5.4.** Spatially resolved two-dimensional ICCD images of the LIF signal for the $CF_2$ (0,11,0) state (a) in the 50/50 $C_2F_6/H_2$ molecular beam (no substrate) and (b) with a 300K polyimide substrate rotated into the path of the molecular beam at a laser surface distance of 2 mm. (c) Difference between the images shown in (a) and (b) and shows only $CF_2$ molecules scattering from the surface. LIF signals with the highest intensity appear as the darkest regions, dashed lines indicate the location of the molecular beam and the laser beam.

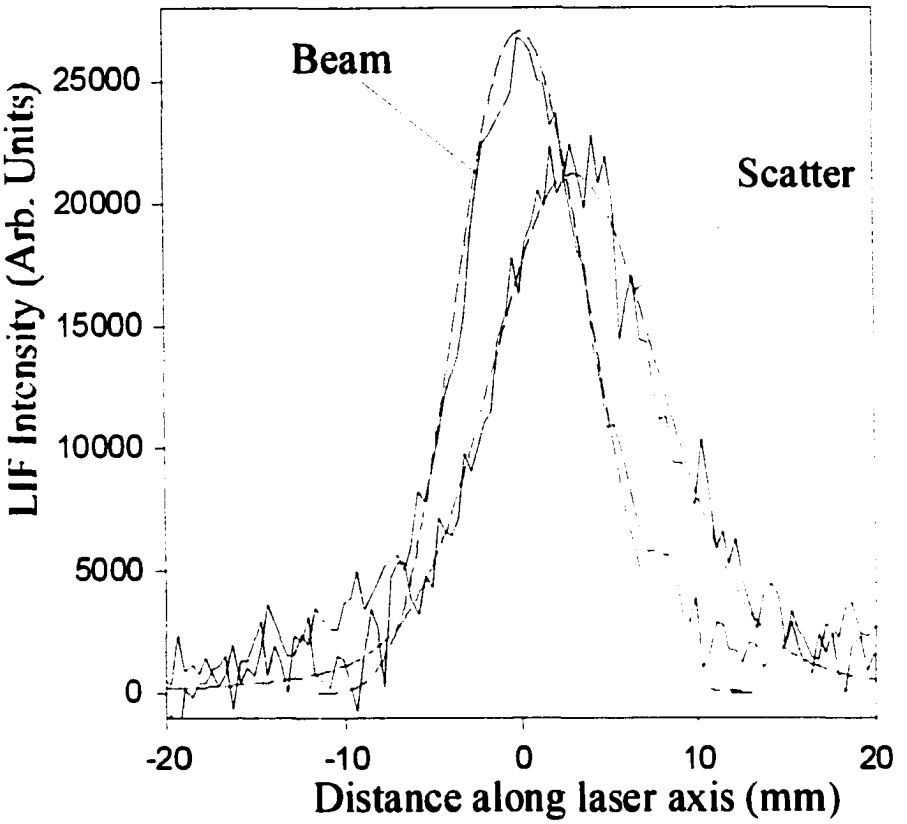


**Figure 5.5.** Cross-sectional data for the LIF of $CF_2$ in the incident molecular beam and scattered from a polyimide (Kapton E) substrate using a 50/50 $C_2F_6/H_2$ plasma molecular beam. The laser-surface distance is 3.0 mm. Dashed lines represent the simulated curves, assuming $S = 0.80$.

**Table 5.1.**[30] Scatter coefficients, *S*, for $CF_2$ in 100% $C_2F_6$ and 50/50 $C_2F_6/H_2$ 50 W plasmas.[a]

| | *S* | |
|---|---|---|
| **Substrate** | 100% $C_2F_6$ | 50/50 $C_2F_6/H_2$ |
| Si | 1.44 ± 0.03 | 0.84 ± 0.02 |
| $SiO_2$ | 1.30 ± 0.06 | 0.86 ± 0.04 |
| Polyimide (Kapton E) | 1.45 ± 0.08 | 0.86 ± 0.09 |
| Polytetrafluoroethylene (PTFE) | 0.98 ± 0.03 | 1.69 ± 0.03 |
| System 8 Photoresist | 1.83 ± 0.03 | - |
| Platinum | 1.15 ± 0.05 | - |

[a]Values obtained using our simulation of the experiment, assuming an adsorption-desorption scattering mechanism. Values given are the weighted average of several data sets.

scatter coefficients determined when a grounded mesh was placed in the path of the molecular beam and for Si substrates biased at +200 VDC.

The behavior of $CF_2$ was also investigated under pulsed plasma conditions utilizing three duty cycles: 5%, 10%, and 33%. Fig. 5.7 shows the incident and scattered beam cross sections obtained for a 33% duty cycle HFPO plasma. Here, $S$ is lower than the values measured for any of the CW HFPO plasmas without the grounding mesh or biasing of the Si substrate. Table 5.3 shows the $S$ values obtained in pulsed HFPO plasmas using different pulse sequences and substrate materials. For all pulse sequences, $S \sim 0.8$, independent of the processed substrate material. The lower $S$ values determined for the pulsed plasma systems indicate that less $CF_2$ is scattered at the substrate surface than under CW conditions.

### 5.2.4. SURFACE CHARACTERIZATION OF FCP PROCESSED MATERIALS

As noted in the Introduction, etching and deposition processes proceed simultaneously in FCPs, in direct competition with each other. For 100% $C_2F_6$ plasmas, the balance between etching and polymer deposition results in very little film growth. To directly correlate $CF_2$ radical scatter coefficients with substrate modifications occurring during plasma processing, IRIS substrates were removed from the instrument after data collection and surface analysis was performed.

Fig. 5.8 shows FTIR reflection spectra of silicon and ATR-FTIR spectra of polyimide and photoresist substrates after exposure to 100% $C_2F_6$ plasma molecular beams. The FTIR spectrum of the silicon substrate shows no evidence of fluorocarbon

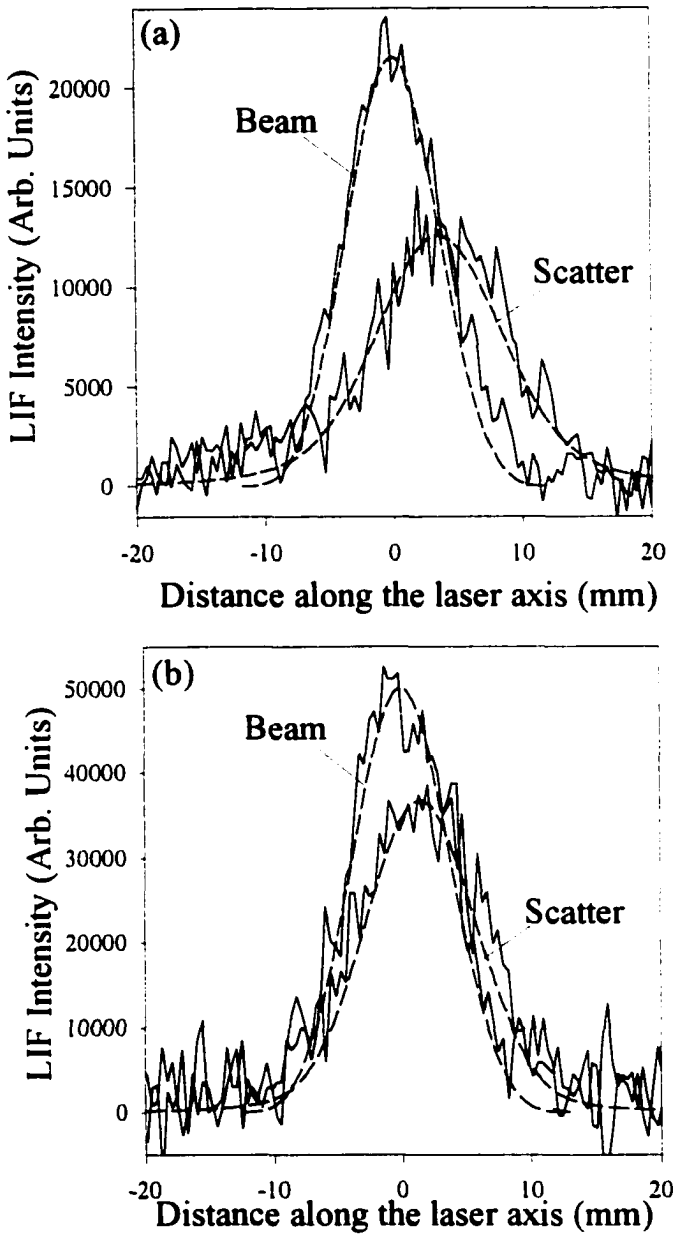


**Figure 5.6.** Incident and scattered beams in 135 W HFPO plasma. The Si (100) was placed 3.0 mm from the laser beam. (a) The best fit was obtained for $S = 1.1$ . (b) The Si substrate was biased at + 200 VDC. The laser-surface distance was 1.5 mm and the best fit was obtained for $S = 0.80$.

**Table 5.2.** $CF_2$ scatter coefficients using a CW HFPO plasma molecular beam.

| Substrate Conditions | RF Power | | | | |
|---|---|---|---|---|---|
| | v'' [a] | 35 W | 135 W | 200 W | |
| Silicon | (0,11,0) | 0.97 ± 0.03 | 1.15 ± 0.03 | 1.29 ± 0.05 | |
| | (0,10,0) | | 1.16 ± 0.03 | | |
| | (0,12,0) | | 1.10 ± 0.07 | | |
| | (0,11,0) | 0.80 ± 0.07 | 0.77 ± 0.05 | | Grounded mesh |
| | (0,11,0) | 0.82 ± 0.02 | 0.81 ± 0.06 | 0.85 ± 0.07 | + 200 V |
| Silicon [b] | (0,11,0) | 1.07 ± 0.06 | 1.05 ± 0.15 | | |
| $SiO_2$ | (0,11,0) | 1.00 ± 0.07 | 1.15 ± 0.07 | 1.25 ± 0.05 | |
| Copper | (0,11,0) | | | 1.20 ± 0.10 | |
| | | | | 0.80 ± 0.05 | + 200 V |
| Teflon | (0,11,0) | 1.01 ± 0.04 | 1.10 ± 0.10 | | |
| | (0,11,0) | 0.82 ± 0.04 | 0.68 ± 0.07 | | Grounded mesh |

[a] Vibrational level of the $A^1B_1$ electronic excited state of $CF_2$ radicals.
[b] Silicon wafer was processed 28 cm downstream in a CW HFPO plasma for 3 hrs.

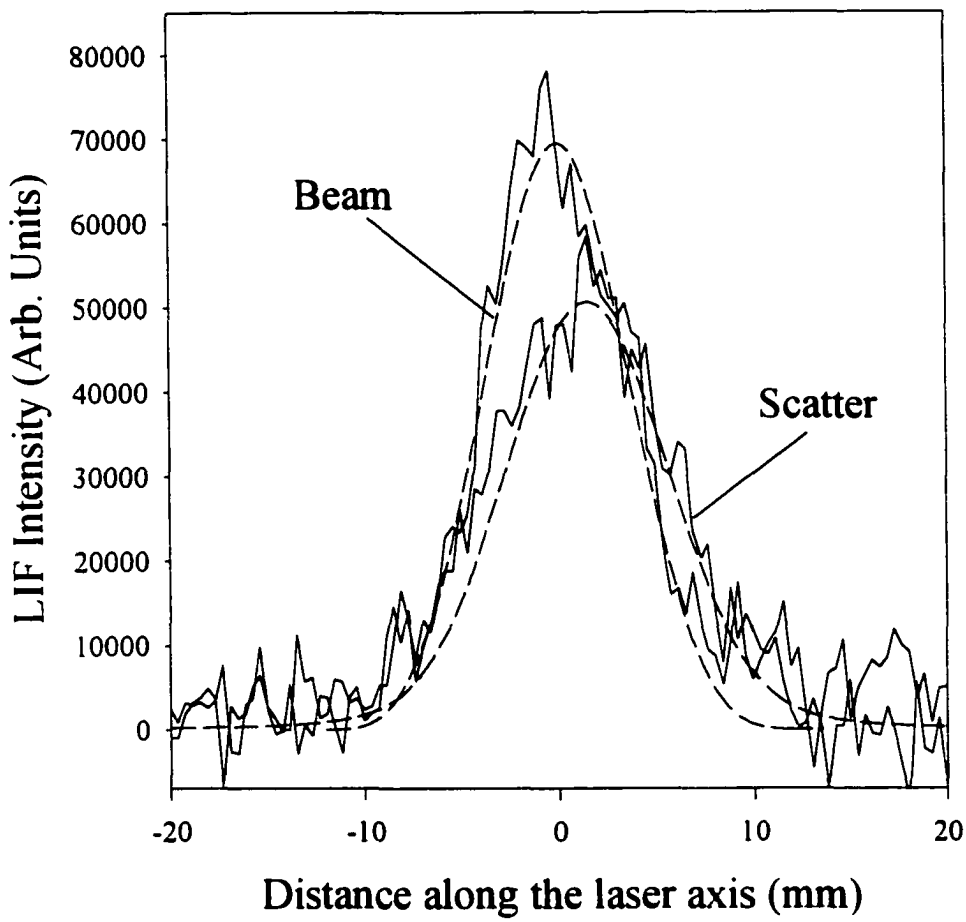


**Figure 5.7.** Cross-sectional experimental and simulated curves for $CF_2$ radicals present in the incident and scattered beams in a 33% duty cycle HFPO plasma. The laser-surface distance was 1.5 mm and the best fit was obtained for S = 0.77.

**Table 5.3**. $CF_2$ scatter coefficients, $S$, using a pulsed HFPO plasma molecular beam.

| Substrate | Duty cycle (%) | $S$ |
|---|---|---|
| Silicon | 5 % | 0.82 ± 0.10 |
| | 10 % | 0.86 ± 0.09 |
| | 33 % | 0.77 ± 0.06 |
| Silicon [a] | 5 % | 0.74 ± 0.04 |
| $SiO_2$ | 5 % | 0.85 ± 0.05 |
| | 10 % | 0.83 ± 0.08 |
| | 33 % | 0.81 ± 0.05 |
| PTFE | 5 % | 0.75 ± 0.05 |
| | 10 % | 0.78 ± 0.10 |

[a] See Table 5.2.

film deposition. There are, however, prominent features attributable to SiO stretching at 1070 $cm^{-1}$,[31] and to SiF at 723 $cm^{-1}$.[32] This has been observed previously, and is the result of F atoms etching the walls of our glass reactor.[33]

Due to the low reflectivity of the polymer materials studied, ATR-FTIR was performed on polyimide and system 8 photoresist materials before and after processing with a 100% $C_2F_6$ plasma molecular beam. These materials show little change in film structure from the native polymer after plasma processing. The ATR-FTIR spectrum of the polyimide sample, Fig. 5.9, shows characteristic peaks for C=O amide stretch at 1712 $cm^{-1}$, C-O ether stretch at 1342 $cm^{-1}$, and two distinct peaks due to para-substituted phenyl rings at 820 $cm^{-1}$ and 717 $cm^{-1}$. Although the ATR-FTIR spectrum of the photoresist sample is more difficult to characterize, OH and $sp^3$ CH stretching frequencies at 3300 $cm^{-1}$ and 2900 $cm^{-1}$, respectively, are observed. There are also contributions from ketone C=O at 1728 $cm^{-1}$ and olefinic C=C bonding at 1650 $cm^{-1}$.

In contrast to the silicon substrate, the polyimide and photoresist substrates show no significant changes after plasma processing with the 100% $C_2F_6$ plasma molecular beam. There are two possible reasons for this. First, the polymer modifications may be restricted to the very surface of the polymer and therefore below the sampling depth of the ATR technique (~0.1 $\mu$m). Second, because of the low species flux in our IRIS experiment, the degree of plasma modification may be below the sensitivity of this IR technique. To address this second point, polyimide and photoresist polymers were processed in an inductively coupled reactor nearly identical to the source on IRIS. After processing with a 50 W 100% $C_2F_6$ plasma for 10 minutes, the polyimide sample did not

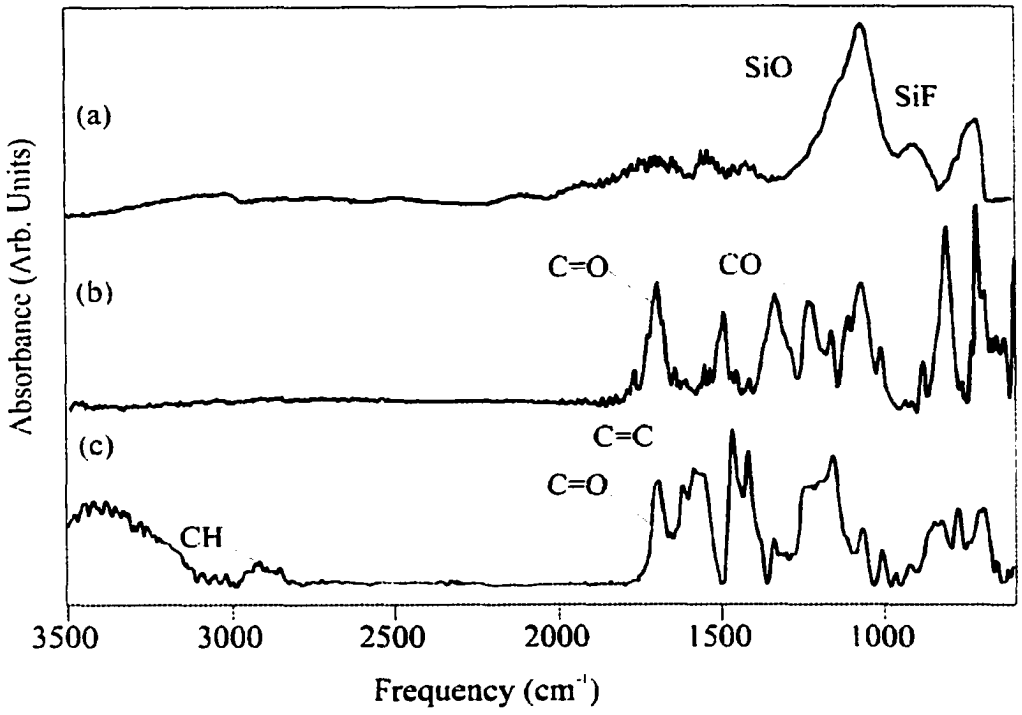


**Figure 5.8.**[30] FTIR spectra of (a) silicon (reflection), (b) polyimide (ATR), and (c) System 8 photoresist (ATR) substrates after processing in IRIS with a 100% $C_2F_6$ 50 W plasma molecular beam.

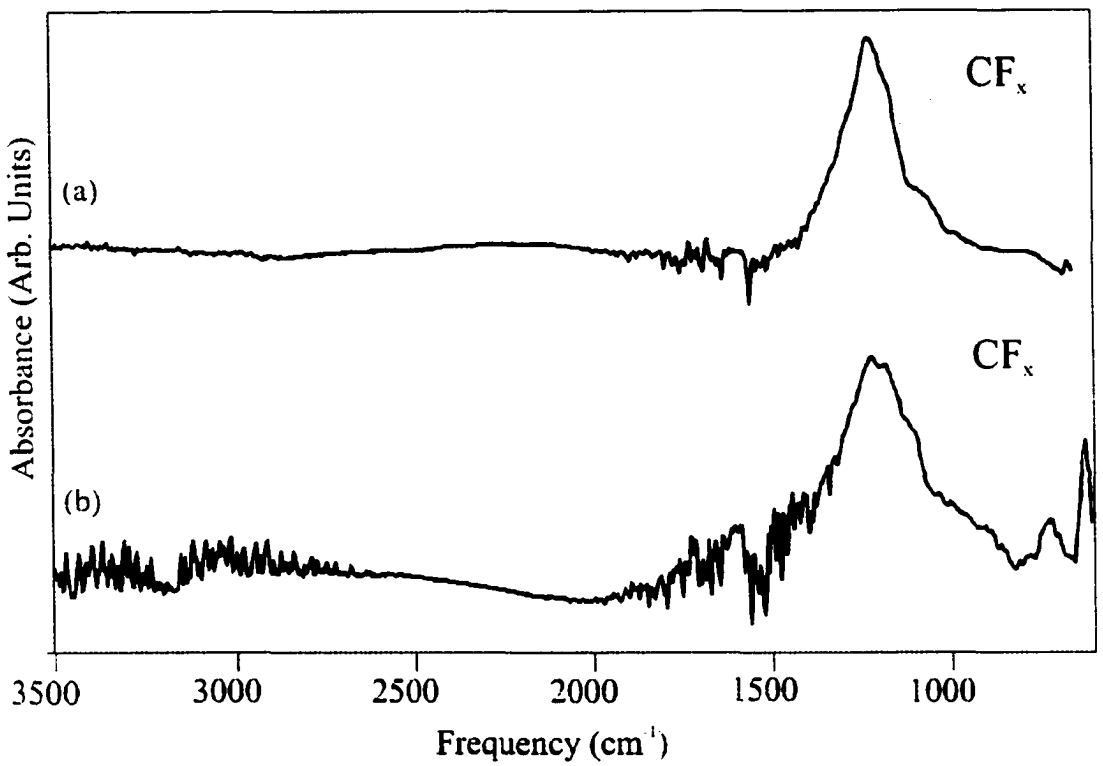


**Figure 5.9.**[30] FTIR spectra of (a) silicon (reflection) and (b) polyimide (ATR) substrates after processing in IRIS with a 50/50 $C_2F_6/H_2$ 50 W plasma.

show any change due to the plasma treatment. A 5 minute exposure of the photoresist polymer, however, resulted in visible etching and film removal. ATR-FTIR analysis of the etched photoresist sample showed no observable chemical modification.

Fig. 5.9 shows FTIR reflection spectra of silicon and FTIR-ATR spectra of polyimide substrates after processing with 50/50 $C_2F_6/H_2$ plasmas during IRIS experiments. As can be seen from this figure, there is an identical, relatively thick, fluorocarbon film deposited on the silicon and polyimide substrates. This fluorocarbon film shows only one broad absorption band from 1100 - 1400 $cm^{-1}$, attributable to all $CF_x$ (x = 1-3) stretching modes.[31,34] This suggests a very amorphous material is deposited under these plasma conditions.

Using the 100% $C_2F_6$ plasma, only very thin fluorocarbon films were produced (≤80 Å), even after several hours of exposure to the molecular beam. Indeed, the films are so thin that the FTIR analysis reveals only fluorine incorporation, and little, if any film formation. However, XPS analysis revealed that very thin fluorocarbon polymer films were indeed being deposited on the $SiO_2$, polyimide, PTFE, and Pt substrates.[30] For these materials, similar film compositions, and F/C ratios of ~1 were found. This was in direct contrast to XPS results for substrates placed directly in the plasma tube, which showed no film deposition. Films formed on the Si substrate, had somewhat lower F/C ratios of ~0.8.[30] This difference may be the result of different film thicknesses on the different substrates or the relative balance between etching and deposition may be different in the Si substrate system.[26]

We have reported a detailed analysis of films produced in HFPO plasmas in

Chapter 3. Briefly, this plasma system produces high $CF_2$ content materials downstream from the rf coil in our inductively coupled plasmas ($P$ < 50 W CW). Fig. 5.10 shows the transmission FTIR spectra of materials generated in CW and pulsed HFPO plasmas. In Fig. 5.10a, the FTIR spectrum of a film obtained in a 30 W CW HFPO plasma is displayed. The broad absorption band at ~ 1200 $cm^{-1}$ indicates that this is a highly amorphous fluorocarbon material. When the plasma is pulsed (5% duty cycle), however, two distinctly separated absorption features appear in the FTIR spectrum of the material generated, Fig. 5.10b. These correspond to the symmetric (1165 $cm^{-1}$) and asymmetric (1217 $cm^{-1}$) stretching frequencies of $CF_2$ groups,[12] indicating that this material is significantly less amorphous than the one generated under CW conditions. Interestingly, when charged species were deflected away from the substrate surface in a 30 W CW HFPO plasma, Fig. 5.10c, the FTIR spectrum of the deposited material is virtually identical to the one shown in Fig. 5.10b. It is also important to note that at rf powers > 50 W CW, etching becomes the dominating process, as seen from lack of $CF_2$ present in FTIR spectra combined with the emergence of intense SiO peaks, Fig. 3.2.

### 5.2.5. OPTICAL EMISSION FROM $C_2F_6$, $C_2F_6/H_2$, AND HFPO PLASMAS

OES is a useful spectroscopic tool that allows the identification of excited state species in a plasma. We collected emission spectra for our three plasma systems using the independent plasma reactor described in Chapter 2. Plasma emission in the range of 249 to 713 nm was analyzed from 100% $C_2F_6$, 50/50 $C_2F_6/H_2$, and 100% HFPO plasmas, Fig. 5.11. The spectrum of the 100% $C_2F_6$ spectra is dominated by emission of $CF_2$ from the

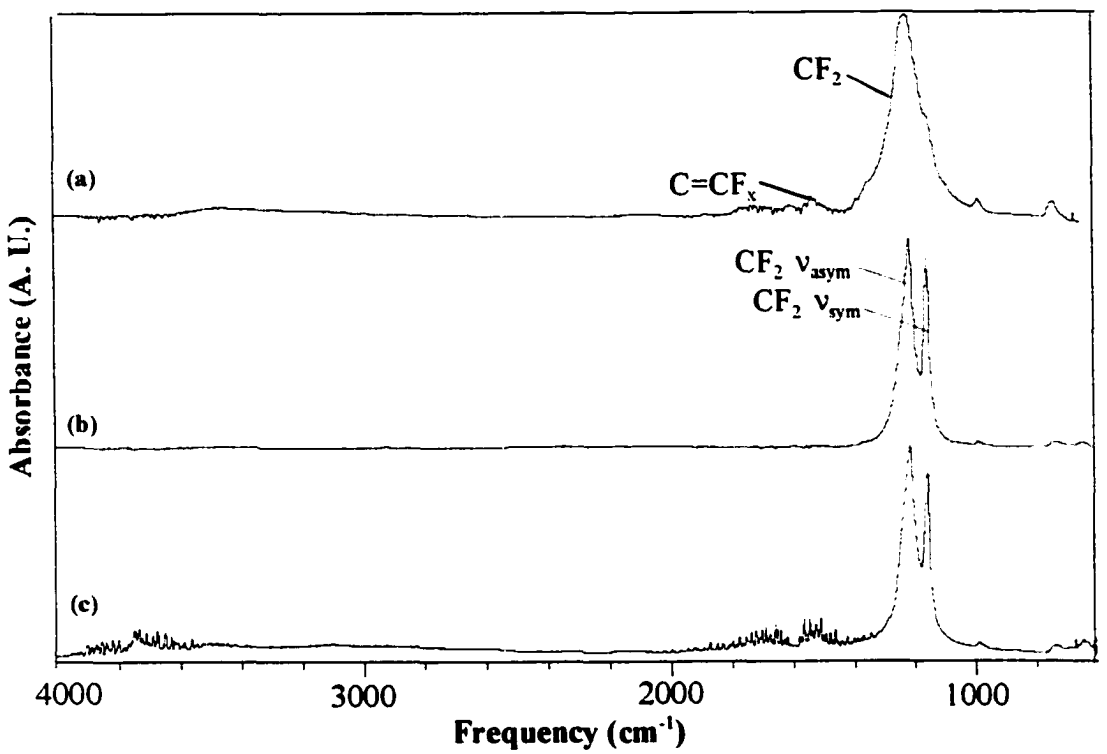


**Figure 5.10.** Transmission FTIR spectra of films obtained from HFPO plasmas under the following experimental conditions: (a) 30 W CW applied rf power, 9.5 cm downstream from rf coil; (b) pulsed plasma: 5 % duty cycle, applied peak power of 300 W, 8 cm downstream from the rf coil; (c) 30 W CW applied rf power with charged species deflected away from the substrate, 9.5 cm downstream from rf coil.

bending mode of the $A^1B_1$ - $X^1A_1$ system, characterized by vibronic transitions $A(0,v_2,0)$ - $X(v_1, v_2, 0)$ from 249 to 300 nm.[12] The small peak at 387 nm is attributable to $N_2$, which is a residual component of the plasma reactor. The spectrum of a 50/50 $C_2F_6/H_2$ plasma also shows intense emission from $CF_2$. In addition, there are peaks attributed to $H_\alpha$ and $H_\beta$ atomic emission at 656.3 nm and 486.1 nm, respectively, which are not present in the spectrum of the 100% $C_2F_6$ plasma.[35] In the OES spectrum of 100% HFPO plasma, Fig. 5.11c, the emission line progression observed in the 249 - 280 nm region shows the presence of $CF_2$ radicals in this system as well. In addition, emission peaks between 280 and 330 nm attributable to the presence of CO molecules in the gas phase are observed.[36]

## 5.3. DISCUSSION

As noted in the Introduction, the interactions of radicals with surfaces are important to thin film formation and etching. Our IRIS work has focused on the surface reactions of radicals primarily in systems where thin films are being deposited or substrates are etched using low-temperature plasmas. With FCPs, both processes are occurring simultaneously such that the effects of radical-surface interactions are very complex. Although many aspects of FCPs have been examined in detail, past studies have rarely discussed both gas-phase characterization and substrate processing effects. Indeed most researchers concentrate on only one aspect of these highly complicated systems.[16,37] Yet, determining how gas phase radicals interact with a substrate is critical to understanding the chemistry of plasma processing. This is especially important in FCPs as the balance between film growth and etching depends on the interactions of active plasma species

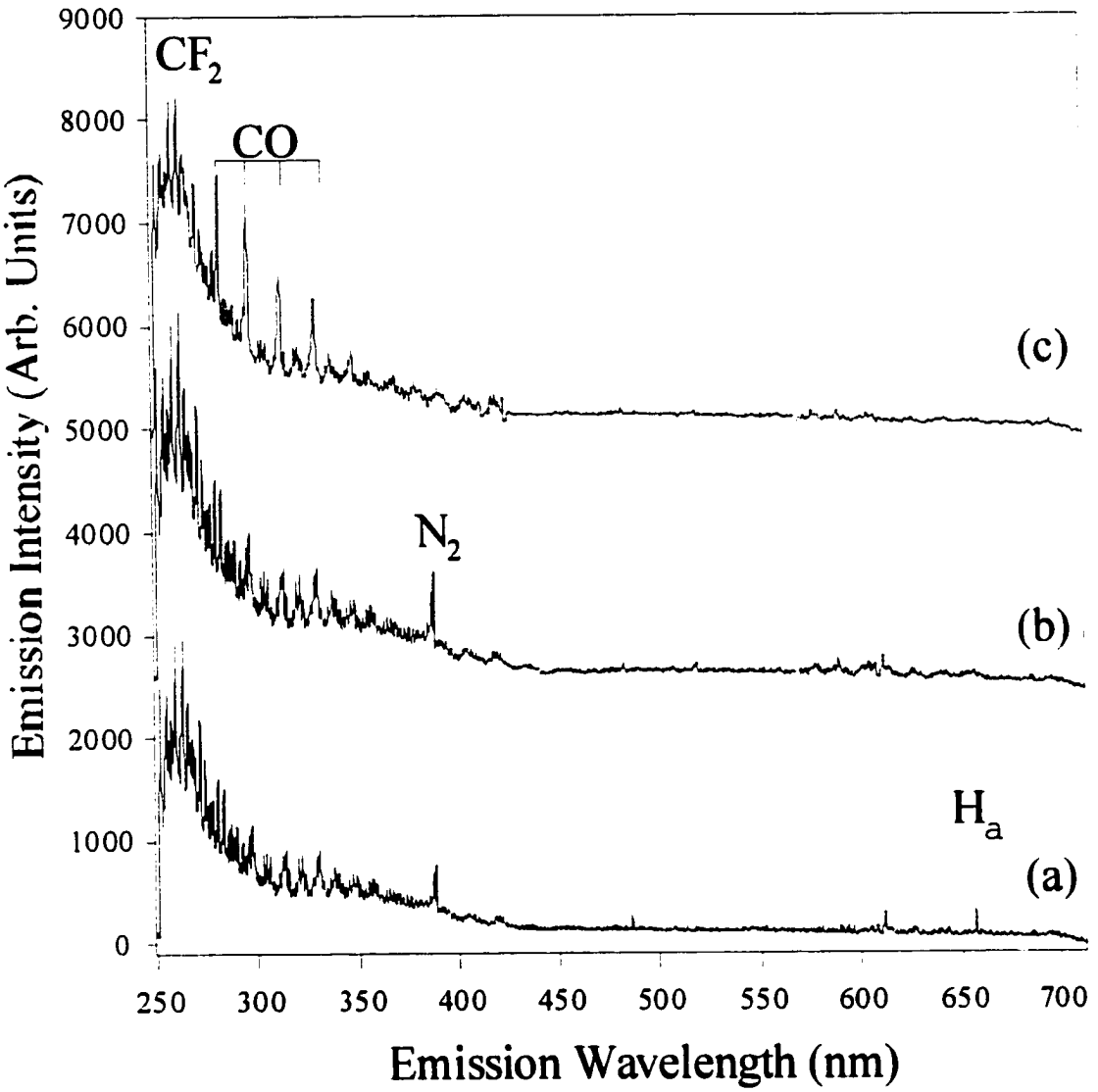


**Figure 5.11.** Optical emission spectra of (a) 100% $C_2F_6$, (b) 50/50 $C_2F_6/H_2$, and (c) 100% HFPO plasmas with applied rf powers of 50 W.

(ions, radicals, electrons) with the surface being processed.

A few past studies have concentrated on directly correlating the presence of different gas phase species such as ions, $CF_x$(x=1-3) radicals, and F atoms to Si and $SiO_2$ etching and film formation. Most notably, Sawin and coworkers explored these effects by emulating a plasma environment through the use of $Ar^+$ ion, $CF_2$ radical, and F atom beams.[38] They found that sticking of $CF_2$ molecules to a Si surface occurs and significantly decreases the $Ar^+$ sputtering rates. In contrast, $Ar^+$ induced etching of $SiO_2$ substrates was enhanced by the presence of both $CF_2$ and F species.[39] However, they did not study these species in their native plasma environment. While it is important to determine how each species affects processing of substrates without other plasma species being present, it is difficult to extrapolate how they will behave in the presence of the multitude of species created in a plasma. This type of research reemphasizes the importance of using our IRIS technique which allows the study of one specific molecule interacting with a particular surface while it is being bombarded by the full range of plasma species.

### 5.3.1. FILM COMPOSITION DEPENDENCE ON PLASMA SYSTEM

Comparison of results for the three plasma systems studied here illuminates some of the chemical and physical processes that occur during FCP processing of materials. First, although no substantial fluorocarbon film is deposited from 100% $C_2F_6$ plasmas, our FTIR analyses reveal that some fluorine is implanted into the surface of Si (100) substrates. This is supported by the XPS results which show significant fluorine content,

and the presence of a thin fluorocarbon polymer.[30] In contrast, relatively thick amorphous fluorocarbon films are deposited from the 50/50 $C_2F_6/H_2$ plasma on Si (100), $SiO_2$, and polyimide substrates. XPS and FTIR analyses reveal that these materials are similar in composition and are highly crosslinked.[30] Fluorocarbon materials are also deposited in HFPO plasmas under CW ($P < 50$ W) and pulsed conditions. These films contain high $CF_2$ concentrations (~80%) and little crosslinking for processing performed far downstream from the rf glow.[8]

It is important to note that ion bombardment of the substrate occurs in all three systems. In the 100% $C_2F_6$ system, ion bombardment is partly responsible for removal of the thin film of fluorinated material deposited during processing.[13] In the 50/50 $C_2F_6/H_2$ system, ion bombardment also causes crosslinking of the resulting film and likely aids in the deposition process.[12] In HFPO plasmas, ions cause crosslinking in the deposited fluorocarbon material as shown by the FTIR spectra of films deposited with and without ions present in a 30W CW system, Figs. 5.10a and 5.10c. In addition, increased ion bombardment at P > 50W results in etching becoming the predominant plasma process in HFPO plasmas.[8]

Many researchers have proposed $CF_2$ radicals as film deposition precursors in a variety of FCP processing systems.[12-14] Consequently, we concentrate our efforts on correlating $CF_2$ radical behavior and substrate processing differences for $C_2F_6$, $C_2F_6/H_2$ and HFPO plasmas.

### 5.3.2. $CF_2$ REACTIVITY DEPENDENCE ON PLASMA SYSTEM AND SUBSTRATE MATERIAL

The three plasma systems investigated here are representative of the major fluorocarbon plasma types: etching ($C_2F_6$), depositing upon adding $H_2$ to the feedgas ($C_2F_6/H_2$), and slow depositor (HFPO). Our results show that $CF_2$ radical interactions with substrates in the three systems can be related to the type of overall substrate processing.

100% $C_2F_6$ PLASMAS. In the 100% $C_2F_6$ plasma, the nearly linear increase of gas-phase difluorocarbene concentration with rf power (slope≈1.6), Fig. 5.1, is mostly the result of the higher number of parent gas molecules dissociating in the gas phase at higher powers. We observe $S > 1$ for $CF_2$ radicals on many substrates (Si, $SiO_2$, polyimide, photoresist, and platinum) under these conditions. This demonstrates that $CF_2(g)$ is being produced at these surfaces during plasma processing. In addition, it also indicates that difluorocarbene generation at reactor walls is a possible contributor to the gas phase density of $CF_2$ at high rf power.

Interestingly, there is some dependence of the observed scatter on the substrate material. This differs from what was observed in the $CHF_3$ system,[6] where nearly identical $S$ values were obtained for Si, $SiO_2$, $Si_3N_4$, photoresist, and 304 stainless steel at 50 W applied power. Likewise, the $C_2F_6/H_2$ and HFPO plasmas also show little substrate dependence. In the $CHF_3$ system, however, a fluorocarbon polymer of the same composition was formed on all substrates. Therefore, the nature of the underlying substrate does not affect the observed $S$ values. Among the substrates that produce $CF_2$

radicals upon interaction with the 100% $C_2F_6$ molecular beam, Pt gives a smaller scatter coefficient of 1.15 compared to Si, $SiO_2$, polyimide, and photoresist, Table 5.1. One possible explanation for this is that the platinum substrate is not as easily fluorinated as the other substrates. Thus, formation of volatile products is more difficult. The smaller production of $CF_2$ could also be attributed to the catalytic action of Pt with one of the beam species (e.g. $CF_3$ radicals). This seems plausible as platinum is know to activate C-F bonds in a variety of organic and organometallic complexes.[40]

While difluorocarbene radicals are generated when 100% $C_2F_6$ plasmas interact with most materials, they are neither produced nor generated at the plasma-PTFE interface. Here, the flux of $CF_2$ radicals incident on the substrate is essentially the same as the flux of $CF_2$ leaving the substrate, $S = 0.98 \pm 0.03$. This is likely a function of the nature of the PTFE substrate, which is a fully fluorinated, relatively inert material. Since there is no net film deposition in this system, and PTFE is very resistant to F atom etching,[41] we observe a low reactivity and near unity scattering for $CF_2$ radicals.

One possible mechanism of $CF_2$ surface generation is ion assisted sputtering of the deposited fluorocarbon adlayer.[3,24] Here we directly demonstrate that this type of process is partly responsible for the production of difluorocarbene at the substrate surface. When a grounded mesh screen removed ions from the 100% $C_2F_6$ molecular beam, Fig. 5.3, the scatter coefficient of $CF_2$ decreases from 1.44 to 1.07. This phenomenon is discussed further in the HFPO section below.

50/50 $C_2F_6/H_2$ PLASMAS. The dependence of relative $CF_2$ densities on rf power is different in this system compared to that observed in the 100% $C_2F_6$ rf discharge. A

linear increase in $CF_2$ signal with rf power (slope≈4.1) is observed up to 80 W followed by a decrease at higher powers. The increase in relative $CF_2$ densities, however, is more dramatic than for 100% $C_2F_6$, as shown by the larger slope. There are two possible explanations for the faster increase in steady state $CF_2$ density in the $C_2F_6/H_2$ system. First, it is well known that the addition of hydrogen quenches reactant F atoms, thereby preventing recombination pathways of $CF_x$ (x = 1-3) radicals.[42] Second, the reaction of H atoms with $CF_3$ radicals to produce $CF_2$ and HF is known to progress at a significant rate ($k = 8.9 \pm 1.8 \times 10^{-11}$ $cm^3$ $s^{-1}$).[43] This reaction may explain the reduction in $CF_2$ intensity at P > 80 W, where the density of $CF_3$ radicals is lower due to increased dissociation. Thus, depletion of gas-phase $CF_3$, and not the direct removal of $CF_2$ results in the observed $CF_2$ density trend. This observation is also supported by kinetics studies which show that the reaction of $CF_2$ with H atoms to form CF and HF is relatively slow ($k = 1.65 \pm 0.40 \times 10^{-13}$ $cm^3$ $s^{-1}$),[43] whereas the reaction of $CF_3$ with $H_2$ is relatively rapid ($2.56 \pm 0.7 \times 10^{-11}$ $cm^3$ $molecule^{-1}$ $s^{-1}$).[44]

The $CF_2$ scatter coefficients determined for Si, $SiO_2$, polyimide and PTFE substrates exposed to the 50/50 $C_2F_6/H_2$ plasma also differ from what was observed in the 100% $C_2F_6$ system. First, for the first three materials, S < 1, indicating surface loss of $CF_2$. This correlates well with the highly depositing nature of the 50/50 $C_2F_6/H_2$ plasma, Fig. 5.9. Second, all scatter loss coefficients are equal to ~0.8 for Si, $SiO_2$ and polyimide. This lack of substrate dependence is caused by the presence of deposited fluorocarbon material, comparable to what was observed for $CHF_3$ plasmas.[3,6] Interestingly, we do observe large production of difluorocarbene on PTFE substrates ($S = 1.69 \pm 0.03$). Some

of the $CF_2$ generated at the PTFE surface must come from the film deposited there. The rest is most likely produced through etching of the substrate's polymeric network by hydrogen. H atoms can scavenge F atoms from the PTFE substrate decreasing the inertness of the material and allowing $CF_2$ species to be etched. Egitto et al. have proposed that fluorine abstraction from the polymer surface would lead to scission of the polymer chains,[45,46] resulting in the formation of $CF_2$ radicals and the high $S$ value obtained in this system.

HFPO PLASMAS. The qualitative behavior of $CF_2$ radicals in HFPO plasmas closely resembles observations made for depositing systems such as $C_2F_6/H_2$ and $CHF_3$ plasmas in that there is no dependence of the difluorocarbene scatter coefficients on substrate material.[3,6] However, for all substrates, $S \geq 1$, unlike what was seen for the 50/50 $C_2F_6/H_2$ system, where $S < 1$ for Si, $SiO_2$, and polyimide materials. This difference in $CF_2$ production correlates well with deposition rates observed for HFPO and 50/50 $C_2F_6/H_2$ plasmas.[3,8] For a 25W CW HFPO plasma, the deposition rate is ~7 Å/min, much smaller than the ~200 Å/min rate observed at 40W in a $C_2F_6/H_2$ system.[3,8] If gas phase $CF_2$ groups are directly involved in film formation at the substrate surface, a faster deposition rate corresponds to a higher fraction of difluorocarbene radicals being lost at the substrate surface.

While this type of behavior is observed for the three plasma systems discussed in this work, the correlation between film deposition and $CF_2$ radical reactivity is not as easily understood for the $CHF_3$ system.[6] In $CHF_3$ plasmas, film deposition rates are fairly high, but difluorocarbene scatter coefficients > 1.5 were measured. One possible

explanation is that in the $CHF_3$ system, $CF_2$ is not a major film precursor. Another possibility is that there are $CF_2$(g) surface generation mechanisms that are inactive in the three FCPs discussed here that are active in the $CHF_3$ system. One such mechanism is F atom abstraction from the surface of the film by gas phase CF radicals to form $CF_2$(g) groups. We have previous reported the scatter coefficient of CF radicals interacting with a Si surface during $CHF_3$ plasma processing is ~0.6.[6] This shows that surface loss of CF molecules occurs in this system and may result in $CF_2$(g) production through CF radical recombination reactions.

Very interesting behavior was also observed for difluorocarbene *S* values when ions were eliminated from the HFPO molecular beam via a grounding mesh. *S* decreased by ~0.17-0.36 (35 W- 135 W) to a value of ~0.8 for all applied rf powers, Table 5.2. Thus, removal of ions eliminates ion assisted film sputtering and lowers $CF_2$ surface production, similar to what was observed in the 100% $C_2F_6$ plasma. In the $C_2F_6$ system, however, ion removal did not lead to loss of $CF_2$ at the substrate surface as indicated by *S* = 1.07 determined in the grounded mesh experiments. In contrast, when ions were eliminated from the HFPO molecular beam, loss of $CF_2$ at the substrate surface occurred, as indicated by $S < 1$. This shows that ion-assisted sputtering plays a significant role in $CF_2$ surface production in both plasmas, but that eliminating ions does not cause difluorocarbene surface loss in etching systems such as $C_2F_6$ plasmas.

To further substantiate the role of ion impact on fluorocarbon material polymerization in HFPO plasmas, the substrate was biased at +200 V. Again, $CF_2$ surface loss coefficients decreased to ~ 0.8, Table 5.2. The large positive substrate bias prevents

the positively charged species from colliding with the surface, eliminating ion-assisted sputtering of $CF_2$. Interestingly, $S$ is equal to ~0.8 in both cases discussed above, suggesting that ions are removed in equal amounts. Theoretical studies performed by Graves and coworkers for $CF_3^+$ ions impinging on a Si surface showed that ~30% of the ions desorbed as $CF_2$ radicals.[47] This value is close to the decrease observed for scattered $CF_2$ radicals when ionic species were prevented from colliding with the substrate surface. Thus, it is possible that a fraction of $CF_3^+$ ions in our experiments undergo dissociative adsorption at the substrate surface followed by $CF_2$ desorption.

For CW HFPO plasma experiments where a grounded mesh was not utilized, the higher rf powers generated the highest levels of scattered $CF_2$, $S = 1.16 \pm 0.02$ and $S = 1.27 \pm 0.07$, respectively. For comparison, the scatter coefficient was $0.97 \pm 0.03$ for a 35W CW HFPO plasma. The use of high rf powers has a twofold effect on the ion population in the plasma: 1) the ion density increases, and 2) higher energy ions are generated. Consequently, at these applied powers, the substrate surface is bombarded by larger numbers of energetic ionic species than at lower rf powers, accounting for an increased degree of ion-assisted sputtering of the deposited fluorocarbon film. In contrast, when ions are removed by the grounded mesh, or repelled by the substrate positive bias, there are no significant differences between the $CF_2$ $S$ values obtained at 35 W, 135 W, and 200 W because ion-assisted sputtering is eliminated from the experiment.

As noted in the Introduction, previous studies in our labs found significant differences between the fluorocarbon materials deposited with CW and pulsed HFPO plasmas.[7,8] Pulsing the plasma can reduce ion effects on film deposition if their decay

pathways alter during the time off periods.[48,49] Ions have shorter lifetimes than plasma neutral species, and consequently most of them undergo fast recombination reactions during the off time period of the plasma modulation, while neutral molecules remain involved in deposition processes at the substrate surface. Consistent with this, $CF_2$ scatter coefficients measured in pulsed $C_2F_6$ plasmas were lower than those observed in CW systems.[24] The *S* values determined from pulsed HFPO plasma experiments also provide a compelling argument in favor of reduced ion effects in pulsed plasmas. Table 5.3 shows that pulsed plasma $CF_2$ scatter values are smaller than those observed in CW HFPO discharges but are equal to those measured for CW plasmas with a grounded mesh or with a positively biased Si substrate, Table 5.2. Note that the composition of materials deposited in pulsed HFPO plasmas is virtually identical to that of films generated under CW conditions where the ions were removed, Figs. 5.10b and 5.10c. This shows that just as with $C_2F_6$ and $C_2F_6/H_2$ plasmas, a clear connection between $CF_2$ radical reactivity and the type of material deposited is observed in HFPO systems

## 5.4. SUMMARY

This work shows that $CF_2$ radicals behave differently in FCPs based on the regime to which the plasma belongs, etching or depositing. In the 100% $C_2F_6$ system, although a thin fluorocarbon polymer is formed on the substrates, the dominant process occurring at the surface is etching. Thus, we see a marked substrate dependence for $CF_2$ scatter coefficients measured in 100% $C_2F_6$ plasmas. In addition, for all substrates except PTFE, $CF_2$ surface generation was observed ($S > 1$). In contrast, we observed surface loss of

$CF_2$ radicals when $H_2$ was added to the $C_2F_6$ feed gas coupled with fast deposition rates of amorphous film on the substrates processed. We attribute these changes to a shift in the etching/deposition balance towards the latter regime caused by hydrogen-fluorine interactions absent in 100% $C_2F_6$ plasmas. Finally, HFPO plasmas were found to deposit films downstream from the rf coil with high $CF_2$ content and low degree of crosslinking. Unlike in 50/50 $C_2F_6/H_2$ plasmas, all rf powers under CW conditions resulted in $CF_2$ surface production. However, the deposition rates of these films were much lower than those observed for the 50/50 $C_2F_6/H_2$ system, which shows that HFPO plasmas are shifted towards the etching regime more than 50/50 $C_2F_6/H_2$ systems. The decreased *S* values obtained when ions were removed from the plasma molecular beam for both $C_2F_6$ and HFPO systems, clearly demonstrate that some of the difluorocarbene surface production is caused by ion assisted sputtering.

Although ions play significant roles in surface processes for all three plasma systems, it is the gas phase chemistry which determines the regime to which the discharge belongs. In this work we have shown that monitoring $CF_2$ radicals can provide a reliable gauge for identifying the regime to which FCPs belong: $S \gg 1$ is prevalent for etching systems ($C_2F_6$), $S \geq 1$ for slower depositors with ions present (HFPO), and $S < 1$ for faster depositors (50/50 $C_2F_6/H_2$), or slow depositors without ions present (HFPO).

## 5.5. REFERENCES


1. H. Yasuda, *Plasma Polymerization*, Academic Press, New York, 1985.

2. F. Yamagishi, D. D. Granger, A. E. Schmitz, and L. J. Miller, *Thin Solid Films* **84**, 427 (1981).

3. N. M. Mackie, V. A. Venturo, and E. R. Fisher, *J. Phys. Chem. B* **101**, 9425, (1997).

4. N. M. Mackie, D. G. Castner, and E. R. Fisher, *Langmuir* **14**, 1227, (1998).

5. M. A. Leich, N. M. Mackie, K. L. Williams, and E. R. Fisher, *Macromolecules* **31**, 7618, (1998).

6. N. E. Capps, N. M. Mackie, and E. R. Fisher, *J. Appl. Phys.* **84**, 4736 (1998).

7. C. I. Butoi, N. M. Mackie, J. E. Barnd, L. J. Gamble and D. G. Castner, and E. R. Fisher *Chem. Mater.* **11**, 862 (1999).

8. C. I. Butoi, N. M. Mackie, L. J. Gamble and D. G. Castner, J. E. Barnd, A. M. Miller, and E. R. Fisher, *Chem. Mater.* **12**, 2014-2024 (2000).

9. K. Endo, *Mat. Res. Soc. Bull.* **22,** 55 (1997), and references therein.

10. F. Neuilly, G. Cunge, J. P. Booth, and N. Sadeghi, "Frontiers in Low Temperature Plasma Diagnostics II", Bad Honnef, Germany, (1997).

11. G. Cunge, and J. P. Booth, *J. Appl. Phys.* **85,** 3952 (1999).

12. R. d'Agostino, F. Cramarossa, F, Fracassi, and F. Illuzzi, in *Plasma Deposition Treatment and Etching of Polymers*, R. d'Agostino, Ed., Academic Press, San Diego, 1990, pp. 95-162.

13. R. D'Agostino, F. Cramarossa, V. Colaprico, and R. d'Ettole, *J. Appl. Phys.* **54**, 1284 (1983).

14. M. M. Millard and E. Kay, *J. Electrochem. Soc.* **129**, 160 (1982).

15. C. R. Savage, and R. B. Timmons, *Chem. Mater.* **3**, 575 (1991).

16. S. J. Limb; D. J. Edell, E. F. Gleason, and K. K. Gleason, *J. Appl. Polym. Sci.* **67**, 1489 (1998).

17. S. G. Hansen, and G. Luckman, *J. Appl. Phys.* **68**, 2013 (1990).

18. A. D. Tserepi, J. Derouard, J. P. Booth, and N. Sadeghi, *J. Appl Phys.* **81**, 2124 (1997).

19. M. A. Lieberman and A. J. Lichtenberg, *Principles of Plasma Discharges and Material Processing*; Wiley and Sons, New York, 1994.

20. X. Li, M. Schaepkens, S. Oehrlein, R. E. Ellefson, L. C. Frees, N. Mueller, and N. Korner, *J. Vac. Sci. Technol. A.*, **17**, 2438 (1999).

21. K. L. Williams, C. I. Butoi, and E. R. Fisher, manuscript in preparation.

22. P. R. McCurdy, K. H. A. Bogart, N. F. Dalleska, and E. R. Fisher, *Rev. Sci. Instrum.* **68**, 1684 (1997).

23. N. M. Mackie, N. E. Capps, and E. R. Fisher, *Fluorinated Polymers, Surfaces and Films, ACS Symp. Proc.*, in press.

24. C. I. Butoi, N. M. Mackie, P. R. McCurdy, J. H. D. Peers, and E. R. Fisher, *Plasmas Polym.* **4**, 77 (1999).

25. C. W. Mathews, *Can. J. Phys.* **45**, 2355 (1967).

26. M. R. Cameron, S. H. Kable, and G. B. Bacskay, *J. Chem. Phys.* **103**, 4476 (1995).

27. C. Wang, C. Chen, J. Dai, and X. Ma, *Chem. Phys. Lett.* **288**, 473 (1988).

28. P. J. Hargis, and M. J. Kushner, *Appl. Phys. Lett.* **40**, 779 (1982).

29. M. Kitamura, H. Akiya, and T. Urisu, *J. Vac. Sci. Technol. B* **7**, 14 (1989).

30. N. M. Mackie, "Investigation of Mechanisms for Plasma Polymerization of Organic Thin Films", Doctoral Thesis, Colorado State University (1998).

31. R. T. Conley, in *Infrared Spectroscopy*, Allyn & Bacon, Boston, 1966.

32. T. Masuoka, and H. Yasuda, *J. Polym. Sci.: Polym. Chem.* **20**, 2633 (1982).

33. A background spectrum of this wafer, taken prior to processing, was subtracted from the experimental spectrum. This should account for the presence of any native oxide present on the substrate.

34. D. F. O'Kane, and D. W. Rice, *J. Macromol. Sci. Chem. A* **10**, 567 (1976).

35. H. C. Barshilia, B. R. Mehta, and V. D. Vankar, *J. Mater. Res.* **11**, 2852 (1996).

36. R. W. Pearse, and A. G. Gaydon, *The Identification of Molecular Spectra*, Chapman & Hall, London, 1965.

37. (a) J. G. Langan, J. A. Shorter, X. Xin, S. A. Joyce, and J. I. Steinfeld, *Surf. Sci.* **207,** 344 (1989); (b) J. W. Thoman, Jr., K. Suzuki, S. H. Kable, and J. I. Steinfeld, *J. Appl. Phys.* **60,** 2775 (1986); (c) S. Joyce, J. G. Langan, and J. I. Steinfeld, *J. Chem. Phys.* **88,** 2027 (1988).

38. D. C. Gray, H. H. Sawin, and J. W. Butterbaugh, *J. Vac. Sci. Technol. A* **9**, 779 (1991).

39. J. W. Butterbaugh, D. C. Gray, and H. H. Sawin, *J. Vac. Sci. Technol. B* **9**, 1461 (1991).

40. M. Crespo, and M. Martinez, J. Sales, *Organometallics* **12,** 4297 (1993).

41. F. D. Egitto, V. Vukanovik, and G. N. Taylor, in *Plasma Deposition, Treatment and Etching of Polymers*; R. d'Agostino, Ed., Academic Press, San Diego, 1990, pp. 321-422.

42. J. P. Booth, G. Hancock, N. D. Perry, D. C. W. Blaikley, J. A. Cairns, and R. Smailes, *Mat. Res. Soc. Symp Proc.* **98**, 135 (1987).

43. K. R. Ryan, and I. C. Plumb, *Plasma Chem. Plasma Process.* **4**, 141 (1984).

44. J. Hranisavljevic, and J. V. Michael, *J. Phys. Chem.* **102**, 7668 (1998).

45. F. D. Egitto, *Pure Appl. Chem.* **62,** 1699 (1990).

46. N. Inagaki, *Plasma Surface Modification and Plasma Polymerization*, Technomic, Lancaster, (1996).

47. C. F. Abrams and D. B. Graves, *J. Appl. Phys.* **86**, 5938 (1999).

48. V. Panchalingam, X. Chen, C. R. Savage, R. B. Timmons, and R. C. Eberhart, *J. Appl. Polym. Sci., Polym. Symp.* **54,** 123 (1994).

49. C. L. Rinsch, X. Chen, V. Panchalingam, R. C. Eberhart, J. H. Wang, and R. B. Timmons, *Langmuir* **12,** 2995 (1996).

# CHAPTER 6

## $NH_2$ RADICAL SCATTER AND TRANSLATIONAL TEMPERATURE STUDIES IN $NH_3$ GLOW DISCHARGES

This chapter contains the manuscript of a full paper submitted for publication to the *Journal of Physical Chemistry B*. The paper coauthors are M. L. Steen, J. R. D. Peers, and E. R. Fisher. The interactions of $NH_2$ radicals with polymeric, metallic and silicon substrates during $NH_3$ plasma processing are investigated. $NH_2$ scatter coefficients and scattered $NH_2$ translational temperatures are determined. By correlating the two, insight into the types of reactions occurring at the substrate surface is gained. Plasma ions are shown to significantly influence the behavior of $NH_2$ radicals at the plasma-substrate interface.

## 6.1. INTRODUCTION AND BACKGROUND

Ammonia plasmas have a wide range of applications in modifying surfaces for specific uses.[1] Previous work has shown that $NH_3$ plasma treatment of polymers can result in improved adhesion and higher wettability relative to the untreated surfaces.[2,3,4] Modification occurs via implantation of amine functionalities, which are hydrophilic and have been shown to facilitate the preparation of blood compatible substrates.[5,6] Ammonia-based glow discharges have also been used to apply nitride passivation layers on polycrystalline silicon and GaAs in integrated circuit manufacture.[7,8] Additional uses of $NH_3$ plasmas include preparation of metal nitride layers and sensor materials.[9]

A number of studies investigating the effects of $NH_3$ plasma treatment on surface properties have been published. For example, processing of hydrocarbon polymers with $NH_3$ rf discharges has been studied extensively.[10,11,12] Griesser and coworkers investigated the treatment of perfluorinated polymers with $NH_3$ plasmas and found that treated fluorinated ethylene propylene and polytetrafluoroethylene (PTFE) exhibited high wettability immediately after treatment.[2] They believe this high wettability is caused by radical incorporation into the treated polymer which subsequently leads to oxidative reaction initiation following $NH_3$ plasma exposure.[13] Additional studies showed that amine group incorporation occurs upon $NH_3$ plasma treatment of polymers, but exposure to air results in a decrease in amine concentration and an increase in amide group content.[14] This results in a loss of hydrophilicity upon aging. We have found similar effects with $NH_3$ plasma treatment on metallic and polymeric substrates, most notably that the hydrophilicity gained by the treated substrates was virtually lost after a period of three

weeks. d'Agostino and coworkers also investigated $NH_3$ plasmas and discovered that amine surface concentration in treated polyethylene can be tuned relative to other N-containing groups by adjusting plasma parameters.[15] While these results provide insight into the surface modifications that occur upon exposure to $NH_3$ plasmas, a complete understanding of surface alteration mechanisms in these systems has not been achieved.

As the above studies demonstrate, it is generally believed that radical species in $NH_3$ plasmas play significant roles in surface modification processes.[16,17,18] Unfortunately, the complexity of glow discharge systems renders the study of specific radical-surface interactions difficult. One of the few techniques which surmounts this problem is the imaging of radicals interacting with surfaces (IRIS) technique which combines laser induced fluorescence (LIF) and dynamic imaging techniques to gain information on specific plasma radicals as they interact with a substrate surface.[19,20] Using IRIS, we have investigated a number of different plasma species. It is instructive to discuss recent results from our extensive IRIS studies of the difluorocarbene molecule in a variety of fluorocarbon glow discharges. The interactions of $CF_2$ with a variety of substrates were investigated for fluorocarbon plasmas such as $C_2F_6$ and $C_2F_6/H_2$,[21,22] $CHF_3$,[23] and hexafluoropropylene oxide (HFPO).[24,25] As discussed in Chapter 5, these studies show that $CF_2$ radicals display different behavior in etching and depositing plasma systems. Specifically, larger amounts of difluorocarbene were produced at the substrate surface under etching conditions than under depositing conditions. In addition, the elimination of ion bombardment during HFPO plasma processing resulted in loss (consumption) of $CF_2$ radicals at the substrate surface along with deposition of highly oriented, high $CF_2$-content

materials.[26,26,27]

We have also published IRIS results on $NH_2$ radical interactions in $NH_3$ glow discharges.[28,29] The first of these studies demonstrated that IRIS could be used to measure the translational temperature of $NH_2$ radicals in a $NH_3$ plasma molecular beam, $\Theta_{Tmb}$. Moreover, $\Theta_{Tmb}$ for $NH_2$ was shown to increase linearly with applied rf power.[29] In the second study, scatter coefficients and translational temperature data on $NH_2$ radicals scattering from substrates were presented.[30] Although this latter study clearly demonstrated that the IRIS technique can be used in conjunction with Monte Carlo simulation methods to determine the velocity profiles of scattered $NH_2$ radicals, the amount of data presented was limited. Indeed, the majority of the data were collected for one rf power, and ion effects were essentially unexplored. Thus, we undertook the present work in an effort to gain a deeper understanding of surface modification mechanisms during $NH_3$ plasma processing.

Here we present a systematic investigation of $NH_2$ radicals in $NH_3$ plasmas. Different types of substrates (i.e. metals, polymers, and semiconductors) were studied while applied rf power, $P$, was varied between 50 W and 175 W. In addition, we directly investigate the effects of ion bombardment on both $NH_2$ surface reactivity and scattered $NH_2$ velocity, $\Theta_{Tsc}$. These data provide the basis for a discussion of possible surface interaction mechanisms for the different substrates examined.

## 6.2. RESULTS

We have previously reported the spectroscopy of $NH_2$ radicals in the $NH_3$ system from our IRIS instrument.[29,30] As with our previous work, the majority of data presented here were collected using the intense line at 597.725 nm, which contains three overlapping rotational transitions ($3_{03}$-$3_{13}$, $4_{04}$-$4_{14}$, and $5_{05}$-$5_{15}$). The data are presented in two categories: (A) surface reactivity or scatter coefficients for $NH_2$ radicals using a variety of substrates; and (B) velocity distributions which have been converted to translational temperatures of the scattered $NH_2$ radicals using the same substrates.

### 6.2.1. SCATTER COEFFICIENTS OF $NH_2$ RADICALS

Figure 6.1 shows a series of three spatially resolved LIF images of $NH_2$ radicals interacting with a polyimide surface using a 75 W CW $NH_3$ plasma. In Fig. 6.1a, the substrate is rotated out of the path of the molecular beam, and only incident $NH_2$ radicals are imaged. In Fig. 6.1b, the substrate was rotated into the path of the $NH_3$ plasma molecular beam, and thus, both incident and scattered $NH_2$ radicals are imaged. Figure 6.1c displays the LIF signal due to scattered $NH_2$ radicals only, and is obtained by subtracting Fig. 6.1a from Fig. 6.1b. As was seen previously,[25,30] there is clearly a significant amount of $NH_2$ scattering from the polyimide substrate.

Figure 6.2a shows the 1-D cross sections corresponding to the ICCD images in Fig. 6.1a and 6.1c. The broad spatial distribution combined with the shift from the molecular beam maximum intensity position are indicative of an adsorption-desorption mechanism for the scattered $NH_2$. Also shown in Fig. 6.2a are the simulated 1-D

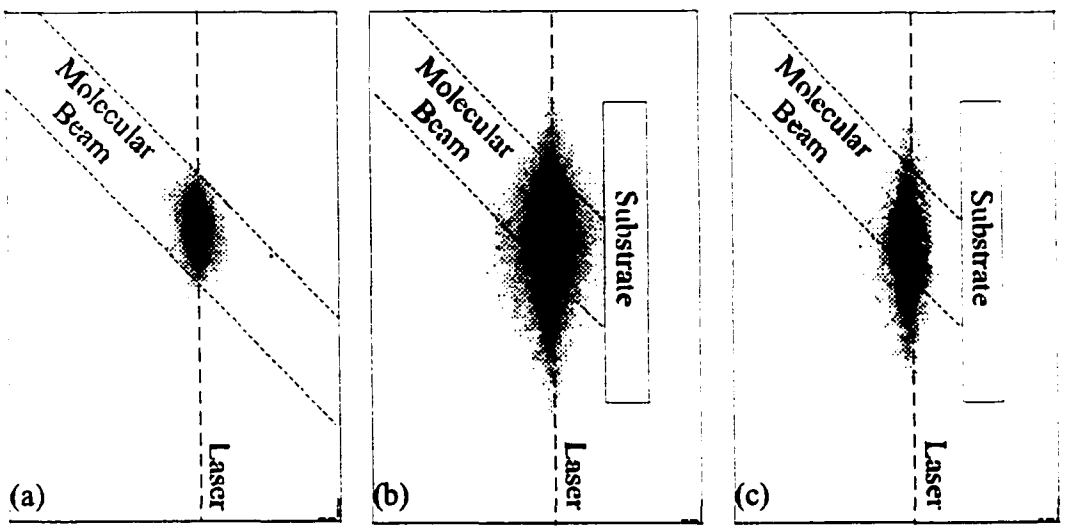


**Figure 6.1.** Spatially resolved two-dimensional ICCD images of the LIF signal for the $NH_2$ $3_{03}$-$3_{13}$, $4_{04}$-$4_{14}$, $5_{05}$-$5_{15}$ rovibronic bands of the $NH_2$ $X^2B_1$ - $A^2A_1$ electronic transition in (a) 75 W CW$NH_3$ molecular beam (no substrate) and (b) with a 300K polyimide substrate rotated into the path of the molecular beam at a laser surface distance of 2.7 mm. (c) Difference between the images shown in (a) and (b) displaying only $NH_2$ molecules scattering from the surface.

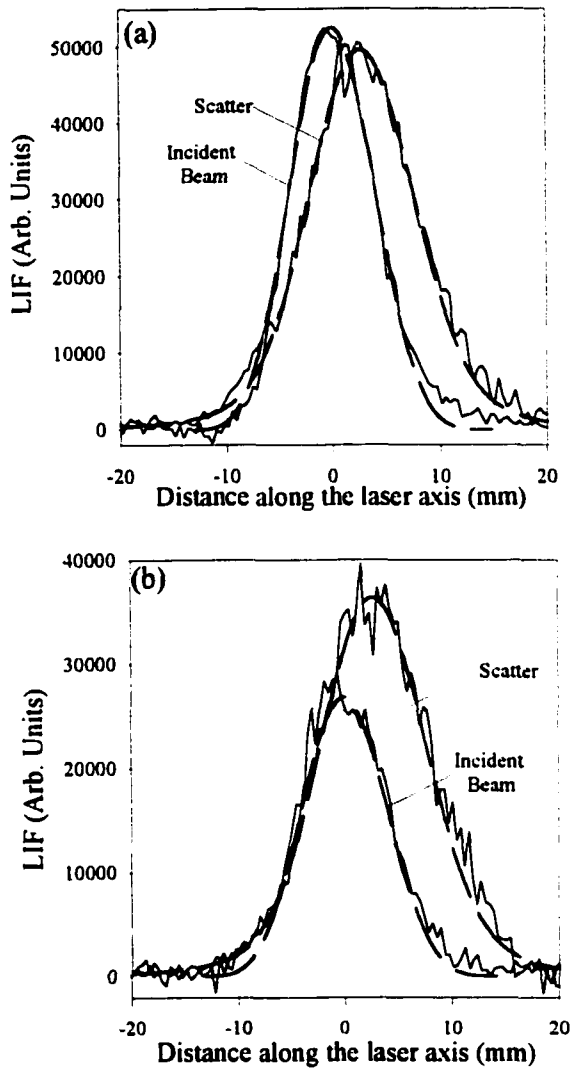


**Figure 6.2.** (a) Cross-sectional data for the LIF of $NH_2$ in the incident molecular beam and scattered from the polyimide substrate using a 75 W CW $NH_3$ plasma molecular beam. The laser-surface distance is 2.7 mm. Dashed lines represent the simulated curves from the geometric model, assuming $S \approx 1.09 \pm 0.05$ and adsorption-desorption scattering. (b) Cross-sectional data for the LIF of $NH_2$ in the incident molecular beam and scattered from a polyimide surface using a 150 W CW $NH_3$ molecular beam. The laser surface distance is 2.7 mm. Dashed lines represent the simulated curves from the geometric model assuming $S \approx 1.7 \pm 0.07$

profiles for the incident beam and scattered radicals. In this case, the best fit is obtained for a scatter coefficient, $S = 1.38 \pm 0.05$, which becomes $S = 1.09 \pm 0.05$ after scaling. Figure 6.2b displays the experimental and simulated 1-D cross-sections for incident and scattered $NH_2$ radicals generated at the polyimide substrate using a 150 W $NH_3$ plasma. Here, the intensity of the scatter signal is clearly larger than with the 75 W plasma, and, when modeled, yields $S = 1.98 \pm 0.07$ before scaling and $S = 1.7 \pm 0.07$ after scaling.. It is important to note that Doppler effects were previously investigated for this system and found to be insignificant (< 0.002 nm at 600 nm excitation wavelength).[30] Thus, these effects were not included in determining $S$ values here.

Scatter coefficient values obtained for different substrate materials (Si, Pt, polyimide, Cu, and PTFE) and different applied rf powers (50 -175 W) are shown in Table 6.1. The $S$ dependence on rf power for these substrates is clearly shown in Figure 6.3. Both metals, Pt and Cu, exhibit similar interactions with $NH_3$ plasmas. A relatively small increase in $S$ occurs as the rf power increases from 50 W to 125 W, followed by a leveling off at higher powers, Fig. 6.3a. In contrast, a more significant increase in $S$ is observed for $NH_2$ radicals desorbing from the polyimide, PTFE and Si substrates, Fig. 6.3b.

*Ion effects on $NH_2$ scatter coefficients.* To investigate the role of ion bombardment in the significant $NH_2$ surface generation observed at the polyimide substrate, ions were removed from the incident molecular beam by placing a grounded mesh screen on the last defining slit.[26,30] The term "ion-free" is used below to describe data taken with this configuration. With the grounded mesh in place, $NH_2$ scatter coefficients were again measured. Figure 6.4 shows the 1-D profiles (experimental and simulated) for polyimide

**Table 6.1** $NH_2$ scatter coefficients for CW $NH_3$ plasma processing

| | Substrate | | | | | | |
|---|---|---|---|---|---|---|---|
| **Power (W)** | Cu | Platinum | Platinum (gm) | Silicon | Polyimide | Polyimide (gm) | PTFE |
| **50** | 1.08 ± 0.05 | 1.10 ± 0.07 | 0.78 ± 0.05* | 1.29 ± 0.05 | 0.82 ± 0.08 | 0.72 ± 0.02 | 1.34 ± 0.09 |
| **75** | 1.08 ± 0.06 | 1.08 ± 0.04 | 0.91 ± 0.03 | 1.39 ± 0.05 | 1.08 ± 0.01 | 0.77 ± 0.07 | 1.40 ± 0.05 |
| **100** | 1.20 ± 0.08 | 1.16 ± 0.03 | 0.94 ± 0.03 | 1.34 ± 0.07 | 1.29 ± 0.03 | 1.0 ± 0.04 | 1.38 ± 0.1 |
| **125** | 1.35 ± 0.06 | 1.21 ± 0.03 | 1.00 ± 0.03 | 1.53 ± 0.09 | 1.45 ± 0.03 | 1.02 ± 0.05 | 1.74 ± 0.06 |
| **150** | 1.33 ± 0.05 | 1.23 ± 0.04 | 1.00 ± 0.06* | 1.70 ± 0.05 | 1.71 ± 0.11 | 1.14 ± 0.1 | 1.64 ± 0.08 |
| **175*** | 1.42 ± 0.09 | 1.20 ± 0.1 | 1.00 ± 0.09 | 1.84 ± 0.03 | 1.70 ±0.03 | 1.20 ± 0.1 | 2.25 ± 0.06 |

* Scatter velocity used to calculate the scaling factor was determined from linear regression.

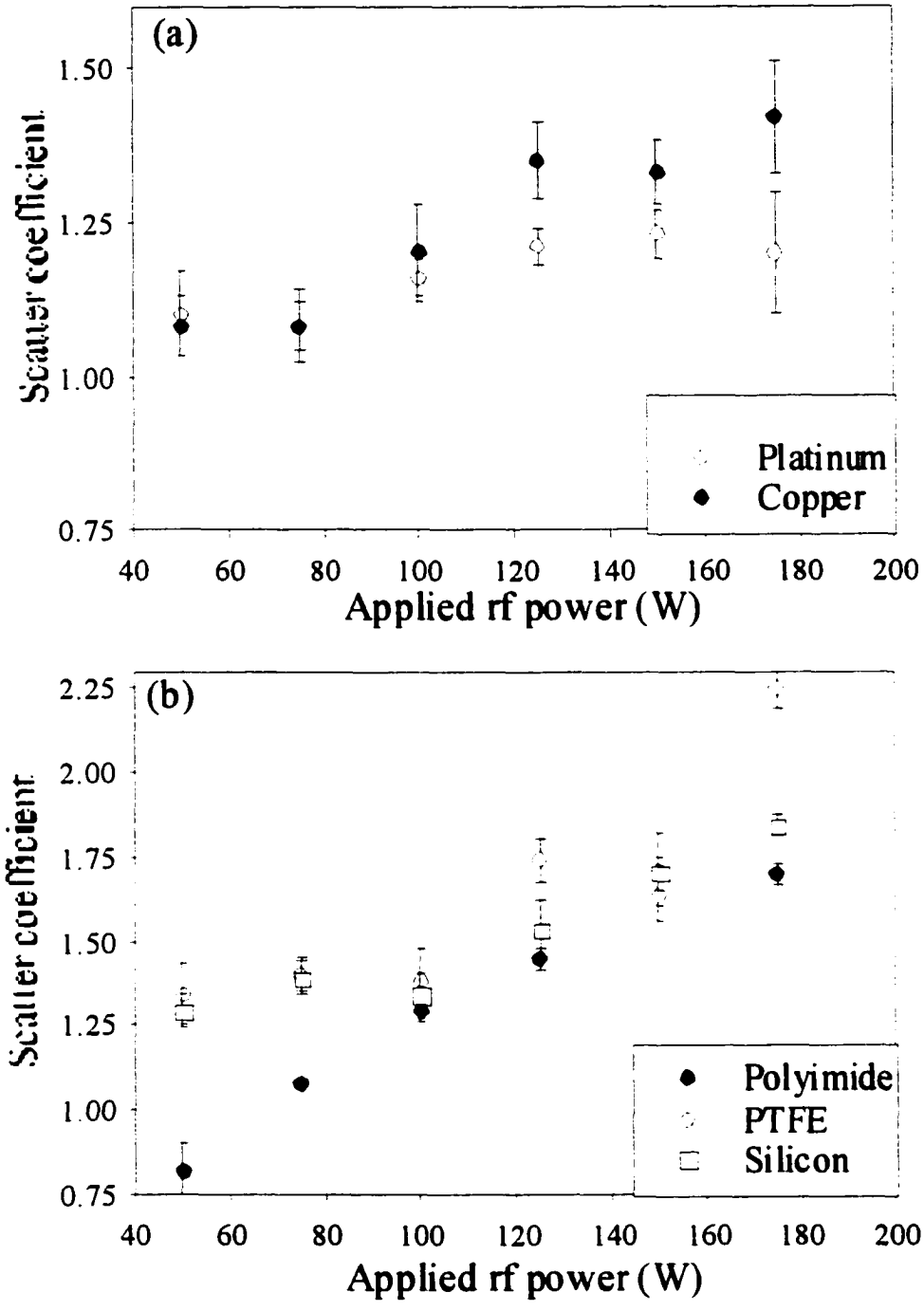


**Figure 6.3.** Substrate material and $NH_3$ plasma power effects on scattered of $NH_2$ radicals. The substrates investigated were (a) Pt and Cu, and (b) polyimide, PTFE, and Si. The applied power ranged between 50 W and 175 W.

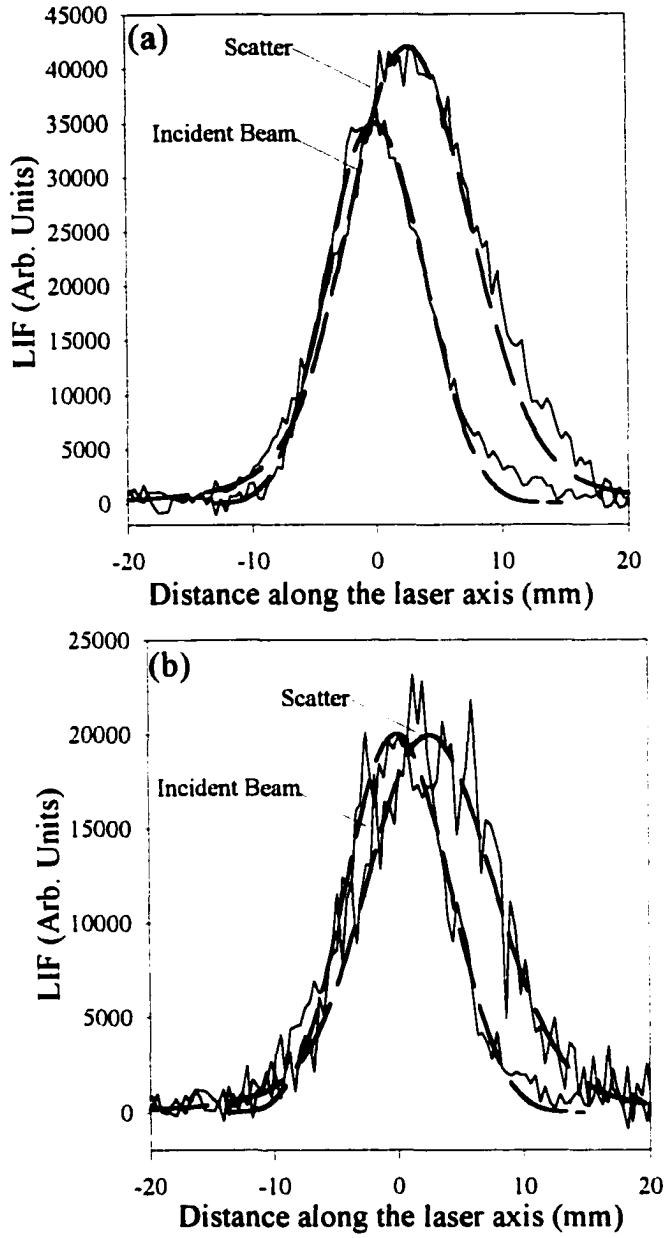


**Figure 6.4**. (a) 1-D profiles (experimental and simulated) for polyimide substrates processed with a 125 W $NH_3$ plasma with ions present at a laser-surface distance of 2.7 mm. The best scatter fit is obtained for $S = 1.44 \pm 0.05$. (b) $NH_2$ radical 1-D profiles when ions were removed from the molecular beam with a grounding mesh. The scatter coefficient decreased to $1.03 \pm 0.08$. Laser-surface distance was measured at 2.6 mm.

substrates processed with a 125 W $NH_3$ plasma with and without ions present. Without the grounded mesh screen (i.e. ions were present), the data are best fit with $S = 1.75 \pm 0.05$, Fig. 6.4a, which becomes $S = 1.44 \pm 0.05$ after scaling. In contrast, when ions were removed from the beam (i.e. with the grounded mesh), the scatter coefficient decreased to $1.4 \pm 0.08$ before scaling and $1.03 \pm 0.08$ after scaling, Fig. 6.4b. This type of decrease in $S$ upon removal of ions from the molecular beam has been observed previously for $NH_2$ radicals;[25,30] $CF_2$ radicals in fluorocarbon systems;[26] and $SiF_2$ radicals in $SiF_4$-based etching plasmas.[30]

Both ion density and ion energy in plasmas are known to increase with applied rf power.[31,32] Thus, we investigated $S$ values as a function of rf power both with and without ion bombardment. The $NH_2$ $S$ values for interactions with the polyimide and Pt substrates as a function of applied rf power are shown in Figures 6.5a and 6.5b, respectively. Interestingly, with both substates, the $S$ values are lower for all powers (50 - 175 W) when the grounded mesh was used, but they closely follow the power dependence trend observed in the experiments with ions. The decrease measured without ions in the molecular beam is more pronounced for the polyimide substrate, Fig. 6.5a, than for Pt, Fig 6.5b.

### 6.2.2. TRANSLATIONAL TEMPERATURES OF SCATTERED $NH_2$ RADICALS

Energy transfer processes between $NH_2$ radicals and plasma processed substrates were investigated through examination of velocity profiles for the scattered radicals. These data were obtained as a function of substrate material, applied rf power, and the

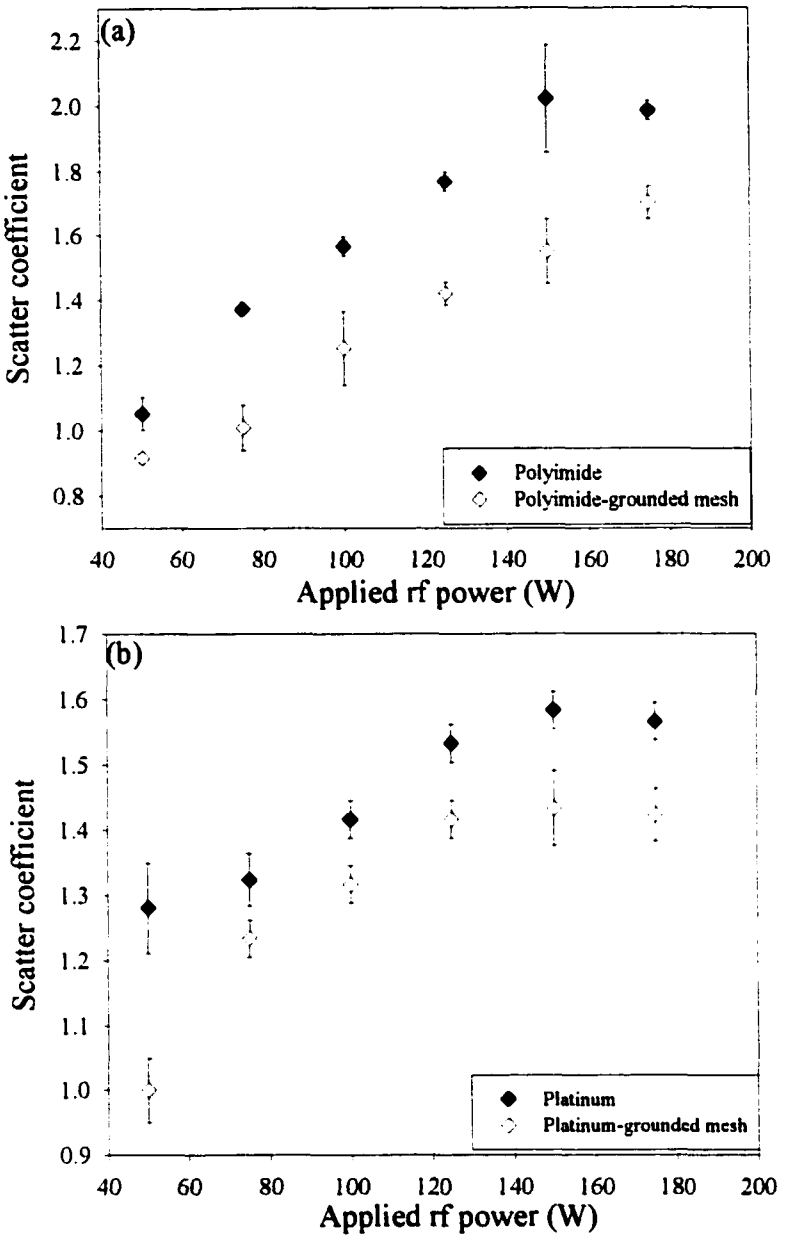


**Figure 6.5.** Ion effects on $NH_2$ *S* values for $NH_3$ interactions with a (a) polyimide and (b) platinum substrates. Scatter coefficients are determined for P = 50 -175 W in 25 W increments. (◆) ionic species were not removed from the plasma molecular beam; (◇) ions were removed by placing a grounding mesh in the path of the molecular beam.

presence of ions in the incident molecular beam.

Figure 6.6 shows a series of four ICCD images obtained at different time delays: 1.332 $\mu$s, 3.332 $\mu$s, 5.332 $\mu$s, and 7.332 $\mu$s, respectively. Only LIF signals from scattered $NH_2$ radicals are shown in these images. At the longer delay times the scattered molecules have moved along the x axis, and the intensity distribution has become broader than the ones seen at shorter delays.

Figure 6.7 shows the 1-D velocity profiles for $NH_2$ radicals scattering from a polyimide surface using a 125 W $NH_3$ plasma with no grounded mesh (i.e. with ions in the molecular beam). Also shown are the simulated 1-D curves generated with a model that assumes a cosine distribution function for scattered radicals and a Boltzmann distribution of velocities.[30] The best fit obtained for $NH_2$ scattering from a polyimide substrate under these conditions corresponded to $\Theta_{Tsc} = 450 \pm 30$ K.

Table 6.2 and Figure 6.8 show the $\Theta_{Tsc}$ values calculated for $NH_2$ scattering from the same materials used in the scatter coefficient measurements. Similar applied rf powers were also used, ranging from 50 W to 150 W. For metallic substrates such as Pt and Cu, the translational temperature does not change as the applied rf power is raised from 50 W to 150 W, Fig. 6.8a. Likewise, there is no significant rf power dependence for $\Theta_{Tsc}$ values measured using Si substrates. However, the two polymeric substrates, PTFE and polyimide, Fig. 6.8b, display a very strong dependence on the applied rf power. When $NH_2$ radicals interact with polyimide substrates, $\Theta_{Tsc}$ increases from ~330 K at 50 W to nearly 500 K at 150 W. In the case of PTFE, $\Theta_{Tsc}$ = 450 K at 50 W and is ~550 K at 150 W. These increases are nearly linear with rf power, Fig. 6.8, and demonstrate that the

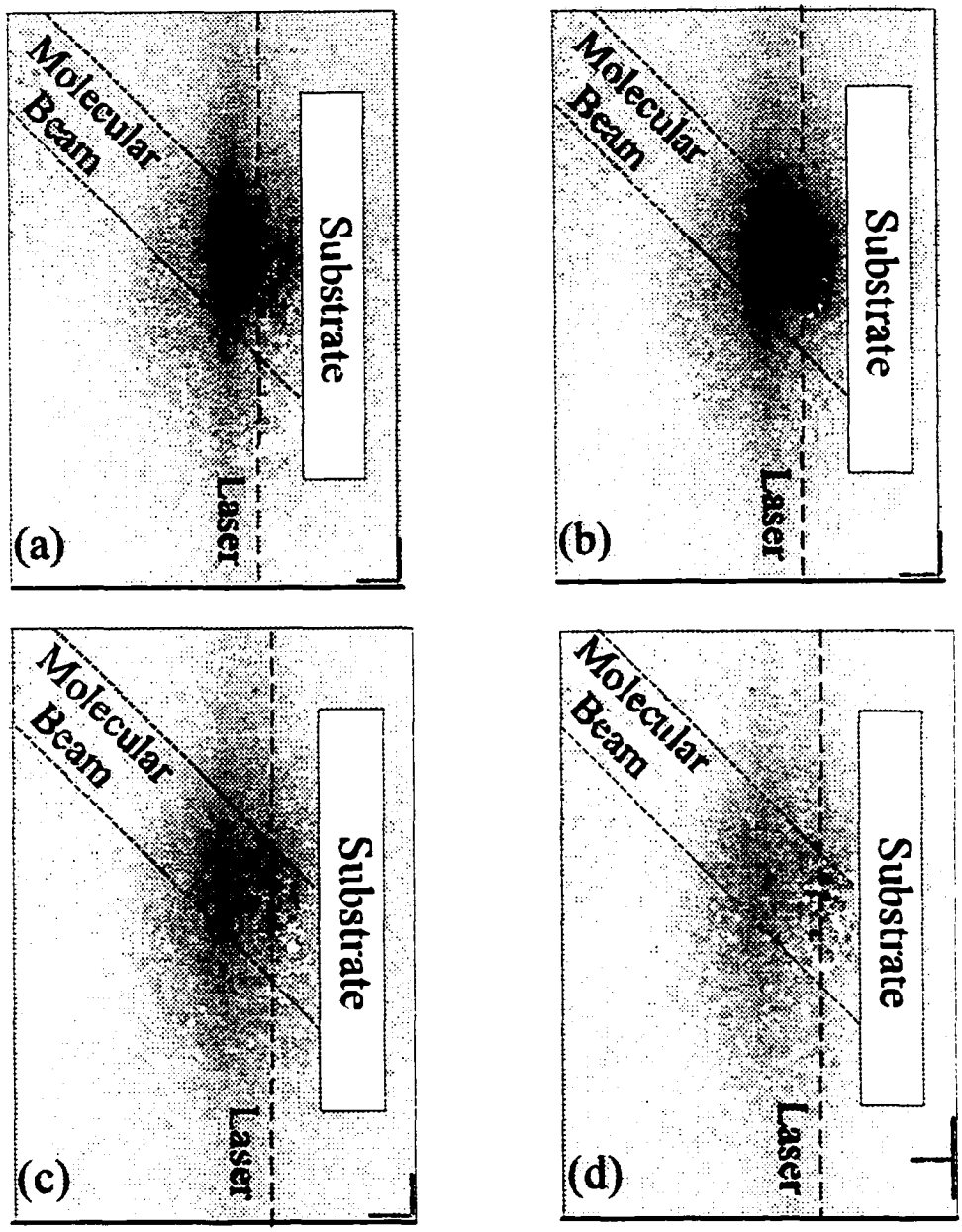


**Figure 6.6.** LIF images of $NH_2$ radicals scattered from a polyimide surface at the following time delays: (a) 1.332 $\mu$s; (b) 3.332 $\mu$s; (c) 5.332 $\mu$s; and (d) 7.332 $\mu$s. The incident molecular beam was produced from a 125 W CW $NH_3$ plasma.

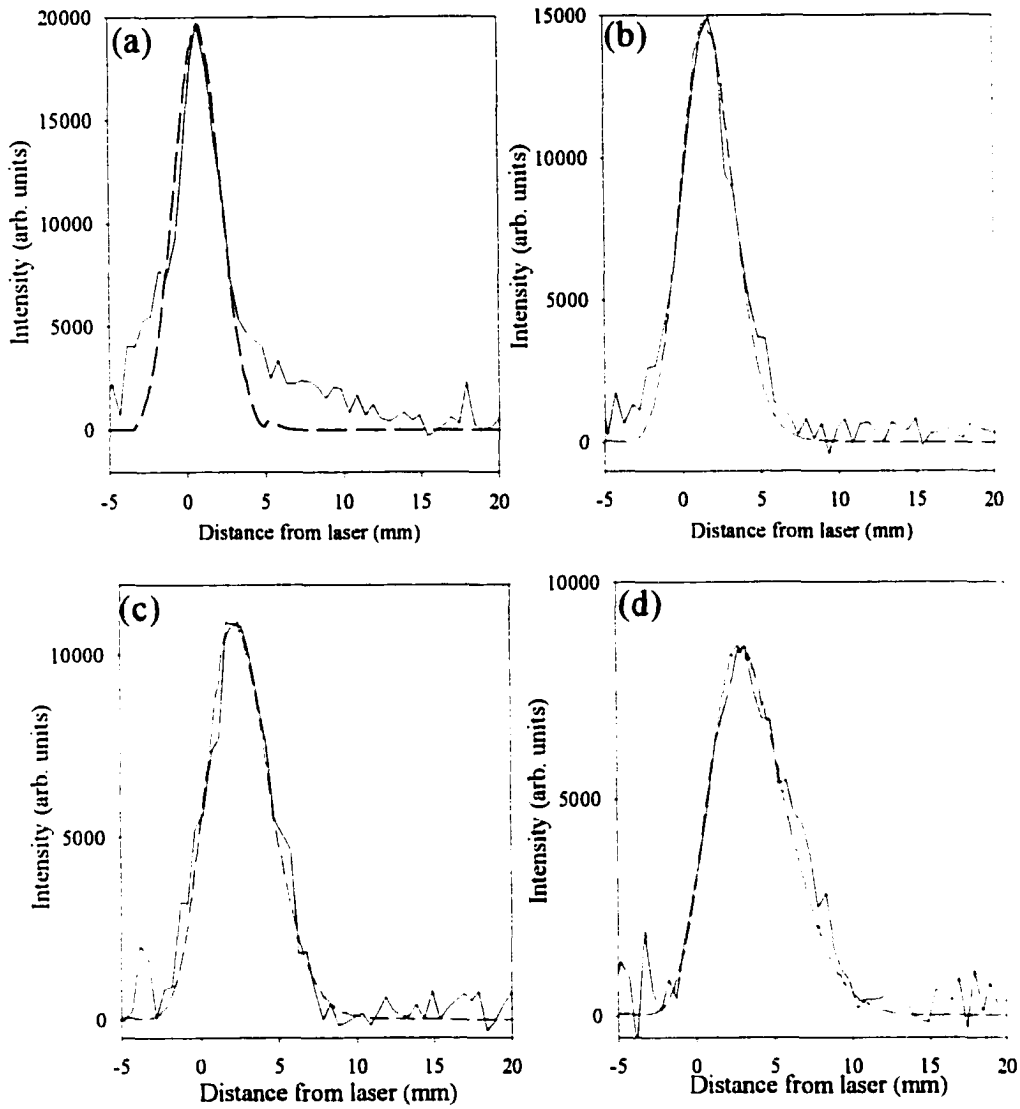


**Figure 6.7.** 1-D profiles obtained from the LIF images presented in Fig. 7 by taking cross-sections *across* the laser axis of scattered $NH_2$ radicals obtained at the following camera gate delays: (a) 1.332 $\mu$s; (b) 3.332 $\mu$s; (c) 5.332 $\mu$s; and (d) 7.332 $\mu$s. The laser-surface distance was 2.4 mm. The continuous lines represent the experimental curves and the dashed lines are the simulated velocity profiles for $\Theta_{Tsc} = 450 \pm 25$ K.

energetics of the incident beam species are clearly affecting the energy of the scattered molecules. As noted above, both ion energy and ion density increase with rf power in these plasma systems. As a consequence, we have examined the effects of ion bombardment on the energy of the scattered $NH_2$ radicals.

*Ion effects on $\Theta_{Tsc}$ for $NH_2$ radicals.* Translational temperatures for scattered $NH_2$ molecules were also determined for "ion-free"plasma molecular beams. Figure 6.9 shows $\Theta_{Tsc}$ data for $NH_2$ radicals scattering from two different substrates, polyimide and Pt, as a function of $P$, with and without the grounded mesh. These data are also listed in Table 6.2. For the polyimide substrate, Fig. 6.9a, $\Theta_{Tsc}$ for $NH_2$ decreases at all $P$ when ions are removed from the molecular beam. At the lowest power ($P$ = 50 W), $\Delta\Theta_{Tsc}$ is only ~ 6 K, whereas at the highest power ($P$ = 150 W), $\Delta\Theta_{Tsc}$ is 120 K. It should also be noted that $\Theta_{Tsc}$ is close to the substrate temperature, $T_S$, of 300 K. A similar decrease in $\Theta_{Tsc}$ when ions are removed from the molecular beam is observed with the Pt substrate, Fig. 6.9b, with $\Delta\Theta_{Tsc} = 26 \pm 11$ K, and $\Theta_{Tsc} \sim T_S$. Thus, for all types of substrates, ion bombardment raises the kinetic energy of $NH_2$ radicals desorbing from the substrate surface.

### 6.2.3. SUBSTRATE MODIFICATION STUDIES

Tables 6.3 and 6.4 display the dependence of static contact angle on time elapsed after treatment with a 50 W $NH_3$ glow discharge for four materials: polyimide, PTFE, Cu and Si. In Table 6.3 the contact angle values of substrates treated directly in the plasma glow are shown. Also shown are the contact angles for the untreated materials. Table 6.4 shows contact angle information for treated substrates of the same materials placed 12 cm

**Table 6.2.** $NH_2$ translational temperature values for CW $NH_3$ plasma processing.

| | Substrate | | | | | | |
|---|---|---|---|---|---|---|---|
| **Power (W)** | Cu | Platinum | Platinum (gm) | Silicon | Polyimide | Polyimide gm | PTFE |
| **50** | 460 ± 20 | 400 ± 30 | -------- | 415 ± 21 | 328 ± 22 | 322 ± 20 | 450 ± 28 |
| **75** | 467 ± 17 | 395 ± 35 | 321 ± 19 | 450 ± 15 | 367 ± 28 | 342 ± 10 | 450 ± 35 |
| **100** | 462 ± 11 | 410 ± 28 | 308 ± 15 | 450 ± 28 | 408 ± 25 | 350 ± 30 | 510 ± 15 |
| **125** | 482 ± 12 | 400 ± 21 | 325 ± 30 | 455 ± 21 | 428 ± 31 | 344 ± 25 | 550 ± 35 |
| **150** | 490 ± 20 | 400 ± 42 | -------- | 455 ± 35 | 494 ± 10 | 375 ± 35 | 550 ± 42 |

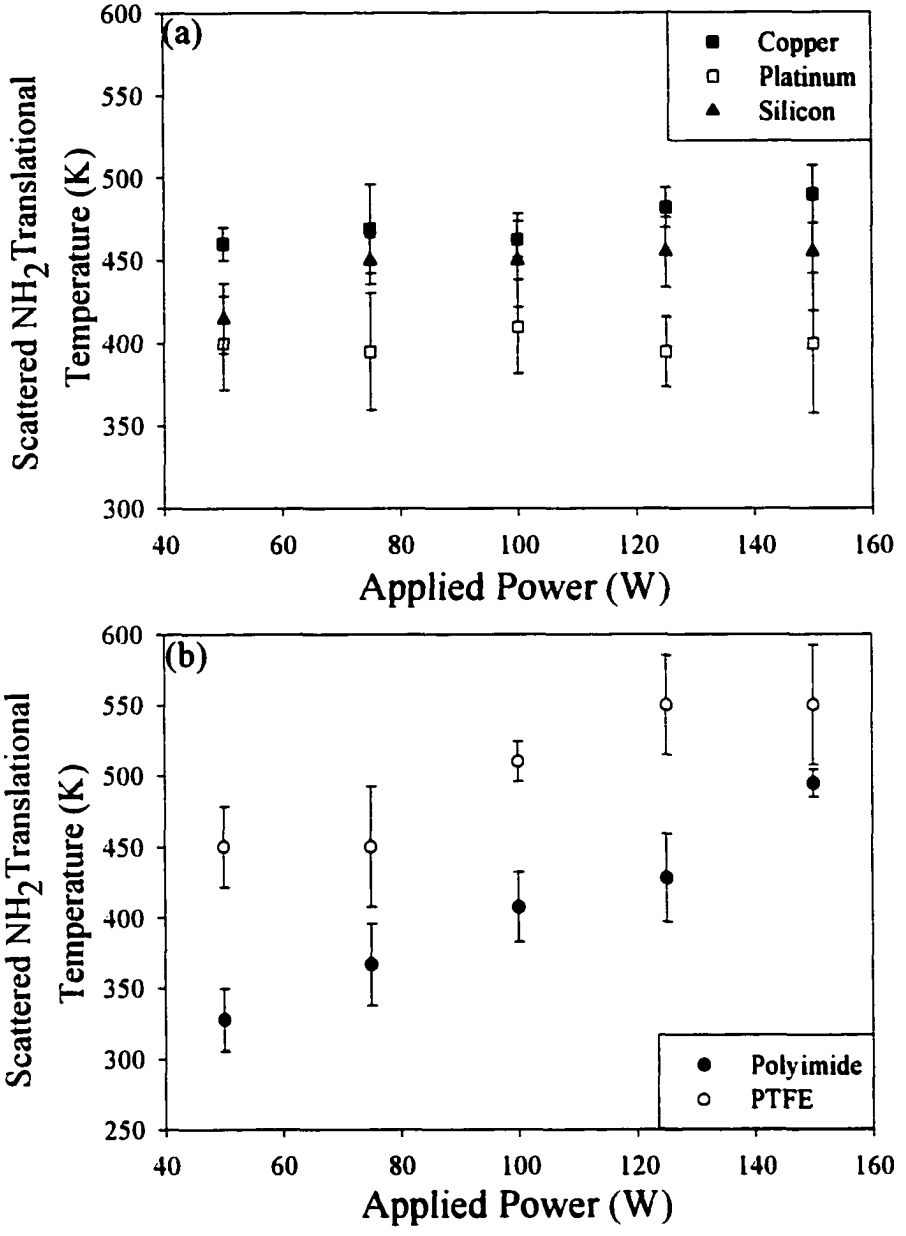


**Figure 6.8.** Substrate material and $NH_3$ plasma power effects on scattered $NH_2$ translational temperatures. The substrates used were (a) Pt, Cu, and Si, and (b) polyimide, and PTFE. The applied power ranged between 50 W and 150 W.

downstream from the rf coil. For both treatment positions, in the glow and 12 cm, all substrate materials became hydrophilic. However, the contact angles measurements clearly show that the samples treated further downstream, Table 6.4, lose hydrophilicity slower than the ones processed in the plasma glow .

Tables 6.5 and 6.6 show that a similar behavior was observed for samples treated in the glow and 12 cm downstream from the rf coil in a 100 W $NH_3$ plasmas. However, the samples shown here lose their hydrophylic attributes faster than the samples treated at 50 W.

## 6.3. DISCUSSION

Understanding radical-surface interactions in glow discharges is of paramount importance for controlling and tailoring the plasma process. While research involving radicals produced in other plasmas does exist,[22-26] little has been published about radicals generated in $NH_3$ plasmas. NH radical reactivity with silicon nitride substrates was found to be 0-10 % for a 45 W ammonia glow discharge and $T_S$ = 300-700 K.[33] No additional applied rf powers were investigated. In our previous work, the energies of $NH_2$ radicals present in $NH_3$ plasma molecular beams were studied.[29] We have also performed a limited study on $NH_2$ molecules scattered from substrate surfaces during $NH_3$ plasma processing. Here, we present a more in-depth investigation of rf power and substrate effects on the reactivity and translational temperature of scattered $NH_2$ radicals. One motivation behind this study is that $NH_2$ radicals are thought to play a significant role in the mechanism through which surfaces are rendered hydrophilic during $NH_3$ plasma

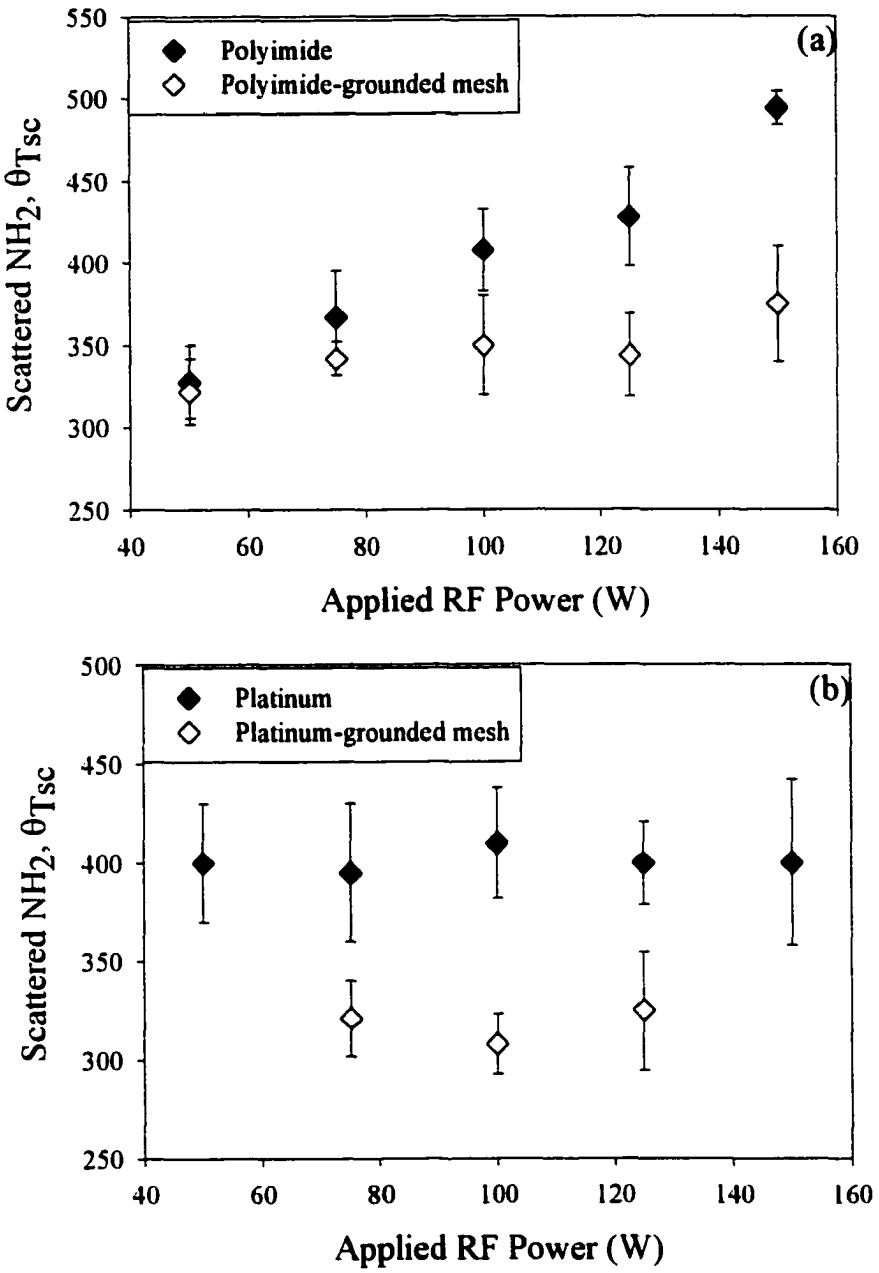


**Figure 6.9.** Ion effects on scattered $NH_2$ translational temperature for $NH_3$ interactions with a (a) polyimide and (b) platinum substrates. $\Theta_{Tsc}$ values are determined for $P$ = 50 -150 W in 25 W increments. (◆) ionic species were not removed from the plasma molecular beam; (◇) ions were removed by placing a grounding mesh in the path of the molecular beam.

**Table 6.3.** Static contact angle measurements as a function of time after treatment with a 50 W $NH_3$ plasma. The substrates were placed in the plasma glow. Also shown are the pretreatment contact angles of the four materials.

| | 0 days | 1.5 day | 5 days | 7.5 days | 18 days | 25 days | pretreatment |
|---|---|---|---|---|---|---|---|
| PI | 62 ± 2.1 | 63 ± 0.8 | 69.9 ± 4.4 | 76.7 ± 4.2 | 83.4 ± 3.6 | 88 ± 3.7 | **94.9** ± 1.1 |
| PTFE | 89 ± 1.4 | 88.2 ± 5 | 98.4 ± 2.5 | 99.6 ± 4.6 | 102.6 ± 5 | 109 ± 3.5 | **107** ± 2 |
| Cu | 56.8 ± 3.3 | 59.9 ± 2.4 | 85.1 ± 5.6 | 88.4 ± 6 | 98.2 ± 5.5 | 99.6 ± 2.6 | **85.6** ± 1.7 |
| Si | 25 ± 2.1 | 41.5 ± 2.2 | 53.4 ± 5.6 | 55.1 ± 3.8 | 66.6 ± 3.8 | 64 ± 3.9 | **42.2** ± 0.5 |

**Table 6.4.** Static contact angle measurements as a function of time after treatment with a 50 W $NH_3$ plasma. The substrates were placed 12 cm downstream from the rf coil. Also shown are the pretreatment contact angles of the four materials.

| | 0 days | 1.5 days | 5 days | 7.5 days | 18 days | 25 days | pretreatment |
|---|---|---|---|---|---|---|---|
| PI | 31.8 ± 2.6 | 43 ± 2.2 | 58.9 ± 6 | 60.6 ± 4.2 | 68.5 ± 2.2 | 71.8 ± 4.6 | **94.9** ± 1 |
| PTFE | 25.3 ± 1.2 | 35.6 ± 3.2 | 50 ± 4.5 | 69.1 ± 2.3 | 75 ± 3 | 79.1 ± 3.9 | **107** ± 2 |
| Cu | 67.8 ± 4 | 68.3 ± 3.6 | 80.1 ± 5.4 | 87.6 ± 5.9 | 89.1 ± 5.6 | 93.3 ± 4.3 | **85.6** ± 1.7 |
| Si | 37.4 ± 1 | 30 ± 4 | 36.1 ± 1.2 | 38.3 ± 2.2 | 45.5 ± 0.7 | 47.9 ± 0.9 | **42.2** ± 0.5 |

**Table 6.5.** Static contact angle measurements as a function of time after treatment with a 100 W $NH_3$ plasma. The substrates were placed in the plasma glow. Also shown are the pretreatment contact angles of the four materials.

| | 0 days | 1.5 days | 5 days | 7.5 days | 18 days | 25 days | pretreatment |
|---|---|---|---|---|---|---|---|
| PI | 19.3 ± 4.5 | 45.6 ± 5 | 60.1 ± 4 | 64.6 ± 6.7 | 75.5 ± 4.8 | 91.8 ± 5 | **94.9** ± 1.1 |
| PTFE | 70 ± 4 | 85.9 ± 6 | 93.6 ± 3 | 91.9 ± 2.8 | 92.8 ± 0.8 | 98.9 ± 2.5 | **107** ± 2 |
| Cu | 59.2 ± 4.5 | 74 ± 3.8 | 85.3 ± 5 | 90.2 ± 2.7 | 93.8 ± 4.4 | 90.9 ± 5 | **85.6** ± 1.7 |
| Si | 15 ± 2 | 31.5 ± 4.9 | 41.5 ± 1.4 | 54.1 ± 3 | 68 ± 2.8 | 66.2 ± 4.3 | **42.2** ± 0.5 |

**Table 6.6.** Static contact angle measurements as a function of time after treatment with a 100 W $NH_3$ plasma. The substrates were placed 12 cm downstream from the rf coil. Also shown are the pretreatment contact angles of the four materials.

| | 0 days | 1.5 days | 5 days | 7.5 days | 18 days | 25 days | pretreatment |
|---|---|---|---|---|---|---|---|
| PI | 31 ± 4 | 43.3 ± 6 | 48.4 ± 5 | 54.3 ± 5.6 | 59.3 ± 3.4 | 58.6 ± 4.5 | **94.9** ± 1.1 |
| PTFE | 51.7 ± 4 | 66.5 ± 5 | 89.2 ± 5 | 92.9 ± 6.7 | 88.1 ± 2 | 98.7 ± 3.2 | **107** ± 2 |
| Cu | 80.3 ± 2.1 | 80.4 ± 4.4 | 77.8 ± 4.9 | 81.4 ± 5 | 88.3 ± 6.7 | 86.9 ± 6 | **85.6** ± 1.7 |
| Si | 20 ± 2 | 28.1 ± 2.2 | 32.5 ± 1.6 | 36.7 ± 1 | 45 ± 1.4 | 48 ± 1.3 | **42.2** ± 0.5 |

treatments.[2] Past research has shown that amine group implantation occurs with polymer substrates that are exposed to ammonia glow discharges.[13] This implantation process is believed to occur through the interactions of $NH_x$ species and the polymer surface. The results presented here and in our past studies [25,30] demonstrate that $NH_2$ radicals are not consumed at the surface of a variety of substrates, including polymers. Thus, the primary question originated by these data revolves around the mechanism for the observed surface production of $NH_2$. This fundamental question is further addressed below. A secondary issue that then arises is identification of the process that is actually contributing to the observed surface modification. This issue will be discussed in future publications after investigating the interactions of other radicals produced in ammonia glow discharges.[34]

### 6.3.1. REACTIVITY OF $NH_2$ RADICALS

As noted in the Introduction, previous research has shown that $NH_2$ group implantation is a major contributor to increasing the hydrophilicity of substrates processed in ammonia glow discharges.[11-13] However, our results show that $NH_2$ radical production occurs at the substrate surface during $NH_3$ plasma processing since $S > 1$ under most experimental conditions, Table 6.1. This suggests that other species in the molecular beam are contributing to the surface production of $NH_2$. The most likely contributing reactions occurring at the plasma-substrate interface are discussed below.

*Possible Reactions Contributing to $NH_2$ Surface Production.* Scattering of incident $NH_2$ molecules can occur through a simple adsorption-desorption type of mechanism, reaction 1,

$$NH_2(g) + * \rightarrow NH_2(ads) \rightarrow NH_2(g) \quad (1)$$

where * represents an active site on the substrate surface. $NH_2$ radicals formed through this process would be expected to have a Maxwell-Boltzmann distribution of energies characterized by the substrate temperature and a cosine angular distribution about the surface normal.[35] We believe this reaction accounts for a large fraction of the desorbed $NH_2$ observed in our system. It does not, however, account for the surface generation of $NH_2$ (i.e. $S > 1$) observed under nearly all of the conditions studied here, Table 6.1.

There are many other possible interactions that could account for the production of $NH_2$ radicals at a substrate surface during plasma processing. Three plausible pathways involving neutral species in the plasma molecular beam are shown in processes 2-4:

$$NH_3(g) + * \rightarrow NH_2(ads) + H(ads) \rightarrow NH_2(g) \quad (2)$$

$$NH(g) + H(ads) \rightarrow NH_2(g) \quad (3)$$

$$NH(g) + * \rightarrow NH(ads); \qquad NH(ads) + H(ads) \rightarrow NH_2(g) \quad (4)$$

Process 2 can be considered as a dissociative adsorption reaction followed by desorption of one of the dissociated species. The last two processes represent Eley-Rideal-type (ER) interactions, wherein a reaction occurs between a gas-phase species and an adsorbed species before the gas-phase reactant has equilibrated with the surface, process 3; and a Langmuir-Hinschelwood-type (LH) process where both reactants have equilibrated on the surface prior to reaction, process 4. While reactions 3 and 4 are primarily used to describe reactions that occur under ultrahigh vacuum (UHV) conditions,[36] they afford a means with which to discuss the results of the present work.

Additionally, reactions involving ions must also be considered. Specifically,

surface bombardment by ions can result in ion dissociation and neutralization, reaction 5, ion neutralization, reaction 6, and ion induced sputtering, reaction 7, where $I^+$ is any gas-phase ion.

$$NH_3^+(g) + * \rightarrow NH_2(ads) + H(ads) \rightarrow NH_2(g) \quad (5)$$

$$NH_2^+(g) + * \rightarrow NH_2(ads) \rightarrow NH_2(g) \quad (6)$$

$$I^+(g) + NH_2(ads) \rightarrow NH_2(g) \quad (7)$$

We explicitly assess the influence of ion-assisted processes in the surface generation of $NH_2$ radicals during plasma processing of two materials, polyimide and platinum using the grounded mesh experiments. For both substrates, less $NH_2$ desorbs from the surface when ions are removed from the plasma molecular beam. While we cannot distinguish between processes 5-7 in these experiments, we can state with certainty that ion-induced reactions are partly responsible for $NH_2$ generation at the substrate surface.

Another interesting result obtained when comparing the $NH_2$ $S$ values obtained in the "ion-free" experiments to those measured with ions present is that the $S$ values decrease by a nearly constant amount at all $P$, specifically 22-29% for polyimide, and 16-18% for platinum, Fig. 6.4. This is unlike what we observed when exploring ion effects on $CF_2$ scatter coefficients in HFPO plasmas.[26] As the HFPO plasma rf power increased from 35 W to 200 W, $CF_2$ S values increased from ~1 to ~1.3. However, the elimination of ion bombardment resulted in a constant difluorocarbene scatter coefficient of ~0.8 at all rf powers.

Two observations from our surface reactivity data suggest that ion bombardment reactions (processes 5-7) are not the only mechanisms through which $NH_2$ surface

generation occurs. First, the data for both the polyimide and Pt substrates taken without ions present follow nearly parallel courses to the data taken with ions present. Second, even when ions are removed from the plasma molecular beam, $S$ values remain above unity at the highest $P$. We will discuss two possibilities for inducing surface generation in the absence of ions. The first possibility is that at higher $P$, the neutral species exhibit higher energy, resulting in increased $NH_2$ surface generation through higher energy transfer or increased dissociation as these species collide with the substrate surface. Our previous studies of the translational temperatures of $NH_2$ radicals produced in $NH_3$ plasmas showed that, indeed, as the rf power increased from 50 W to 150 W, $\Theta_{Tmb}$, also increased from 510 K to 660 K. The energy difference between these two temperatures, however, is relatively small (~0.01 eV). Thus, this mechanism is an unlikely contributor to $NH_2$ surface generation.

The second possibility for $NH_2$ surface generation in our "ion-free" ammonia plasmas is that at higher rf powers there are different species densities than at low $P$. Hence, the surface reactions of such species can gain importance at higher applied rf powers. Studies of $NH_2$ relative density dependence on $P$ show that at $P$ >100 W, $NH_2$ signal decreases significantly. This decrease is consistent with a higher degree of $NH_2$ dissociation at higher rf powers. A likely dissociation product is NH, which can be involved in the generation of $NH_2$ radicals through the pathways given in equations 3 and 4. Thus, it is possible that for high $P$, NH radical densities increase, leading to a larger amount of $NH_2$ produced by NH at the subsrate surface. To directly demonstrate that this type of process takes place, NH radical interactions must be investigated further than has

been done to date. Experiments designed to determine the effects of ions and $NH_3$ plasma rf power on the scatter coefficients of NH are underway.

### 6.3.2. $NH_2$ SCATTER COEFFICIENT DEPENDENCE ON SUBSTRATE MATERIAL

The $NH_2$ scatter coefficients determined in our IRIS experiments under most experimental conditions are > 1. There are, however, significant differences in the $S$ values obtained with different substrate materials. Table 6.1 and Fig. 6.3 show that $NH_2$ radicals exhibit different scatter behavior with the metallic substrates compared to Si and the polymeric materials. First, the $NH_2$ scatter coefficients for Pt and Cu are lower than those determined for the polymers and Si substrates for $P > 75$ W. This indicates that the reactivity of $NH_2$ on the metallic substrates is higher than with the other substrate materials in this study. One can explain these differences by examining the chemistry of the substrates.

To understand these differences, it is helpful to consider molecule-surface reactions in terms of Lewis acid-base type interactions. In general, metals can be considered Lewis acids due to their ability to easily accept electrons, while amines are considered Lewis bases because they are electron donors and have no high-lying donor orbitals. With these definitions, Pt and Cu are expected to exhibit a higher reactivity towards incoming $NH_x$ molecules in the plasma relative to surfaces that do not easily accept electrons. This could result in stronger binding between these substrates and both $NH_2$ and $NH_3$, leading to less $NH_2$ scatter. In other words, reactions 1 and 2 may not contribute as much to the observed scatter. This type of molecule-surface interaction can

be contrasted with that observed on the polymers. For example, polyimide has a strong π-network, replete with electrons, such that it can be classified as a Lewis base. Likewise, PTFE contains large concentrations of F atoms which are not readily polarizable and thus, will not accept electron density easily. Hence, these substrates are expected to exhibit a lower reactivity (higher scatter) than the metallic substrates. Indeed, the highest scatter coefficients we measure are for the polymeric substrates, Table 6.1.

The relatively strong $NH_2$ scatter measured using the silicon substrate is not easily understood in terms of acid-base characteristics. It is generally believed that $SiO_2$ is a weak acid. Thus, with our Si substrate with native oxide, we would expect a high reactivity for $NH_2$. However, upon exposure to the $NH_3$ plasma molecular beam, a $Si_xN_y$ or $Si_xO_yN_z$ type of layer is formed at the substrate surface.[36,37] This has been explicitly demonstrated using $NH_3$ plasma treatment of both Si and $SiO_2$ substrates. The $Si_xN_y$ or $Si_xO_yN_z$ layer formed on our substrates would behave more like a base than an acid, resulting in the high scatter coefficients observed for Si substrates.

### 6.3.3. TRANSLATIONAL TEMPERATURE STUDIES OF SCATTERED $NH_2$ RADICALS

By investigating kinetic energy disposal at the surface, we can obtain information on which of the processes given in reactions 1-7 are more likely to occur. For example, as noted above if only process 1 occurs, the energy of desorbed $NH_2$ would be characterized by the substrate temperature.[38] Likewise, reaction 4 involves species that are fully accommodated at the surface. Hence desorbed $NH_2$ formed by this process would also be

characterized by $T_s$. Since $\Theta_{Tsc} \geq T_s$ under most of the experimental conditions we examine, $NH_2$ radicals must be generated (at least in part) through pathways other than 1 and 4. One possibility is reaction 3, which is expected to produce scattered $NH_2$ molecules that possess kinetic energies independent of $T_S$, and dependent on the translational energy of the incident species.[36,38] Because we do not have any information on the translational energy of NH radicals in the incident beam, we can not fully assess the contribution of this mechanism to the observed $NH_2$ surface generation.

In addition to process 3, the ion-induced $NH_2$ surface production pathways (reactions 5-7) are also likely to result in radicals that desorb with $\Theta_{Tsc} > T_s$. Our data for "ion-free" $NH_3$ plasma molecular beams provide direct evidence that ion-induced reactions do increase the kinetic energy of desorbing $NH_2$ radicals, Table 6.2. With the ion-free plasma molecular beam, $\Theta_{Tsc}$ decreases to values that are close to $T_s$. Thus, ion-induced processes appear to be the main reactions responsible for $\Theta_{Tsc} > T_s$. It is important to note that we cannot distinguish between the three ion-induced reactions discussed earlier. If reaction 7 is contributing, energy transfer must be occurring directly between an incident ionic species and adsorbed $NH_2$. Conversely, if process 5 and 6 are occurring, energy transfer between the incident ionic species and the substrate lattice is not complete such that the desorbing species has an elevated kinetic energy.

As discussed above, the nature of the reactions transpiring at the $NH_3$ plasma-substrate interface is also influenced by the reactivity of the surface with respect to incident species. Indeed, we observe different $NH_2$ scatter behavior for the metallic and polymeric substrates. The same is true for the $\Theta_{Tsc}$ of scattered $NH_2$ radicals. The results

presented in Table 6.2 show a significant difference in the rf power dependence for $\Theta_{Tsc}$ values using different substrates. Specifically, $NH_2$ radicals scattered from Pt and Cu surfaces display virtually no dependence of $\Theta_{Tsc}$ on applied rf power. Similar to the metallic substrates, $\Theta_{Tsc}$ for $NH_2$ desorbing from the Si surface also displayed little dependence on $P$, with $\Theta_{Tsc}$ = ~450 K. In contrast, $\Theta_{Tsc}$ of radicals desorbing from the polymeric substrates shows a substantial increase with rf power.

The complexity of plasma-surface interactions makes it difficult to interpret these energy transfer trends definitively. It is instructive, however, to examine the UHV surface literature for possible analogous behavior. Specifically, the two dissociative adsorption process, reactions 2 and 5, are likely to be contributors to the observed scatter. Indeed, previous reports have expressly shown that $NH_3$ dissociatively adsorbs onto Si and Pt substrates.[39,40] Moreover, Auerbach and Rettner have shown that dissociative adsorption of $N_2$ and $O_2$ on tungsten surfaces can occur through two mechanisms: a precursor-mediated process and a direct adsorption process.[41] The dissociation mechanisms are, however, dependent on the energy of the incident species and both are thought to occur in these systems. For incident energies <0.2 eV, the precursor mediated adsorption dominates, whereas for higher incident energies the direct adsorption process governs the interaction. Since most neutrals in our glow discharges have kinetic energies <0.2 eV, it is likely that they adsorb at the surface through a precursor state. In this type of process, the incident molecule becomes temporarily bound to the surface in a precursor state, and must overcome an intermediate barrier before chemisorption can be attained.[42,43] If the barrier can not be surmounted, the molecule resides on the surface for a short time and then

desorbs.

In our system, the ions have energies > 0.2 eV. Therefore, it is likely that direct adsorption is the preferred mechanism for the ion-mediated reactions, processes 5-7. This is also supported by the observation that if the precursor state does not exist, one expects to see a dependence of adsorption on the incident gas temperature.[43] This is indeed what we observe for our $NH_2$ scattering experiments. Namely, at higher rf powers, the translational temperature of radicals in the plasma is higher than at the lower rf powers.[29] At the higher powers, the amount of $NH_2$ scatter increases, Table 6.1, suggesting that less adsorption occurs. If no precursor state exists, then it is more likely that the scattered molecules will not have had the opportunity to equilibrate fully with the surface. Thus, when they leave the surface, they will exhibit elevated $\Theta_{Tsc}$, relative to $T_S$.

It should also be noted, however, that there are additional factors that will control the plasma-surface interactions. First, with a precursor-mediated process, the height of the barrier to chemisorption is likely to be controlled by the chemical structure of the incident molecule as well as the chemical nature of the substrate material.[39] Second, there is a complex mix of species interacting simultaneously with the surface, such that is is difficult to distinguish between processes. Finally, it is well known that energy transfer between gas molecules and surfaces can occur not only via kinetic energy exchange, but also through vibrational and rotational energy transfer.[33,36,39] Thus, with the high number of variables involved in this complicated process, it is difficult to completely interpret the translational energy transfer trends observed in our IRIS experiments.

## 6.4. SUMMARY AND FUTURE WORK

This work shows that $NH_2$ radicals are generated at the substrate surface during ammonia plasma processing. The $NH_2$ scatter coefficients are >1 under most experimental conditions, but decrease when ionic species are eliminated from the incident molecular beam. The power dependence of scatter coefficients is believed to be the result of two main effects: neutral species increased dissociation at higher rf powers combined with higher energy ions created as the power is increased.

Translational temperatures studies for scattered $NH_2$ molecules show that ions are the main cause for increases in $\Theta_{Tsc}$ with applied power for polyimide substrates. We also hypothesize that differences between Si, polymer substrates and metals are mainly due to the different Lewis acidity characteristics of these materials. To further elucidate $NH_3$ plasma-substrate interactions studies of other species, such as NH radicals, are underway.

## 6.5. REFERENCES


1. J. P. Badey, E. Espuche, T. M. Duc, *Polymer* **37**, 1377 (1996); M. Tatoulian, F. Arefi-Khonsari, J. Amorooux, *Int. J. Adhes.* **15**, 177 (1995).

2. T. R. Gengenbach, X. Xie, R. C. Chatelier, and H. J. Griesser, *J. Adhesion Sci. Technol.* **8**, 305 (1994).

3. E. M. Liston, L. Martinu, and M. R. Wertheimer, *J. Adhesion Sci. Technol.* **7**, 1091 (1993).

4. F. E. Egitto and L. J. Matienzo, *IBM J. Res. Dev.* **38**, 423 (1994).

5. J.-C. Lin and S. L. Cooper, *J. Appl. Polym. Sci.: Appl. Polym. Symp.* **54**, 157 (1994).

6. B. D. Ratner, A. Chilkoti, and G. P. Lopez, *Plasma Deposition , Treatment, and Etching of Polymers*, 464, R. d'Agostino ed. (1990).

7. H.-C. Cheng, F.-S. Wang, and C.-Y Huang, *IEEE Trans. Elec. Devices* **44**, 64 (1997).

8. M. E. Jones, J. R. Shealy, and J. R. Engstrom, *Appl. Phys. Lett.* **67**, 542 (1995).

9. references 4 and 5 in reference 29.

10. D. L. Cho, and H. Yasuda, *J. Vac. Sci. Technol. A* **4**, 2307 (1986).

11. N. Inagaki, S. Tasaka, and H. Kawai, *J. Adhesion Sci. Technol.* **3**, 637 (1989).

12. C. Munkholm, D. R. Walt, F. P. Milanovich and S. M. Klainer, *Anal. Chem.* **58**, 1427 (1986).

13. R. C. Chatelier and H. J. Griesser *Surface and Interface Analysis* **24**, 611, (1996).

14. T. R. Gegenbach, R. C. Chatelier and H. J. Griesser *Polymer* **38**, 1045 (1997).

15. P. Favia, M. V. Sternardo, and R. d'Agostino, *Plasmas Polym.* **1**, 91 (1996).

16. N. Inagaki, *Plasma Surface Modification and Plasma Polymerization*, Technomic, Lancaster, 1996.

17. d'Agostino, R. in *Plasma Deposition, Treatment and Etching of Polymers*; R. d'Agostino, Ed., Academic Press, San Diego, 1990.

18. H. Yasuda, *Plasma Polymerization*, Academic Press, New York, 1985.

19. P. Ho, W. G. Breiland, and R. J. Buss *J. Chem Phys.* **91**, 2627 (1989).

20. P. R. McCurdy, K. H. A. Bogart, N. F. Dalleska, and E. R. Fisher, *Rev. Sci. Instrum.* **68**, 1684 (1997).

21. N. M. Mackie, V. A. Venturo, and E. R. Fisher, *J. Phys. Chem. B* **101**, 9425, (1997).

22. N. M. Mackie, N. E. Capps, C. I. Butoi, E. R. Fisher, in *Fluorinated Coatings, Surfaces, and Films, ACS Symp. Proc.*, D. G. Castner, D. W. Grainger, eds., in press.

23. N. E. Capps, N. M. Mackie, and E. R. Fisher, *J. Appl. Phys.* **84**, 4736 (1998).

24. C. I. Butoi, N. M. Mackie, P. R. McCurdy, J. H. D. Peers, and E. R. Fisher, *Plasmas Polym.* **4**, 77 (1999).

25. C. I. Butoi, N. M. Mackie, K. L. Williams, N. E. Capps, E. R. Fisher, *J. Vac. Sci. Technol. A* **18**, (2000), in press.

26. C. I. Butoi, N. M. Mackie, L. J. Gamble and D. G. Castner, J. E. Barnd, A. M. Miller, and E. R. Fisher, *Chem. Mater.* **12**, 2014 (2000).

27. C. I. Butoi, N. M. Mackie, J. E. Barnd, E. R. Fisher, L. J. Gamble and D. G. Castner, *Chem. Mater.* **11**, 862 (1999).

28. P. R. McCurdy, V. A. Venturo, and E. R. Fisher, *Chem. Phys. Lett.* **274**, 120 (1997).

29. P. R. McCurdy, C. I. Butoi, K. L. Williams, and E. R Fisher, *J. Phys. Chem B.* **103**, 6919 (1999).

30. K. L. Williams, C. I. Butoi, and E. R. Fisher, *J. Vac. Sci. Technol. A*, manuscript in preparation.

31. M. A. Lieberman, A. J. Lichtenberg, *Principles of Plasma Discharges and Material Processing*; Wiley and Sons: New York, 1994.

32. A. Grill, *Cold Plasma in Materials Fabrication*; IEEE Press: Piscataway, NJ, 1994.

33. E. R. Fisher, P. Ho, G. Breiland, and R. J. Buss *J. Phys. Chem.* **96**, 9855 (1992).

34. M. L. Steen and E. R. Fisher, unpublished work.

35. C. T. Rettner, D. J. Auerbach, J. C. Tully, A. W. Kleyn, *J. Phys. Chem.* **100**, 13021 (1996).

36. This was explicitly shown to be true in a previous IRIS study (see Ref. 34).

37. R. I. Masel, *Principles of Adsorption and Reaction on Solid Surfaces*; John Wiley: New York, 1996.

38. G. A. Somarjai, *Introduction to Surface Chemistry and Catalysis*; John Wiley: New York, 1994.

39. M. J. Dresser, P. A. Taylor, R. M. Wallace, W. J. Choyke, J. T. Yates, Jr *Surf. Sci.* **1989**, *218*, 75.

40. Y.-M. Sun, D. Sloan, H. Ihm, J. M. White, *J. Vac. Sci. Technol. A* **14**, 1516 (1996).

41. D. J. Auerbach, C. T. Rettner, in *Kinetics of Interface Reactions*, M. Grunze, H. J. Kreuzer, Eds.; Springer Verlag: Berlin, 1986, p. 142.

42. W. H. Weinberg, in *Kinetics of Interface Reactions*, M. Grunze, H. J. Kreuzer, Eds.; Springer Verlag: Berlin, 1986, p. 94.

43. J. I. Steinfeld, S. J. Francisco, W. L. Hase, *Chemical Kinetics and Dynamics*; Prentice Hall: Englewood Cliffs, NJ, 1989.

# CHAPTER 7

## CONCLUSIONS AND FUTURE WORK

This chapter provides a comparison between the two types of plasma systems examined in this dissertation: fluorocarbon and ammonia glow discharges. Future experiments designed to further elucidate the mechanisms through which plasmas modify substrates are also discussed.

## 7.1. PLASMA SYSTEM COMPARISON

The investigations of fluorocarbon and ammonia plasma systems discussed in this dissertation provide some insight into the processes involved in glow discharge processing. In general, fluorocarbon plasmas display a dual nature in that both deposition and etching reactions occur concomitantly during substrate processing.[1,2,3,4] Which one predominates determines the overall plasma process. This dissertation discusses two depositing fluorocarbon plasmas: $C_2F_6/H_2$ and HFPO. One difference between the two is the deposition rate of fluorocarbon materials. The $C_2F_6/H_2$ glow discharge is a fast depositing system with a deposition rate of 200 Å/min for 40 W CW conditions, whereas the HFPO system deposits materials more slowly at ~7 Å/min under similar plasma conditions. Interestingly, the interactions between $CF_2$ radicals and substrates during plasma processing are also different for the two systems. For the fast depositing system, $C_2F_6/H_2$, difluorocarbene scatter coefficients were found to be < 1. In contrast, the studies of $CF_2$ radical interactions during HFPO plasma processing resulted in $S \geq 1$. When etching was the predominant process, however, as observed for $C_2F_6$ glow discharges, $CF_2$ scatter coefficients were >> 1.

It is also important to note that for both depositing systems, HFPO and $C_2F_6/H_2$, difluorocarbene-substrate interactions are independent of substrate material, Tables 5.1 and 5.2. Conversely, the $CF_2$ scatter coefficients determined under etching conditions were different for substrates with different chemical composition, Table 5.1. Thus, it is apparent from the study of $C_2F_6/H_2$, HFPO, and $C_2F_6$ glow discharges that the behavior of $CF_2$ radicals provides a means by which the overall plasma process, deposition or etching,

can be gauged.

To assess if radical-surface interactions also gauge the overall process for other systems in addition to fluorocarbon plasmas, $NH_2$ interactions were investigated during $NH_3$ glow discharge processing. It is well known that $NH_3$ plasmas neither deposit significant amounts of film nor etch substrates.[5] Instead, amine group implantation occurs during processing of polymeric materials,[6,7] and nitriding of surfaces takes place for semiconductor and metal substrates.[8] Based on the results obtained from our fluorocarbon plasma investigations, a plasma system that does not result in film deposition is expected to display dependence of radical-surface interactions on the chemical composition of the substrate being processed. Indeed, different $NH_2$ radical scatter coefficients were determined for polymeric, semiconductor, and metallic materials. Clearly, radical-surface interactions provide a reliable gauge for the overall plasma process in glow discharges other than fluorocarbon systems.

## 7.2. FUTURE WORK

The investigations of fluorocarbon and ammonia glow discharges discussed in this dissertation show that radical-surface interactions can be used to determine the regime to which a plasma belongs: depositing or non-depositing. While this is a major finding, it is equally important to determine the individual processes responsible for surface modification during rf plasma processing. Future experiments designed to achieve this goal are discussed below.

For both fluorocarbon and ammonia plasmas, the interactions between substrates

and other plasma radicals other than $CF_2$ and $NH_2$, respectively, must be investigated. CF and $CF_3$ radicals produced in $C_2F_6/H_2$, HFPO, and $C_2F_6$ glow discharges should be examined to determine if these radicals are involved in surface reactions by which difluorocarbene radicals are generated. Since CF radicals fluoresce, the IRIS apparatus used in the $CF_2$ studies can be employed to assess CF scatter coefficients. In contrast, LIF techniques cannot be used to investigate $CF_3$ radicals which photodissociate upon laser irradiation. A technique which circumvents this difficulty is resonance-enhanced multiphoton ionization (REMPI). REMPI analysis of $CF_3$ radical-surface interactions can be used to obtain $CF_3$ scatter coefficients during fluorocarbon plasma processing.

Studies similar to those proposed above must be performed to gain a deeper understanding of surface modification processes during ammonia plasma processing. When $NH_2$ radical-substrate interactions were investigated, $NH_2$ surface generation occurred for most plasma conditions. In Chapter 6, we directly identified ion induced reactions as being partly responsible for the observed radical surface generation. However, we also showed that this type of process cannot be the only reaction causing large densities of $NH_2$ to emanate from the substrate surface. To ascertain if NH surface reactions contribute to the observed $NH_2$ behavior, the IRIS technique can be used.

The future experiments listed in this chapter will reveal if radical loss or generation at substrate surfaces occurs for all significant plasma species. This systematic investigation of glow discharge systems has the potential to illuminate exact substrate modification mechanisms during plasma processing. This would constitute a great accomplishment since a full understanding of plasma modification pathways remains

elusive despite the extensive work already existent in the plasma science field.

## 7.3. REFERENCES


1. R. d'Agostino, F. Cramarossa, F. Fracassi, and F. Illuzi, *Plasma Deposition, Treatment, and Etching of Polymers*, R. d'Agostino ed., Academic Press, San Diego, p. 99 (1990).

2. N. M. Mackie, "Investigation of Mechanisms for Plasma Polymerization of Organic Thin Films", Doctoral Thesis, Colorado State University (1998).

3. N. Inagaki, *Plasma Surface Modification and Plasma Polymerization*, Technomic, Lancaster, (1996).

4. M. A. Lieberman, A. J. Lichtenberg, *Principles of Plasma Discharges and Material Processing*; Wiley and Sons: New York, 1994.

5. B. D. Ratner, A. Chilkoti, and G. P. Lopez, *Plasma Deposition , Treatment, and Etching of Polymers*, 464, R. d'Agostino ed. (1990).

6. T. R. Gengenbach, X. Xie, R. C. Chatelier, and H. J. Griesser, *J. Adhesion Sci. Technol.* **8**, 305 (1994).

7. T. R. Gegenbach, R. C. Chatelier and H. J. Griesser *Polymer* **38**, 1045 (1997).

8. R. I. Masel, *Principles of Adsorption and Reaction on Solid Surfaces*; John Wiley: New York, 1996.